THE DESIGN OF A MOTT-SCHWINGER NEUTRON POLARIMETER AND POLARIZATION IN THE $H^2(d,n)He^3$ REACTION.

by

RAFAEL MARTINEZ LUGO , B.Sc.

Thesis submitted for the degree of

DOCTOR OF PHILOSOPHY

University of Edinburgh

1976

ABSTRACT.

The most commonly used technique to investigate the degree of polarization of a fast neutron beam has been, so far, the He^4 scattering polarimeter. This system is based on the asymmetry of the nuclear scattering cross section introduced by the nucleus spin-orbital angular momentum interaction between the neutron and the nucleus, in which case the analysing power of the scattering nucleus is calculated from a complicated phase shift analysis of the elastic scattering differential cross section data. The asymmetry may be affected by neutron background which in turn may introduce a systematic error in the polarization value, since correction for this effect depends on the judgement of the experimenter.

An alternative technique is the small angle Mott-Schwinger scattering, in which case the polarization is calculated directly from the experimental total cross section and differential elastic scattering cross section for the angle of scattering, and therefore is not influenced by the model used to describe the nucleus. This system has been employed mainly to investigate small angle theory, requiring then, very fine collimation of the neutron beam incident on the analysing scatterer and very small spread in scattering angles accepted by the neutron detectors which have to be positioned very close to the neutron beam with the consequent problem of severe

background. For these reasons the efficiency of data collection is very low when compared with the efficiency of a typical He^4 scattering polarimeter.

The main objective of this thesis is to design and construct a polarimeter for neutrons of a few MeV energy based on small angle Mott-Schwinger scattering which has an efficiency of data collection comparable to that attainable in a conventional He^4 scattering polarimeter based on a gas scintillator. The calculations carried out to obtain an optimum geometry for such a polarimeter are presented and a detailed description of its construction is given. This Mott-Schwinger scattering polarimeter has been assessed by measuring the polarization of fast neutrons emitted from the $H^2(d,n)He^3$ reaction at a laboratory reaction angle of about 45° at several deuteron energies below 500 KeV.

The polarization values obtained agree with recent measurements obtained with a typical He^4 scattering polarimeter and the new technique based on a helium filled proportional chamber. A comparison of the polarization values of D-D neutrons obtained with the present Mott-Schwinger polarimeter and He^4 scattering polarimeter indicated that the efficiency of data collection of both systems are comparable. It is concluded that the advantages of the present Mott-Schwinger scattering polarimeter outweigh the experimental difficulties and that this system can provide an efficient and reliable method to determine the source polarization in various neutron producing reactions.

CONTENTS.

CHAPTER 3.

CHAPTER 1.

CHAPTER 1.

FAST NEUTRON POLARIZATION STUDIES.

1.1 Introduction.

Reliable fast neutron polarization data can be extremely helpful in the analysis of some problems in nuclear physics, namely in obtaining spin-parity information concerning unbound nuclear states; the reaction mechanism of neutron production reactions such as (d,n), (p,n), (He^3,n) etc. and the effect of spin-orbit forces in elastic scattering. Also, an accurate knowledge of polarization of neutrons emitted in the main neutron producing reactions is important for their use in experiments on scattering of polarized neutrons. Thus, measurements of the polarization of neutrons scattered by the lightest nuclei can provide information about nucleon-nucleon forces; information about nuclear energy levels can be obtained in the study of other light nuclei; and for intermediate and heavy nuclei, one can learn something about the neutron-nucleus potential.

A beam of neutrons is polarized if the spins are not randomly distributed but have some preferred orientation. If the number of neutrons in the beam with spin component parallel to

this preferred direction is N+ and the number with antiparallel spin component is N-, the polarization is defined as:

$$P_n = \frac{N+ - N-}{N+ + N-} \qquad (1.1.1)$$

According to Wolfenstein [1], the equation (1.1.1) is equivalent to $P_n = \langle \sigma d \rangle$, the expectation value of the component σd of the spin operator σ along the preferred direction d. If this direction is not selected in advance, P can be defined with respect to arbitrary axes and the direction also found. Thus, the polarization is given by:

$$P_n^2 = \langle \overline{\sigma x} \rangle^2 + \langle \overline{\sigma y} \rangle^2 + \langle \overline{\sigma z} \rangle^2 \qquad (1.1.2)$$

and the preferred direction is specified by the polarization vector:

$$\overline{\sigma} = \langle \sigma x \rangle \hat{i} + \langle \sigma y \rangle \hat{j} + \langle \sigma z \rangle \hat{k} \qquad (1.1.3)$$

Since conventional neutron detectors are not sensitive to the neutron spin direction, the measurement of fast neutron polarization generally involves a double scattering process. Fig. 1 shows a typical geometry for fast neutron polarization measurements. Unpolarized charged particles of energy E in the direction $\underline{k}_d$ are incident on a target T, where a reaction occurs in which neutrons of polarization $P_n(E,\Theta_1)$ are produced. Neutrons of energy E_n emitted in the direction $\underline{k}_n$ are elastically scattered

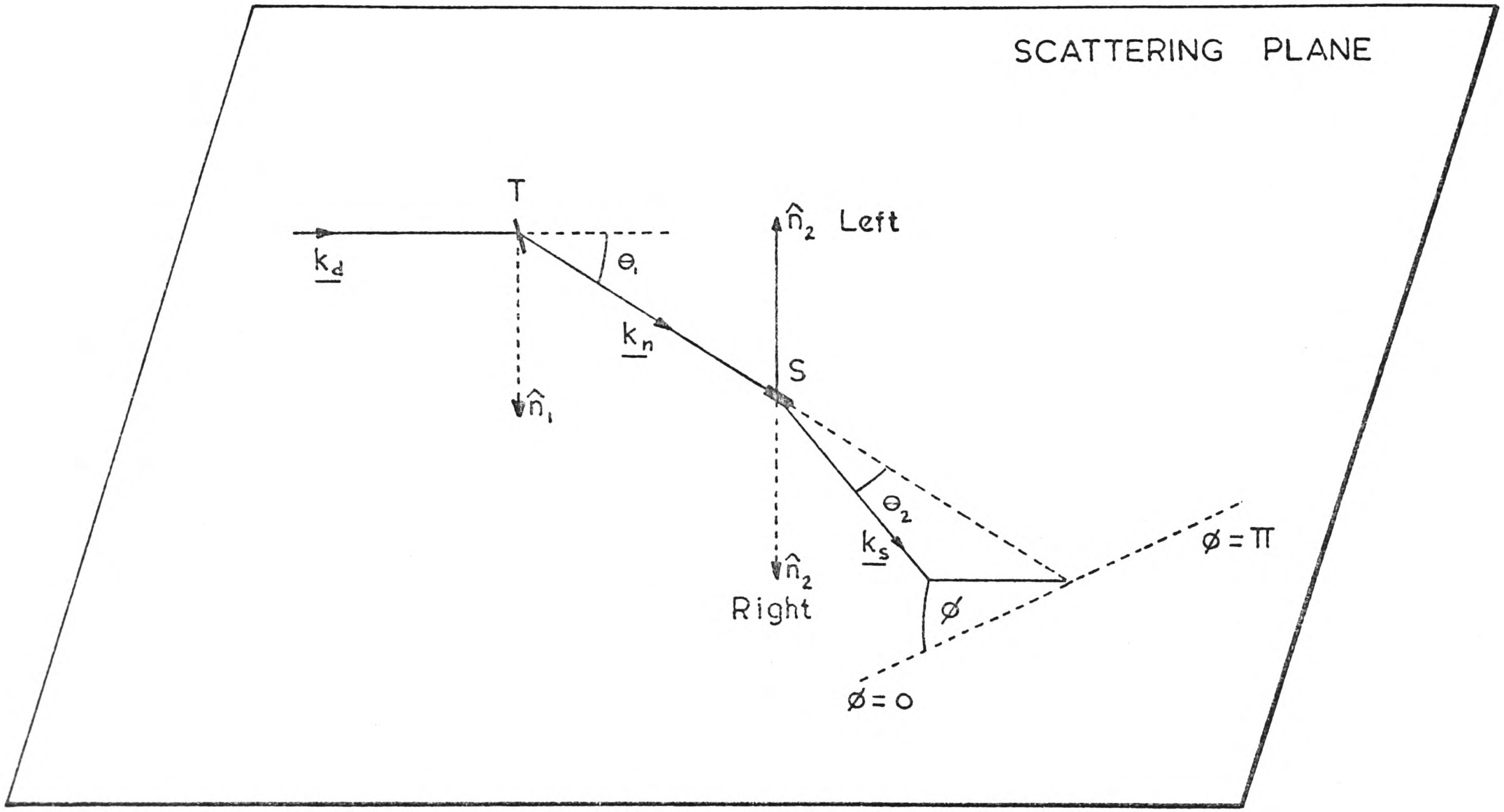

Fig. 1. The principle of fast neutron polarization experiments.

by a scatterer S through angles Θ_2, ϕ.

The polarization $\underline{P_n}$ of the neutrons emitted from the reaction in the target T is normal to the reaction plane [2] defined by the momentum vectors $\underline{k}_d$ and $\underline{k}_n$ of incident and outgoing beam. Thus, the polarization may be written as:

$$\underline{P}_n = P_n \hat{n}_1 \qquad (1.1.4)$$

where P_n is given by equation (1.1.1), and the sign convention [3] for $\hat{n}_1$ is defined by:

$$\hat{n}_1 = \frac{\underline{k}_d \times \underline{k}_n}{|\underline{k}_d \times \underline{k}_n|} \qquad (1.1.5)$$

Wolfenstein [4] pointed out that even with an unpolarized beam falling on a target with random spin orientation, a partially polarized neutron beam may result, due to the interference between the wave describing particles which are scattered without change of spin direction and the wave describing spin-shifted particles. Thus, in any scattering process involving a suitable force coupling spin and space coordinates, there is the possibility of polarization, its sign and magnitude depending on the angle of scattering.

The second reaction, or analyzing reaction, permits observation of the polarization of the neutrons. The analyzing

power of the second scattering is written:

$$\underline{P}_s = P_s(E_n, \Theta_2)\hat{n}_2 \qquad (1.1.6)$$

where:

$$\hat{n}_2 = \frac{\underline{k}_n \times \underline{k}_s}{|\underline{k}_n \times \underline{k}_s|} \qquad (1.1.7)$$

and is equal to the polarization that unpolarized neutrons of energy E_n would have after elastic scattering through Θ_2 by scatterer (or analyzer) S. Because the neutron beam from the target T is polarized, the differential cross section in the elastic scattering process has an azimuthal dependence [2]:

$$\sigma(\Theta_2, \phi) = \sigma_o(\Theta_2)\left[1 + P_n P_s(\Theta_2)\cos\phi\right] \qquad (1.1.8)$$

where $\sigma_o(\Theta_2)$ is the differential cross section for the elastic scattering process for an unpolarized neutron beam, and the azimuthal angle ϕ is the angle between $\hat{n}_1$ and $\hat{n}_2$:

$$\cos\phi = \hat{n}_1 \cdot \hat{n}_2 \qquad (1.1.9)$$

Neutron detectors are then placed at a fixed scattering angle Θ_2 to measure the intensities I_o and I_π for azimuthal angles equal to $\phi = o$ and $\phi = \pi$, respectively. These two detector positions are called R (right) and L (left) respectively. The intensities $I_o = I_R$ and $I_\pi = I_L$ are simply related to the polarization product $P_n P_s$ by the fundamental expression for the

asymmetry ϵ ,

$$\epsilon = P_n P_s = \frac{I_R - I_L}{I_R + I_L} \qquad (1.1.10)$$

It follows then that a direct measurement of either P_n or P_s is not possible. If, however, the analysing power P_s can be calculated for some nucleus, it is then possible to measure P_n for a variety of source reactions. Two different experimental techniques for fast neutron polarization measurements, using different analysers, will be discussed in the following sections.

1.2 Neutron Elastic Scattering by Light Nuclei.

Schwinger has suggested two possible methods to produce polarized neutron beams, which can alternatively be used as analysing processes. The first method [5] involves the elastic scattering of neutrons by light nuclei of spin-zero, in a resonance of the compound nucleus which involves a definite neutron orbital angular momentum $l > o$ (P,D, etc.). Since a given resonance also requires a definite total angular momentum, $J = l + \frac{1}{2}$ or $J = l - \frac{1}{2}$, it follows that the two possible neutron orientations will have different angular distributions after scattering. The current procedure is to select a light nucleus, usually He^4 or C^{12}, as a standard analyser, since in these cases the total cross sections and angular distributions for neutron elastic scattering are rather well known over a wide

range in energy so that a value of the analysing power $P_s(E_n, \Theta_2)$ can be calculated directly from the phase shifts.

However, elastic scattering from helium is the most preferred, because up to a neutron energy of 20 MeV the scattering takes place without excitation of internal degrees of freedom of the α particle and the interaction has a smooth dependence on energy [6], leading therefore, to a large polarization which depends smoothly on energy. This is not the case with C^{12} or O^{16}. At present there are several sets of n - He^4 phase-shifts [7,8,9,10,11], some of them of recent publication [12,13]. It is difficult to estimate the accuracy to which a phase-shift analysis, and therefore, the analysing power is known, due to the complex way in which the errors in the individual phases are interrelated. Davie and Galloway [14] have compared the analysing power of He^4, as a function of laboratory scattering angle, calculated from various sets of phase-shifts and found that the agreement between the analysing powers is much better at the backward scattering angles, where maximum analysing power occurs, than at the forward scattering angles where the minimum analysing power exists. For example, using the phase-shifts of Austin et al. [9] and Morgan and Walter [11], the analysing power of He^4 for 3 MeV neutrons at the forward scattering minimum differs by 20%, while only a 3% difference exists for the backward scattering maximum. Of course, the phase-shift analysis and consequent calculations of the analysing power

is constantly undergoing revision as better n-He^4, n-C^{12} and n-O^{16} experiments are performed.

According to Baumgartner [15], the polarization P resulting from scattering by spin-zero nuclei is given by:

$$P = -\frac{2\mathrm{Im}(g^*h)}{g^2 + h^2} \qquad (1.2.1)$$

where $g = (1/k)\sum_\ell P_\ell(\cos\theta)\left[(\ell+1)\sin\delta_\ell^+ e^{i\delta_\ell^+} + \ell\sin\delta_\ell^- e^{i\delta_\ell^-}\right]$

and $h = (1/k)\sum_\ell P_\ell^{(1)}\sin(\delta_\ell^+ - \delta_\ell^-)\, e^{i(\delta_\ell^+ + \delta_\ell^-)}$

The coefficients P_1 and $P_1^{(1)}$ are the Legendre and associated polynomials respectively. δ_ℓ^+ and δ_ℓ^- are the phase shifts for $J = l + ½$ and $J = l - ½$ respectively. A theoretical discussion of this method has been given by Lepore [16] and a description of different types of He^4 scattering polarimeters can be found in references 17, 18 and 19.

1.3 Mott-Schwinger Scattering.

The second method suggested by Schwinger [20] to produce polarized fast neutron beams is the basis of this thesis and for this reason it will be presented in some detail.

Because of its intrinsic magnetic moment, the neutron will interact with, and consequently be scattered by, magnetic fields. The interaction between the magnetic moment of the neutron $\underline{\mu}$ and the Coulomb field of the nucleus $\underline{B}$ is of the form $\underline{l}\cdot\underline{s}$, since $\underline{\mu}$

is associated with the neutron spin $\underline{s}$ and $\underline{B}$ with the orbital angular momentum $\underline{l}$. Schwinger pointed out that due to this spin-orbit interaction, a large polarization could arise in small angle scattering of neutrons by heavy nuclei. Mott [21] had earlier predicted a similar effect for the scattering of electrons, and so, the effect is called Mott-Schwinger scattering.

In order to produce a spin dependent scattering, the major part of this scattering should take place outside the nucleus but within the screening radius of the atomic electrons. This restricts the range of scattering angles where the effect can be observed. According to Schwinger, the unscreened Coulomb field of a nucleus is effective in the angular range:

$$\frac{1}{ka} \ll 2 \sin(\theta/2) \ll \frac{1}{kR} \qquad (1.3.1)$$

where k, a, θ and R are the neutron wave number, the screening radius of the atom, scattering angle and radius of the nucleus, respectively. Schwinger showed, by the Born approximation method, that the amplitude of such scattering is:

$$f(\theta) = f_o(\theta) + f_s(\theta)$$

where $f_o(\theta)$ is the nuclear scattering amplitude and:

$$f_s(\theta) = \tfrac{1}{2} i \underline{\sigma}.\underline{n} \cot(\theta/2)(\hbar/Mc)(Ze^2/\hbar c) \qquad (1.3.2)$$

where $\underline{\sigma}$ is the Pauli spin vector, $\underline{n}$ is the unit vector defined by:

$$\underline{k} \times \underline{k}_o = \underline{n} k^2 \sin\theta \qquad (1.3.3)$$

where $\underline{k}_o$ and $\underline{k}$ are vectors in the direction of the incident and scattered neutrons respectively. Thus, the polarization of the scattered neutrons resulting from interference between nuclear and electromagnetic scattering is:

$$P_s(\theta) = \frac{-2\mathrm{Im}f_o(\theta)\,\gamma\cot(\theta/2)}{f_o(\theta)^2 + \gamma^2\cot^2(\theta/2)} \qquad (1.3.4)$$

with $\gamma = \tfrac{1}{2}\mu_n Ze^2/Mc^2 = kZ$.

The denominator of equation (1.3.4) is the differential scattering cross section for an initially unpolarized neutron beam, from which it is clear that the Mott-Schwinger interaction is particularly important for heavy nuclei and small scattering angles. Within the angular range defined by equation (1.3.1), the specifically nuclear scattering $f_o(\theta)$ is insensitive to angle and can be replaced by the appropriate value for forward scattering $f_o(0)$, and $\mathrm{Im}f_o(0)$ is related to the total scattering cross section by:

$$\mathrm{Im}f_o(0) = \frac{k\,\sigma_T}{4\pi} \qquad (1.3.5)$$

so that the polarization of the scattered neutrons is given by:

$$P_s(\theta) = \frac{-k\,\sigma_T\,\gamma\cot(\theta/2)}{2\pi\,\sigma_o(\theta)} \qquad (1.3.6)$$

From this last equation, it is seen that the polarization resulting from small angle scattering of neutrons from heavy nuclei can be determined from the measured total cross section

and differential scattering cross section for the angle of scattering, without need for a phase shift analysis.

Using the "hard sphere" model, Schwinger showed that there is an optimum scattering angle Θ_o, for which the polarization is a maximum. This angle is:

$$\Theta_o = 2\text{arc tan}\left(\tfrac{1}{2}\mu_n \frac{Ze^2}{MRc^2}\right) \qquad (1.3.7)$$

according to his calculation, 1 Mev neutrons scattered by lead through a scattering angle of 1.5^o should have practically complete polarization and the polarization should decrease with increasing scattering angle approximately inversely as the angle. It follows then that it is possible to choose angles larger than Θ_o for which the degree of polarization is still reasonable without considerable loss in the experimental effect. Similarly, Sample [22] has carried out a detailed calculation of the perturbation of a "Hard sphere" wave fuction by this magnetic interaction and has developed an expression for the differential scattering cross section for a 100% polarized neutron beam, which is slightly different from Schwinger's. According to Sample's calculations, the differential scattering cross section for 100% polarized 3.1 Mev neutrons scattered by lead is appreciably polarization sensitive, provided the scattering angles are less than 10^o.

1.4 The Differential Scattering Cross Section at Small Angles.

As mentioned before, the study of the elastic scattering of neutrons by intermediate and heavy nuclei can provide information about the neutron-nucleus interaction. In the case of small angle ($< 10^{o}$) scattering of fast neutrons by medium and heavy nuclei, other long range components, besides the Mott-Schwinger scattering, have to be considered in the total potential of the interaction of the neutron with the nucleus. Purcell and Ramsey [23] suggested that the interaction of the induced electric dipole of the neutron, $\underline{p} = \alpha_n \underline{E}$, with the Coulomb field $\underline{E}$ of the nucleus provides another long range component which can contribute to the differential scattering cross section at small scattering angles. The magnitude of the contribution from this electric-dipole interaction depends on the so called polarizability of the neutron. Fox [24] has suggested a long range component resulting from the purely nuclear interaction, which does not decrease as rapidly with increasing distance from the nucleus as is generally assumed. This last component is not normally considered when analysing scattering data, since the possibility of estimating (quantitatively) its effect is limited by the fact that the expected magnitude is of the same order as the uncertainty in the prediction of the optical model.

Applying the Born approximation method, Walt and Fossan [25] have shown that the expression for the differential scattering cross section for an unpolarized neutron beam is:

$$\sigma(\Theta) = |f_n|^2 + |f_s|^2 + 2(\mathrm{Im}B)\gamma\cot(\Theta/2) + f_p^2 + 2(\mathrm{Re}A)f_p \qquad (1.4.1)$$

where the specific nuclear scattering is expressed in the form

$$f_n = A + B(\underline{\sigma} \cdot \underline{n}) \qquad (1.4.2)$$

f_s is the Schwinger scattering amplitude defined by equation (1.3.2), and the term $2(\mathrm{Im}B)\gamma\cot(\Theta/2)$ results from the interference of the Schwinger scattering amplitude with that from nuclear scattering. The scattering amplitude, f_p, results from the induced electric dipole moment, and it is proportional to the electric polarizability of the neutron, i.e. $f_p \propto \alpha_n$. The term $2(\mathrm{Re}A)f_p$ results from the interference of the polarizability amplitude with that from nuclear scattering. The effect of the polarizability of the neutron on the differential scattering cross section is given by the last two terms in equation (1.4.1).

For heavy elements, ReA is negative for scattering angles less than 15° and f_p is positive for small angles and decreases with increasing angle. Thus, these two terms produce a decrease in the differential scattering cross section at small angles when $|2(\mathrm{Re}A)f_p| > f_p^2$ and produce an increase when $|2(\mathrm{Re}A)f_p| < f_p^2$ depending on the value of α_n. The contribution of these two terms to the differential cross section for scattering of 570 kev

neutrons by uranium, for different values of α_n, is illustrated in figure 2a. Figure 2b shows the experimental differential cross sections and calculated values after subtracting the Schwinger scattering term. From this, they concluded that the contribution of the neutron polarizability to the differential scattering cross section at small scattering angles is very small at a value of α_n close to its experimentally determined [26] upper limit. The differential scattering cross section at scattering angles less than 18° did not show evidence for any anomalous long range neutron-nucleus interaction as reported by other experimenters [27, 28, 29].

Aleksandrov [27] carried out an experiment to investigate the possible contribution of the polarizability of the neutron to the differential scattering cross section of 2 Mev neutrons by Pu, U, Sn, Pb, Bi, and Cu in the angular interval from 4° to 25°. He observed a sharp increase in the differential scattering cross section for Pu and U for scattering angles less than 11°, although for the other elements the possible increase was within the limits of the experimental error. He attributed this increase in differential scattering cross section to the polarizability of the neutron and performed some calculations based on the "hard sphere" model from which he obtained a value of $\alpha_n = (8 \pm 3.5) \times 10^{-41}$ cms^3 ; but the more accurate calculation by Fossan and Walt [25] shows that this interpretation of Aleksandrov's results would require $\alpha_n \geq 5 \times 10^{-40}$ cm^3. Both of these values are considerably larger than the estimate

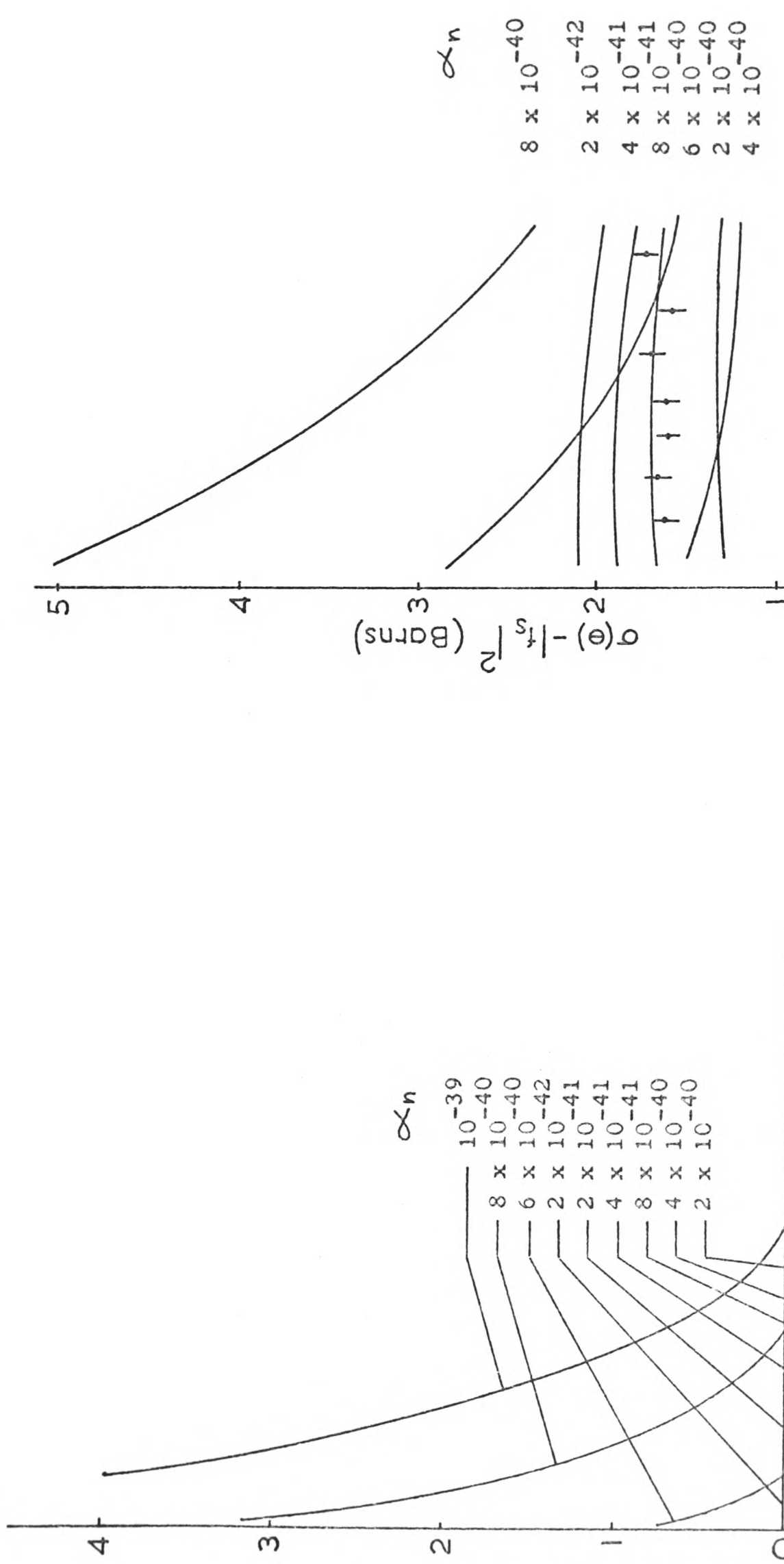

Fig. 2b. Theoretical and experimental differential cross sections.

Fig. 2a. The terms $2(\mathrm{Re}A)f_p + f_p^2$ as calculated for various values of $\alpha_n^{25)}$.

$\alpha_n \approx 2 \times 10^{-42}$ cm^3 obtained from elementary particle theory [30].

As an attempt to establish the possible energy dependence of the mentioned effect, Aleksandrov et al [28] made an experiment to investigate the differential cross section for elastic scattering of 0.8 and 2.8 Mev neutrons by Th, U and Cu in the angular interval from 3° to 25°. Their measurements for 0.8 Mev neutrons agree with Schwinger theory within the limit of error. For 2.8 Mev neutrons, they observed an increase in the differential scattering cross section for U and Th for scattering angles less than 10°.

Elwyn et al [29] undertook an experiment to investigate the polarization and differential scattering cross section of 830 kev neutrons scattered by uranium through angles of 1.65°, 2.35°, 4.6° and 10°. The resulting angular distribution exhibited an anomalous increase with decreasing angle. In order to interpret this effect, they carried out some calculations showing the dependence of the differential scattering cross section and polarization on the neutron polarizability for 830 kev neutrons scattered by uranium in the angular interval mentioned. They considered a potential given by:

$$V(r) = V_m(r) + V_s(r) + V_p(r) \qquad (1.4.3)$$

which accounts for the potential describing the Schwinger scattering $V_s(r)$; the potential describing the interaction between the induced electric dipole and the Coulomb field of

the nucleus $V_p(r)$, and the nuclear interaction represented by an optical model potential $V_m(r)$. Figure 3 shows the differential cross section as calculated for the various potentials described in equation (1.4.3). From this they concluded that the increase in differential scattering cross section due to the polarizability of the neutron is quite small. Also, they suggested that the anomaly in uranium, if it exists, could be attributed to another long range component of the neutron-nucleus interaction, and that it might be associated with the fission threshold, since the fission threshold of U^{238} occurs at a neutron energy of approximately 600 kev and their measurements were made at a neutron energy above this threshold. On this basis, they suggested that Walt and Fossan [25] did not observe any anomaly because their measurements were made at a neutron energy below the fission threshold.

In order to investigate this fission effect, Adam et al [31] measured the differential cross section for elastic scattering of 14.7 Mev neutrons scattered by uranium in the angular interval from 4° to 18°. The measured and calculated differential cross sections were in excellent agreement and they concluded that for neutron energies near 14 Mev and for small scattering angles there is no anomalous scattering. They applied the optical model with the contribution of inelastic scattering to describe, satisfactorily, the differential scattering cross section. Gorlov et al [32] studied the small angle scattering of 4 Mev neutrons and reported the results to be consistent with Schwinger

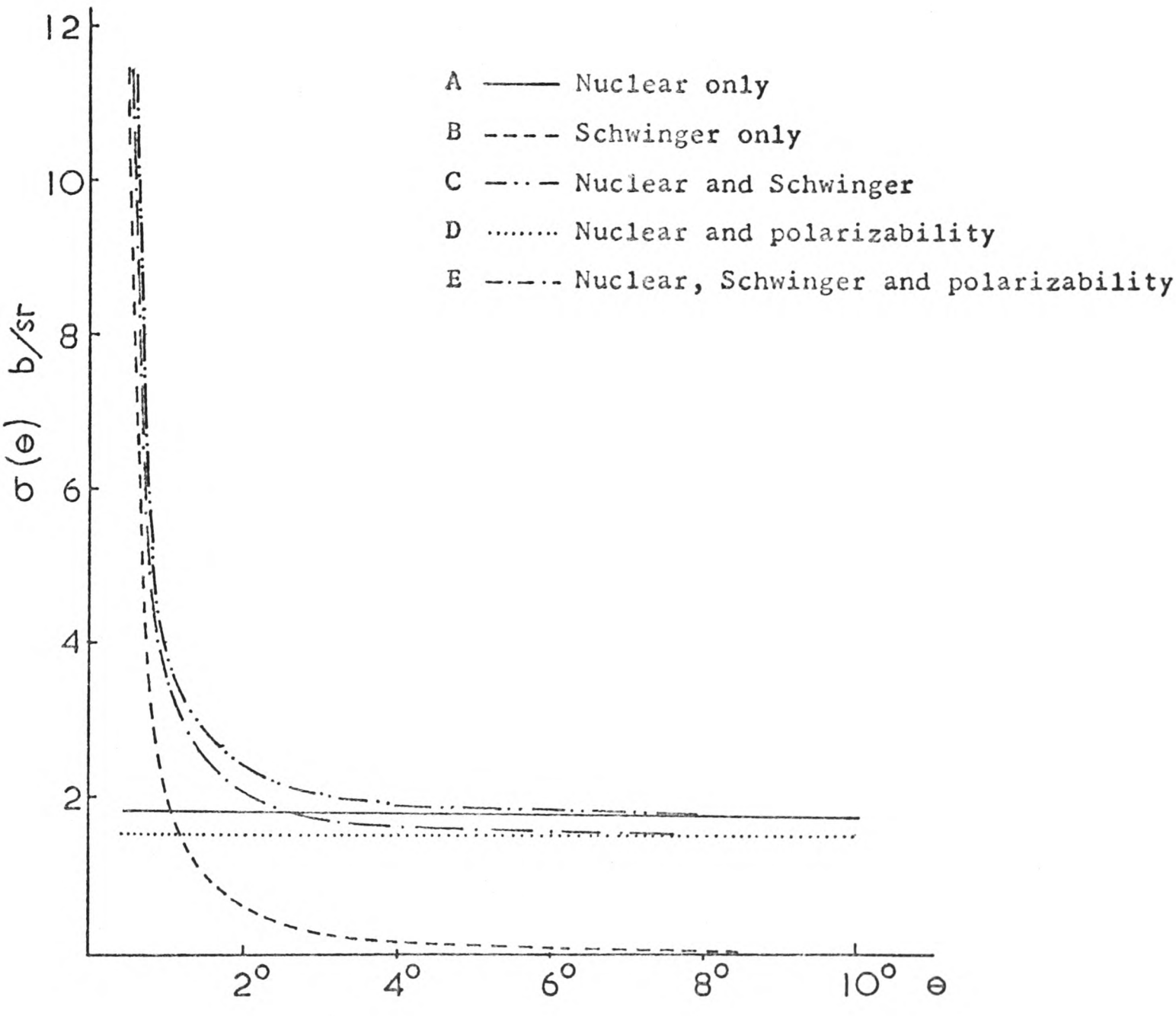

Fig. 3. Calculated differential cross section for the various terms in the neutron-nucleus interaction potential[29].

calculation.

Kuchnir et al [33] have investigated the differential cross section and polarization of neutrons elastically scattered by U, Th, Pb, Au, W and Cd for scattering angles between 1.75° and 15° for neutron energies between 0.6 and 1.6 Mev. The measured angular distributions did not show any anomaly and were consistent with the calculations based on the neutron-nucleus interaction which takes into account the Schwinger scattering, the polarizability of the neutron and the nuclear interaction represented by an optical model potential. Thus they concluded that the polarizability interaction can be neglected so that the electromagnetic interaction is assumed to be entirely given by the Schwinger term.

Anikin and Kotukhov [34] reported differential scattering cross sections in the angular interval from 2.5° to 25° for Cu, Pb and U for neutrons of mean energies 0.575, 1.33, 2.45, 4.5, 5.6 and 8.4 Mev. They suggested that the agreement between the calculated and measured differential scattering cross sections can be improved by correcting the optical model nuclear potential, corresponding to $\alpha_n \approx 2 \times 10^{-40}$ cm^3. This allowed normalization of their calculated differential cross section by up to 15% to fit the experimental points.

A recent report [35] on the question of a contribution to the differential scattering cross section due to the polarizability of the neutron concerned the scattering of 3 Mev polarized neutrons through angles from 1.6° to 7,7° by U, Pb and Cu. In this work, Galloway and Maayouf [35] found that the calculated and measured differential scattering cross sections are in agreement with Schwinger theory and they did not observe a significant effect attributable to the polarizability of the neutron.

Very recently, Martin et al [36] used the associated particle technique to investigate the differential scattering cross section for 4.3 Mev neutrons elastically scattered from U, Bi and Pb through angles of 5°, 10° and 15°. The measured and calculated angular distribution for uranium are in very good agreement with Schwinger theory, but the theoretical fits to the data were not in such good agreement for lead and mainly for bismuth, although in the latter case there were large errors associated with the data points. They suggested that the indication of an enhancement in the case of bismuth at smaller angles might be associated with the diffraction effects due to the presence of alpha particle clusters in the surface of the heavy nucleus. However, they concluded that for 4.3 Mev neutrons the alpha particle cluster model, originally described by Vogt [37], predicts a deviation from the optical model calculations which is too small to detect.

In view of this inconsistency, some authors have reinterpreted with a different model the results obtained by other authors and found that the anomalies are due to the models used for interpreting the experimental data. Thus the anomaly reported by Dukarevich et al [38] for U at 14.2 Mev disappeared when reinterpreted by Anikin et al [39] and for Th when reinterpreted by Palla [40].

Gorlov et al [32] pointed out that the main difficulty in the interpretation of the experimental data on small angle scattering of Mev neutrons by heavy nuclei is the uncertainty in the magnitude of the nuclear cross section predicted by the theory, as there exists an uncertainty of about 10% - 20% in the value of the nuclear cross section as predicted [41] by the optical model.

In order to assess the degree of agreement between experiment and theory, Gorlov et al [32] introduced the quantity

$$\Delta = \sigma(\theta) - \sigma_s(\theta) - \sigma_m(\theta) \qquad (1.4.4)$$

where $\sigma_m(\theta)$ is the cross section described by the nuclear model employed. They analysed the results of various authors [25,28,37,38] who reported an anomalous increase in the differential scattering cross section, and found that in neutron scattering by nuclei of medium atomic weight the neutron scattering cross section is described satisfactorily by different models [28,38] of nuclear scattering as well as by the optical model of the nucleus, in

which case $\Delta = 0$. In the case of heavy nuclei they found that applying different models in the interpretation of the data of one particular experiment can produce conclusions that differ in the sign of the effect, that is $\Delta = 0$, $\Delta > 0$ and $\Delta < 0$ may be found. On this basis, they concluded that the mentioned apparent inconsistency in the results is associated with the model used to interpret the data.

Thus it is possible to conclude that the general systematic trend for heavy nuclei provides evidence that there is no anomaly in the small angle differential scattering cross section at neutron energies with which we are concerned.

1.5 Fast Neutron Polarization Experiments based on Mott-Schwinger Scattering.

The first attempt to measure the degree of polarization of a fast neutron beam by Mott-Schwinger scattering was made by Longley et al [42]. They tried to measure the polarization of neutrons from $H^2(d,n)He^3$ by scattering by Pb, but this experiment did not lead to conclusive results. An attempt by Sample et al [43] failed because of the difficulty in collimating fast neutrons sufficiently well to investigate scattering at very small angles.

The first experiment demonstrating the Mott-Schwinger effect was made by Voss and Wilson [44], who used a polarized neutron

beam of 100 Mev energy from the reaction $Be^9(p,n)B^9$ and a uranium sample as analyser with scattering angles below 1^o. They discovered that the sign of the polarization agrees with the prediction of Fermi that a nuclear spin-orbit coupling responsible for the shell model is also responsible for high energy polarization. Thus the sign of the polarization in neutron-nucleus scattering is indeed in the opposite direction to that of Coulomb field scattering, for neutrons of a few Mev energy with which we are concerned. This was confirmed by Hillman et al [45] who detected again the effect using a technique based on the Larmour precession of the polarization vector through 90^o about the neutron beam axis in the magnetic field of a solenoid inserted between the beryllium target and the uranium analysing scatterer. The scattering angle in this experiment was $1/3^o$.

Elwyn et al [29] have measured both the polarization and the differential cross section of 830 kev neutrons emitted at 51^o from $Li^7(p,n)Be^7$. Although they reported an anomalous increase in the differential scattering cross section, they did not observe an additional polarization effect beyond what was expected from the Mott-Schwinger interaction.

Kuchnir et al [33] have investigated the differential cross sections and polarization of neutrons from the reaction $Li^7(p,n)Be^7$ for neutron energies ranging from 0.6 to 1.6 Mev and scattered through angles from 1.75^o to 15^o from samples of U, Th, Pb, Au, W and Cd. They also reported that the general systematic trend

for all nuclei provides evidence that there is no anomaly in measured small angle differential cross section and polarization at energies below 1.6 Mev.

Gorlov et al [32] obtained both the differential cross section and the polarization of 4 Mev neutrons scattered through angles of 2°, 4° and 6° from samples of Cu, In, Sn, Pb, Bi and U. As mentioned before, the differential cross section values were found to be accurately described assuming only nuclear and Schwinger scattering. These values were used to determine the analysing power of the different nuclei, the differential cross sections for elastic scattering of unpolarized neutrons and elastic forward nuclear scattering. Similarly, these values were used to determine the polarization of the neutrons from the $H^2(d,n)He^3$ reaction averaged over all the angles and elements. They confirmed Schwinger's assumption that the measured polarization of the neutrons should be independent of both the measurement angle and the scattering elements. The reported polarization value for neutrons emitted at 37° Lab. for a mean deuteron energy of 1.2 Mev is in good agreement with the results obtained by other methods. Here again, they concluded that within the accuracy limits of the experiment, quantitative and qualitative agreement was obtained between the prediction of Schwinger's theory and the measured results.

Recently, Galloway and Maayouf [46] have developed a polarimeter for neutrons of a few Mev energy employing elastic scattering by lead through an angle of about 2°. The measured differential cross sections are as predicted by Schwinger theory. The polarization value for neutrons emitted at 46° from $H^2(d,n)He^3$ is in agreement with the values obtained using elastic scattering by He^4. Although they carried out this experiment to test the agreement between observed behaviour and Schwinger theory, they suggested that a fast neutron Schwinger polarimeter with an adequate geometry could be comparable in efficiency of data collection with the commonly used He^4 scattering polarimeter.

Elwyn et al [47] carried out measurements of 1 Mev neutrons scattered from nuclei with $Z \approx 40$ through angles of 24°, 56°, 86°, 118° and 150°. They pointed out that Schwinger scattering may contribute to the polarization at a scattering angle as large as 24°. This is supported by the calculations made by Monahan and Elwyn [48] based on a more generalised Born approximation which takes into account both the nuclear and the electromagnetic interactions. Redmond [49] and Hogan and Seyler [50] have also found that the polarization can be influenced by Schwinger scattering at angles much larger than had been previously considered.

The different calculations, carried out so far, of the polarization resulting from Schwinger scattering lead to different conclusions regarding both the amplitude of the effect and the

range of angles where it extends. However, for scattering angles less than 10^{o}, the contribution of the Schwinger scattering to the polarization has been extensively demonstrated by several experimenters to be in excellent agreement with its theoretical description.

1.6 Polarization of Neutrons Emitted from the $H^2(d,n)He^3$ Reaction.

The different experimental techniques used to measure the degree of polarization of a fast neutron beam can be assessed by measuring, under the same conditions, the polarization of neutrons emitted from a convenient source of polarized neutrons. The Schwinger fast neutron polarimeter object of this thesis is intended to be tested with the $H^2(d,n)He^3$ reaction at deuteron energies below 500 kev.

Historically, the polarization of fast neutrons emitted from the $H^2(d,n)He^3$ reaction was first predicted by Wolfenstein [1] and measured by Huber and Baumgartner [15] and by Ricamo [51]. Since then many measurements of D - D neutron polarization have been made, as may be seen in a review by Galloway [52]. A brief review of results in the deuteron energy region below 1 Mev is given in this section.

Meier et al [53], using C^{12} as analyser, measured the angular dependence of the polarization of the neutrons emitted from a thin D_2O target at a deuteron energy of 600 kev. These

authors reported maximum polarization values at angles of 58° and 122° in the centre of mass system. Similarly, McCormac et al [54] reported maximum neutron polarization at an angle of 53° in the centre of mass system. They used a thick target at deuteron energies between 500 and 700 kev.

Levintov et al [55] measured the energy dependence of the polarization of neutrons emitted at 40° lab. from thick and thin targets at deuteron energies from 0.6 to 1.8 Mev. They employed helium as analyser and observed the recoil alpha particles with directional proportional counters. The reported polarization values for thick and thin targets did not show appreciable difference.

Pasma [56] developed a helium gas scintillation counter to be used both as polarization analyser and detector of the helium recoil nuclei, so that only the scattered neutrons in coincidence with the helium recoil are recorded. With this technique Pasma measured the energy dependence of the polarization of neutrons at 47° lab. and found that the polarization increases from 6% at 200 kev to 9.5% at 500 kev deuteron bombarding energy.

In an attempt to increase the precision of the measurement of the neutron polarization at low incident deuteron energies, Kane [57] measured the polarization of neutrons emitted at 45° and 53° in the laboratory system at an average deuteron energy of 93 kev. His value for the polarization was the same, within the experimental error, as those of the experimenters [53,54,55,56]

just mentioned. From this comparison he suggested that the polarization is independent of the deuteron energy between 93 kev and 700 kev.

Ot-Stavnov [58] investigated the polarization of the neutrons emitted from a heavy ice target at angle of 150° (lab) at deuteron energies from 0.4 to 1 Mev. This author employed a helium gas detector. He found that the polarization increases in absolute magnitude with increasing deuteron energy.

Boersma et al [59] carried out an experiment to investigate the angular and energy dependence of the polarization of the neutrons emitted from a 50 kev thick target. The experimental set-up used helium gas as analyser and included α - n coincidence requirement and gamma - neutron discrimination. They measured the polarization of the neutrons for a deuteron energy of 375 kev at ten different reaction angles between 0° and 80° and for deuteron energies of 275 kev and 450 kev at 50° (lab). The reported values differ by nearly a factor of two in magnitude from the measurements of Pasma [56].

Rogers and Bond [60] reported polarization measurements on the neutrons emitted at an angle of 45° (lab) at average deuteron energies of 99 kev, 81.5 kev and 67.5 kev, which strongly support those made by Kane [57]. Hansgen et al [61] measured the polarization at 50° (lab) for eight different deuteron energies from 57.3 to 116.8 kev with a thick target and found that the polarization

exhibits a strong energy variation with a maximum polarization at an average deuteron energy of 80 kev. In these two experiments C^{12} was used for analysing the emitted neutrons.

Polarization measurements on neutrons scattered through 46.5° by helium were reported by Mulder [62], who used a heavy ice target with a thickness of 50 kev at a mean deuteron energy of 350 kev. This measurement is in very good agreement with the results of Boersma [59].

The polarization of neutrons emitted at 47° lab. from a thick heavy ice target at deuteron incident energies between 60 and 380 kev in 20 kev intervals and an angular distribution of polarization at 340 kev were measured by Behof et al [63] with a helium polarimeter. Their results indicated that the polarization is a slowly varying function of the deuteron energy over most of the range below 400 kev.

Prade and Csikai [64] measured the polarization of neutrons emitted at 50° lab. from a thick TiD target at five deuteron energies between 92 and 173 kev. By using a cloud chamber and He^4 as analyser, they measured the polarization at average deuteron energies of 92 and 173 kev. By using the associated particle method and C^{12} as analyser, they measured the polarization at average deuteron energies of 109, 137 and 169 kev. They found that the polarization has a sudden decrease in this deuteron energy region, which supports the results of Hansgen et al [61].

Roding and Scholermann [65] measured the angular distribution of the polarization of neutrons emitted from a TiD target at five deuteron energies from 0.5 to 2.0 Mev. The experimental set-up employed a high pressure helium-xenon gas scintillator and a time of flight system to detect the scattered neutrons. They observed a polarization maximum at an angle of 50° c.m.s. at a deuteron energy of 500 kev.

Davie and Galloway [14] developed a fast neutron polarimeter based on neutron scattering from a high pressure helium gas scintillator, with which a preliminary measurement of polarization of neutrons emitted at 46° lab. from a thick TiD target at an incident deuteron energy of 390 kev was found to be in good agreement with those measurements of Boersma et al [59] and Mulder [62]. These same authors [66] have measured the energy dependence of the polarization of neutrons emitted at a laboratory reaction angle of 46° from a thin TiD target for deuteron energies ranging from 300 kev to 900 kev. Their results have a marked disagreement with those of Pasma [56], Boersma et al [59] and Roding and Scholermann [65].

Employing a liquid helium scintillator and neutron time of flight technique, Smith and Thornton [67] measured the angular distribution of the polarization of neutrons for several deuteron energies from 0.87 to 5.0 Mev. Their measurement at a laboratory angle of about 45° at deuteron energy below 1 Mev was found in good agreement with those of Levintov et al [55] and Davie and

Galloway [66].

Only three measurements of the $H^2(d,n)He^3$ neutron polarization using the Mott-Schwinger scattering have been reported. The first of these [32] concerned neutrons emitted at 37° lab. at 1.2 Mev deuteron energy, which, according to Walter[68], differs by about two standard deviations from the trend of helium scattering data. The second [46] concerned neutrons emitted at 46° lab. at 575 kev deuteron energy and agreed with the trend of the helium scattering data available, although the statistical accuracy in this experiment was poorer than in the experiment of Gorlov et al [32]. The third experiment based on Mott-Schwinger scattering was carried out by Maayouf and Galloway [69] in order to compare the performance of this polarimeter with the commonly used helium polarimeter. They found that the polarization values obtained with both systems are in very good agreement. These measurements were carried out for neutrons emitted at 47° from a thick TiD target for a mean deuteron energy of 330 kev.

Very recently Alsoraya et al [70] have measured the energy dependence of the polarization of neutrons emitted at 45° lab. from a thin TiD target in the deuteron energy range from 50 to 500 kev. They also have measured the angular dependence of the polarization for mean deuteron energies of 290 and 460 kev at seven different reaction angles between 25° and 90°. Their experimental set-up consisted of a helium gas scintillator

operating at a pressure of 70 atmospheres and a pair of liquid scintillators with pulse shape discrimination against gamma - rays. They have found that their measurements below 200 kev agree reasonably well with the values predicted by the theory of Boersma [71].

Also in a very recent experiment based on a helium filled proportional chamber, Sikkema and Steendam [72] have measured the energy dependence of the polarization of neutrons emitted at a laboratory reaction angle of about 48° from a TiD target with a thickness of about 70 kev in the deuteron energy range from 50 to 700 kev. Their results indicate a monotonic increase of the polarization value with increasing deuteron energy in the range mentioned. The results of these two last experiments are in remarkably good agreement.

From this review it is clear that although many experiments have been carried out, there still is a considerable disagreement between published measurements of neutron polarization for deuteron energies below 1 Mev. The specific purpose of the present work is concerned with polarization measurements of neutrons emitted from the $H^2(d,n)He^3$ reaction at a laboratory angle of about 45° in the deuteron energy range from 100 kev to 500 kev. Figure 4 shows a compilation of ten different experiments, described in the previous review, so far reported in this deuteron energy range and for the raction angle mentioned.

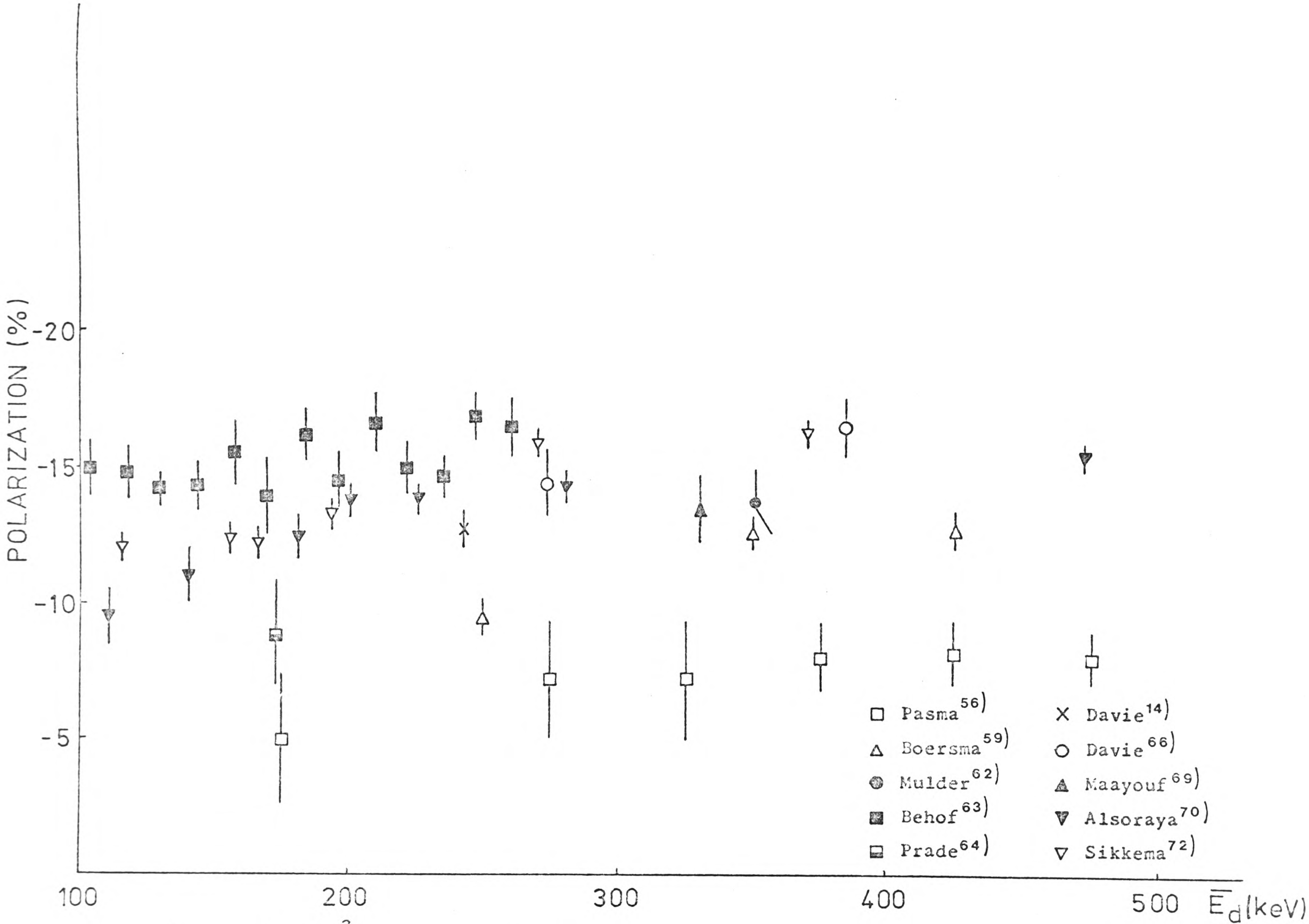

Fig.4. $D(d,n)He^3$ neutron polarization measurements at a laboratory reaction angle of about 45°.

From fig. 4, one finds that excluding the data of Pasma [56], the point of Prade and Csikai [64] and one point of Boersma et al [59], the remaining data follow a trend which supports, at deuteron energy below 200 kev, the theory of Boersma. A reason to exclude the low values reported by Pasma [56] is that they were obtained in an experiment without any gamma ray discrimination technique. The point of Prade and Csikai [64] was obtained using C^{12} as analyser, for which the analysing power is less well established and is much more energy dependent; also, this technique does not permit the detection in coincidence of both the recoil nucleus and the scattered neutron, losing therefore, the advantage of discrimination against background neutrons. The low value reported by Boersma et al at 275 kev belongs to a series of measurements obtained with a helium polarimeter which included α - n coincidence requirement and gamma ray discrimination, but the helium recoil spectra were not recorded and therefore correction for neutron background was not made.

1.7 Thesis Objective.

The most commonly used technique to investigate the degree of polarization of a fast neutron beam has been the He^4 scattering polarimeter. This system is based on the asymmetry of the nuclear scattering cross section introduced by the nucleus spin-orbital angular momentum interaction between the neutron and the nucleus, in which case the analysing power of the scattering nucleus is calculated from a complicated phase shift analysis of the elastic

scattering differential cross section data. The asymmetry may be affected by neutron background, which in turn may introduce a systematic error in the polarization value, since correction for this effect can depend on the judgement of the experimenter.

On the other hand, working with the Mott-Schwinger fast neutron polarimeter, the polarization is determined from the equation [20]:

$$P_n(\theta') = \frac{\sigma(\theta,0) - \sigma(\theta,\pi)}{2\,\sigma_0(\theta)\,P_s(\theta)} \qquad (1.7.1)$$

where the product $\sigma_0(\theta)P_s(\theta)$ is defined by equation (1.3.6):

$$\sigma_0(\theta)\,P_s(\theta) = -\,k\,\sigma_T\,\gamma\,\cot(\theta/2)/2\pi$$

Therefore, the determination of polarization does not depend on a particular nuclear model but on the experimental total cross section and differential cross section for the angle of scattering. This simplicity of calculating the analysing power $P_s(\theta)$ is the main advantage of the Mott-Schwinger polarimeter.

Most of the Mott-Schwinger fast neutron polarimeters have been designed to investigate the Mott-Schwinger theory. For this, they require very fine collimation of the neutron beam incident on the analysing scatterer and very small spread in scattering angles accepted by the neutron detectors which have to be positioned very close to the neutron beam with the consequent problem of severe background. For these reasons the efficiency of data collection is very low.

The objective of this thesis is to design and construct a polarimeter for neutrons of a few Mev energy based on small angle Mott-Schwinger scattering, which has an efficiency of data collection comparable to that attainable in a conventional He^4 scattering polarimeter based on a gas scintillator. This Mott-Schwinger scattering polarimeter will be assessed by measuring the polarization of fast neutrons emitted from the reaction $H^2(d,n)He^3$ at a laboratory reaction angle of about 45^o at several deuteron energies below 500 kev and the results obtained in these measurements will be compared with the corresponding values obtained with a typical He^4 scattering polarimeter.

CHAPTER 2.

CHAPTER 2.

THE DESIGN AND CONSTRUCTION OF A SMALL ANGLE MOTT - SCHWINGER SCATTERING POLARIMETER.

A typical small angle Mott-Schwinger scattering polarimeter is shown diagramatically in figure 5. Briefly, the neutrons emitted from the accelerator target after collimation are incident on a heavy nuclei scatterer, neutrons scattered to 'right' and 'left' in the reaction plane are detected by a pair of neutron detectors symmetrically placed relative to the neutron beam axis. A third neutron detector, hereafter called the collimated neutron monitor, is placed in line with the collimated neutron beam axis and it is used to monitor the neutron flux passing through the collimator and to determine the total cross section for the scatterer employed.

The present chapter describes the calculations carried out in order to obtain an optimum geometry for a more efficient small angle Mott-Schwinger scattering polarimeter. A comparison of the efficiency of the calculated geometry with that attainable in a conventional He^4 polarimeter and in a recent Mott-Schwinger fast neutron polarimeter is presented. Also, a detailed description of the construction of the present experimental set-up is given.

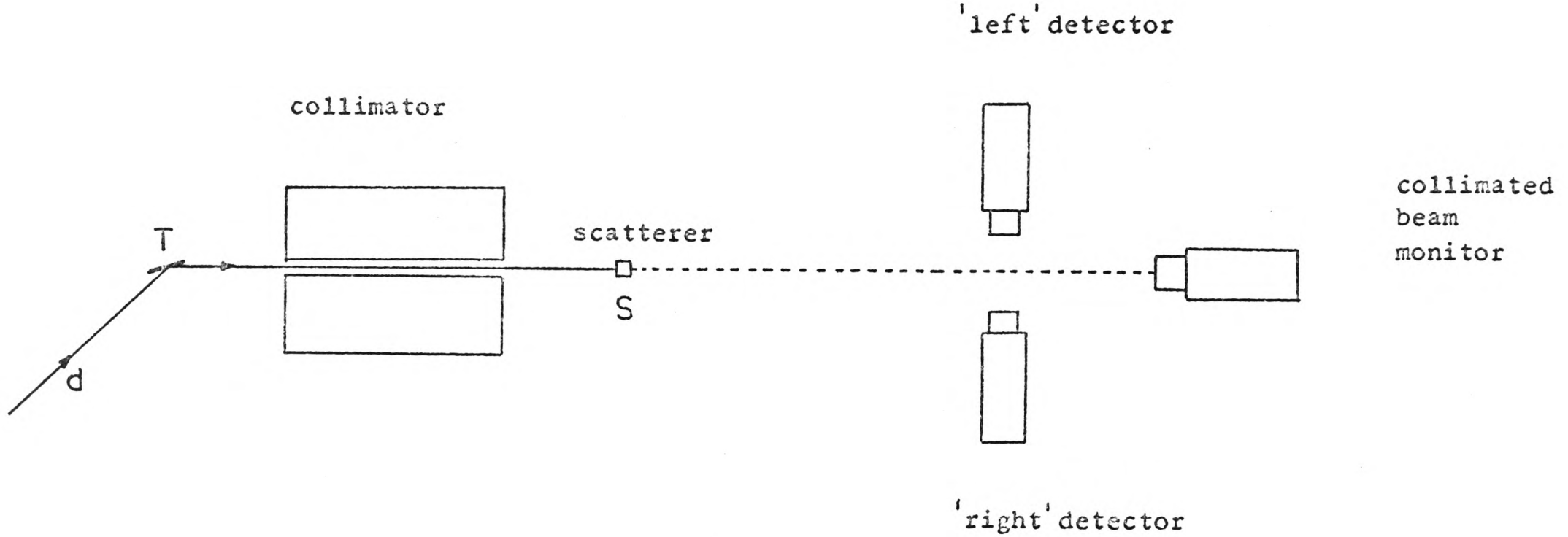

Fig. 5. Typical small angle Mott - Schwinger scattering fast neutron polarimeter.

2.1 Definition of Parameters.

The different parameters involved in the efficiency of polarization determination, in an ideal system with no background, are:

Ω_1: solid angle subtended by the scatterer at the neutron source

Ω_2: solid angle subtended by a side neutron detector at the scatterer

t : thickness of the scatterer

n : the number of scattering nuclei per unit volume

$\sigma_o(\theta)$: the differential scattering cross section for the angle of scattering

$P_s^2(\theta)$: square of the analysing power for the scattering process

In order to compare the efficiency of different experimental arrangements, a figure of merit, f, may be defined as:

$$f = \Omega_1 \Omega_2 t n \sigma_o(\theta) P_s^2(\theta) \qquad (2.1.1)$$

This figure of merit has been employed by Galloway and Maayouf [46] to evaluate the efficiency of both a Mott-Schwinger fast neutron polarimeter and a He^4 scattering polarimeter based on a gas scintillator. They found that a particular Mott-Schwinger fast neutron polarimeter should take 120 times as long to obtain a polarization value with the same statistical accuracy as the particular He^4 scattering polarimeter. This sort of performance is typical of small angle Mott-Schwinger scattering systems employed up to now.

The central idea of the present experiment is to reduce the time of data collection of a Mott-Schwinger fast neutron polarimeter by selecting an adequate geometry with larger spread in scattering angles and collecting in one measurement the polarization information in an angular interval determined by suitable values of analysing power and figure of merit.

2.2 Evaluation of Parameters.

Rough calculations of angular spread suggested the following dimensions:

1) a distance of about 65 cm between target and scatterer (in the experiment this distance was 77 cm).
2) a collimator 46 cm long with a 1 cm side square axial hole.
3) a distance of 60 cm between scatterer and side detectors.

These dimensions form the basis of a workable system and this was investigated in more detail. The geometrical factors involved in the following calculations are referred to figure 6. The target is assumed a point source of neutrons and the collimator has been omitted for clarity.

2.2.1 Solid Angle Subtended by Scatterer at Neutron Source.

By definition, the differential solid angle subtended by an element of surface area ds at a point O outside the surface M is given by:

$$d\Omega = \frac{\underline{r} \cdot \underline{ds}}{r^3} \qquad (2.2.1)$$

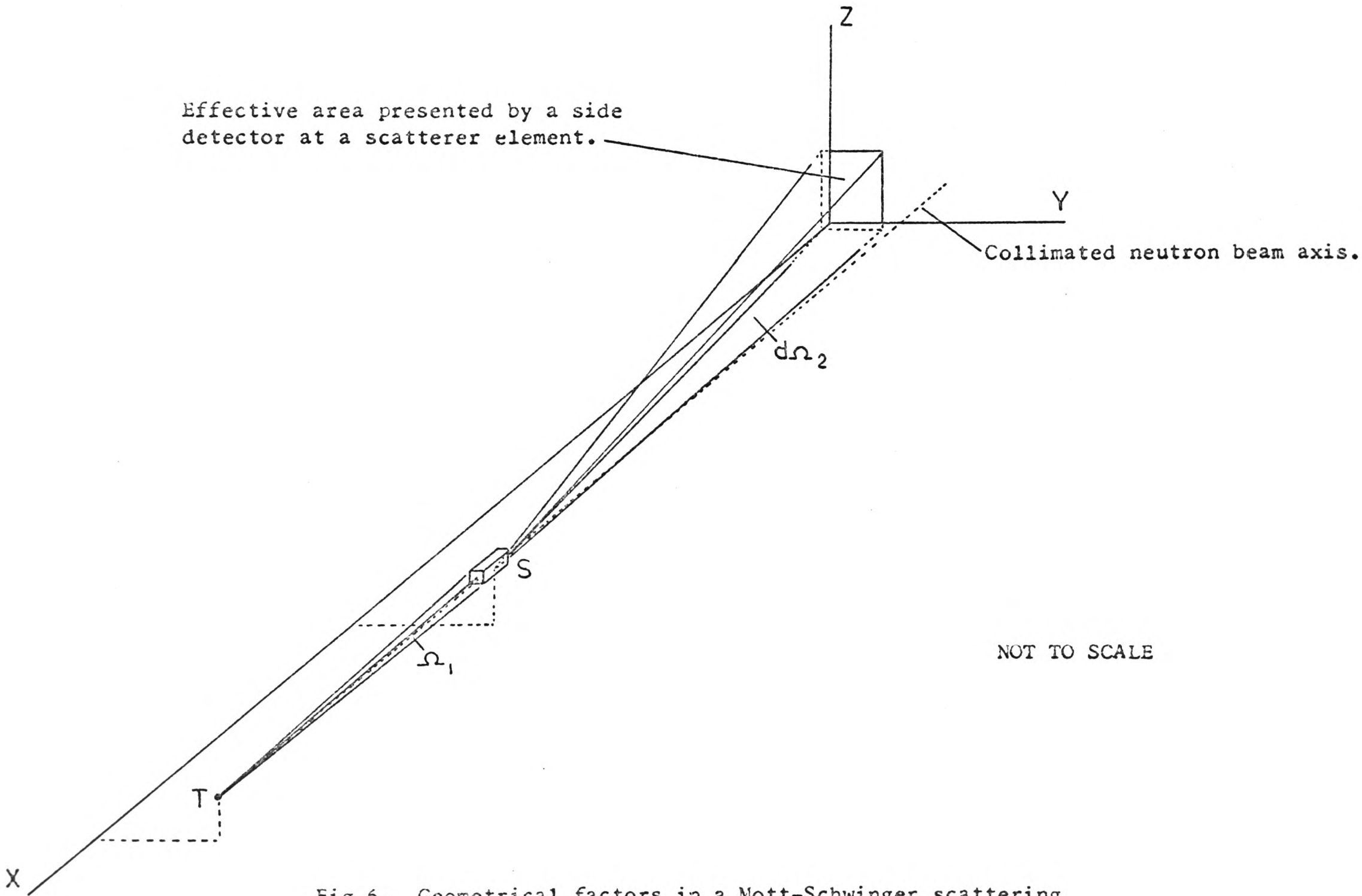

NOT TO SCALE

Fig.6. Geometrical factors in a Mott-Schwinger scattering polarimeter.

where $\underline{r}$ is the vector joining the point O with the element of surface area ds and $\underline{ds}$ is the vector normal to the element of surface area ds. The total solid angle subtended by the surface M at the point O is:

$$\Omega = \int_M \frac{\underline{r} \cdot \underline{ds}}{r^3} \qquad (2.2.2)$$

this equation in scalar form is:

$$\Omega = \iint_M \frac{(a-x)\,dy\,dz + (b-y)\,dx\,dz + (c-z)\,dx\,dy}{\left[(a-x)^2 + (b-y)^2 + (c-z)^2\right]^{3/2}} \qquad (2.2.3)$$

where (a,b,c) and (x,y,z) are the Cartesian coordinates of O and ds respectively.

Applying the equation (2.2.2) it is possible to show that the exact expression for the solid angle subtended by a rectangular pyramid of half angles α and β is:

$$\Omega = 2\pi - 4\left[\arcsin\left(\frac{\cos\alpha\,\tan\beta}{\sqrt{\tan^2\alpha + \tan^2\beta}}\right) + \arcsin\left(\frac{\cos\beta\,\tan\alpha}{\sqrt{\tan^2\alpha + \tan^2\beta}}\right)\right] \qquad (2.2.4)$$

and for the special case of a square pyramid $\alpha = \beta$ and the expression for solid angle is reduced to:

$$\Omega = 2\pi - 8\arcsin\left(\frac{\cos\alpha}{\sqrt{2}}\right) \qquad (2.2.5)$$

In order to maximise the solid angle for acceptance of neutrons from the target, without enlarging the dimension of the collimated neutron beam, a square cross section aperture was chosen for the present experimental arrangement. The solid angle subtended by the scatterer at the target defined by the far end of the collimator is given by equation (2.2.5). A collimator 46 cm long with a 1 cm

side square axial hole was found suitable to meet the previous requirement, and at the same time, permits the side neutron detectors to be positioned as close to the collimated beam axis as to accept a minimum scattering angle of about 1.8°, measured between the collimated neutron beam axis and the line joining the geometrical centre of the scatterer with the nearest point of the side neutron detector to the collimated neutron beam.

2.2.2 Scatterer requirements.

As mentioned in section 1.7, the determination of polarization in a Mott-Schwinger fast neutron polarimeter depends on the experimental total cross section and differential elastic cross section for the angle of scattering, therefore, the scatterer used in the present experiment should meet the requirements of transmission total cross section and differential elastic scattering cross section measurements.

The heavy element selected as scatterer was lead. The scatterer, machined out of a piece of pure lead, has a square cross section dictated by the collimator aperture. The side of the scatterer was chosen a little larger than the dimension of the collimated neutron beam at the scatterer position in order to reduce the correction required for inscattering into the collimated beam monitor. The thickness of the scatterer along the beam direction was determined by a desired transmission of about 50% for neutrons of about 3 Mev with which we are concerned.

This transmission value is a fair choice from the standpoint of multiple scattering and finite geometry corrections, and on the other hand solves the compromise between low statistical error in the measured total cross section by using a thick sample and minimum corrections due to inscattering by using a thin sample. The actual dimension of the lead sample are 2.6 cm thick and 1.7 cm side.

2.2.3 Solid Angle Subtended by Neutron Side Detector at Scatterer.

Although at this stage the dimensions of the neutron side detectors have not been determined, an analytic account will be presented in order to evaluate the total solid angle subtended by a side detector at the scatterer.

The scatterer is divided into differential volume elements and the differential solid angle subtended by the effective area presented by the detector at a particular scatterer element is evaluated using the equation (2.2.3). Now M is the surface area on the plane YZ defined by the projection of the detector on such a plane for a particular scatterer element. Integrating this equation for a given scatterer element, a differential solid angle $d\Omega_2$ is obtained:

$$d\Omega_2 = \arctan \frac{(c-z_2)(b-y_2)}{a\sqrt{(c-z_2)^2+(b-y_2)^2+a^2}} - \arctan \frac{(c-z_1)(b-y_2)}{a\sqrt{(c-z_1)^2+(b-y_2)^2+a^2}} -$$

$$- \arctan \frac{(c-z_2)(b-y_1)}{a\sqrt{(c-z_2)^2+(b-y_1)^2+a^2}} - \arctan \frac{(c-z_1)(b-y_1)}{a\sqrt{(c-z_1)^2+(b-y_1)^2+a^2}} \qquad (2.2.6)$$

In this equation (a,b,c) are the coordinates of the scatterer element and y_1, y_2, z_1 and z_2 are the integration limits determined by the coordinates of the scatterer element selected. The evaluation of equation (2.2.6) for each scatterer element is a repetitive process, and so a computer program was elaborated, in which the total solid angle subtended by a side detector at the scatterer can be obtained evaluating the expression (2.2.6) for each scatterer element and an average was taken.

2.2.4 Analysing Power and Figure of Merit.

As pointed out in chapter 1, the analysing power can be calculated directly from the experimental total cross section σ_T, and differential elastic scattering cross section $\sigma_o(\theta)$. The analysing power has been defined as:

$$P_s(\theta) = k\,\sigma_T\,\gamma\,\cot(\theta/2)/2\pi\,\sigma_o(\theta) \qquad (1.3.6)$$

where θ is the scattering angle. Since the angular resolution for this experimental geometry is finite, account has to be taken of the fact that the differential elastic scattering cross section is not constant with the scattering angle.

In order to evaluate the analysing power, the scatterer and effective area of the detector projected on plane YZ are divided into differential volume and surface area elements respectively. The scattering angle, θ, is then the angle between the line joining the target with a particular scatterer element and the

line joining this scatterer element with a given surface area element on plane YZ. The differential elastic scattering cross section value associated with the scattering angle is obtained from the theoretical curve shown in figure 7. This theoretical curve is based on optical model calculations carried out by Wilmore and Hodgson [73]. The total cross section for lead, in the neutron energy range of interest, used in these calculations is taken from a summary of neutron total cross section made by Hughes and Harvey [74].

Thus, the analysing power, $P_s(\theta)$, and figure of merit, f, can be calculated and averaged over the geometry of both the scatterer and detector. This is also a repetitive process which is included in the computer program mentioned in section 2.2.3.

2.2.5 Dimensions of the Side Neutron Detector.

The dimensions of the side detectors were chosen according to the following requirements:

1) the vertical (azimuthal) dimension of the side detector must be a little larger than the vertical dimension of the neutron beam at the position of the side detectors, so that an intercalibration of detection efficiencies of the collimated beam monitor and the side detectors can be made by scanning each side detector in turn across the collimated neutron beam. This dimension turned out to be 3.0 cm.

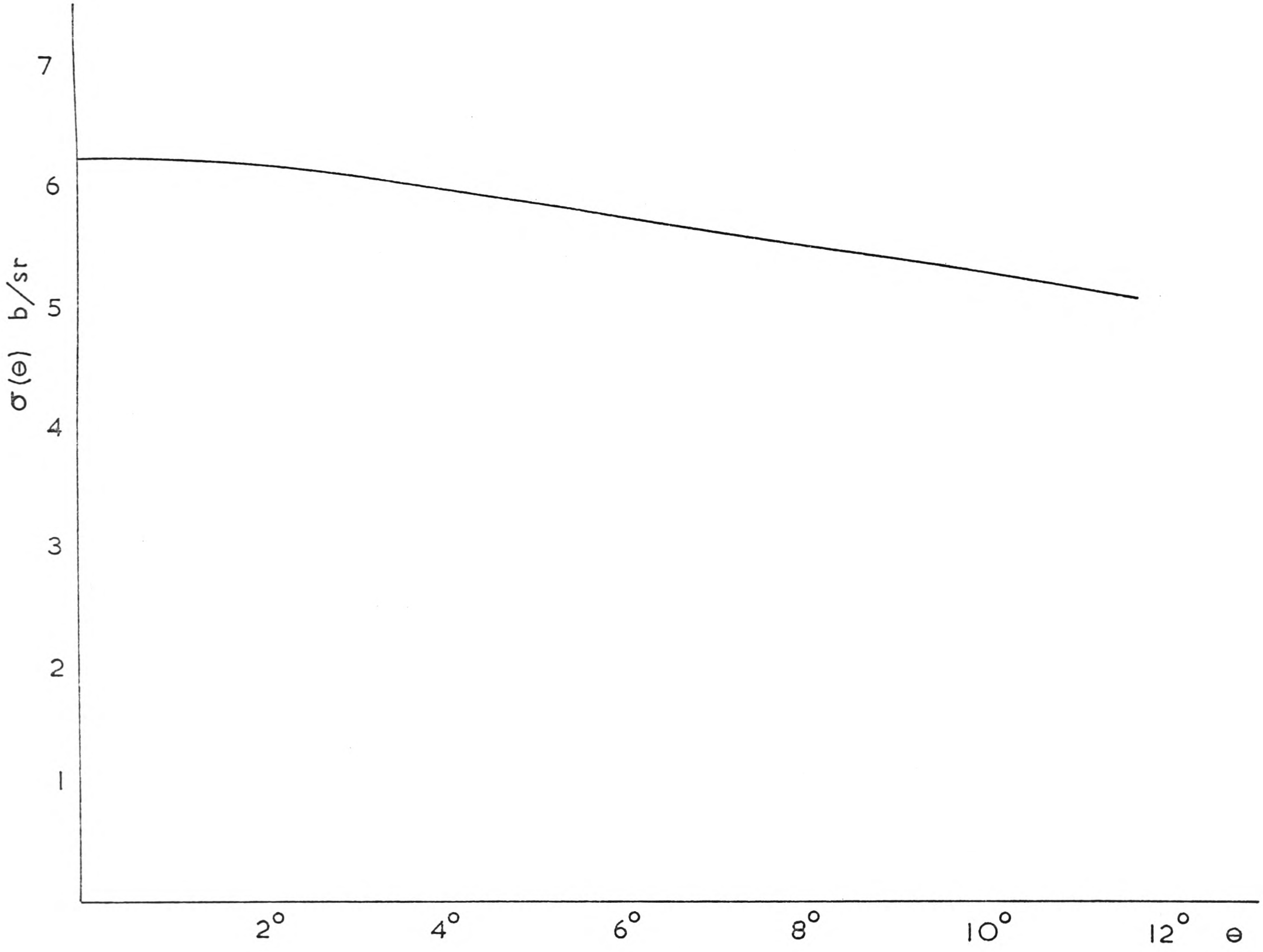

. Fig.7. Differential cross section of Pb at 3 MeV calculated from optical potentials [73].

2) the horizontal dimension (length) of the side detector represents a compromise between two factors affecting the figure of merit of the system. On the one hand, one can get a large analysing power value and small solid angle subtended by the side detector at the scatterer, and therefore low counting rate, by using a short detector. On the other hand, one gets a low analysing power value but large solid angle subtended by side detector at scatterer when using a long side detector.

In order to determine the optimum length for the side detectors, the analysing power and figure of merit for several detector lengths were calculated with a computer program which takes into account all the geometrical factors described above. In these calculations the minimum scattering angle, measured between the collimated neutron beam axis and the line joining the geometrical centre of the scatterer with the nearest point of the side detector, is 1.8^{o}.

The results of these calculations are shown in figure 8. From these curves it is clear that there is little to be gained in figure of merit by having a detector length greater than 4.0 cm and having at the same time a reasonable value in analysing power. It was decided that cylindrical stilbene crystals, 3.8 cm in diameter by 3.5 cm long, commercially** available at that time, should meet the requirements for the side detectors. These

**Footnote: Manufactured and marketed by Nuclear Enterprises Ltd. (U.K.)

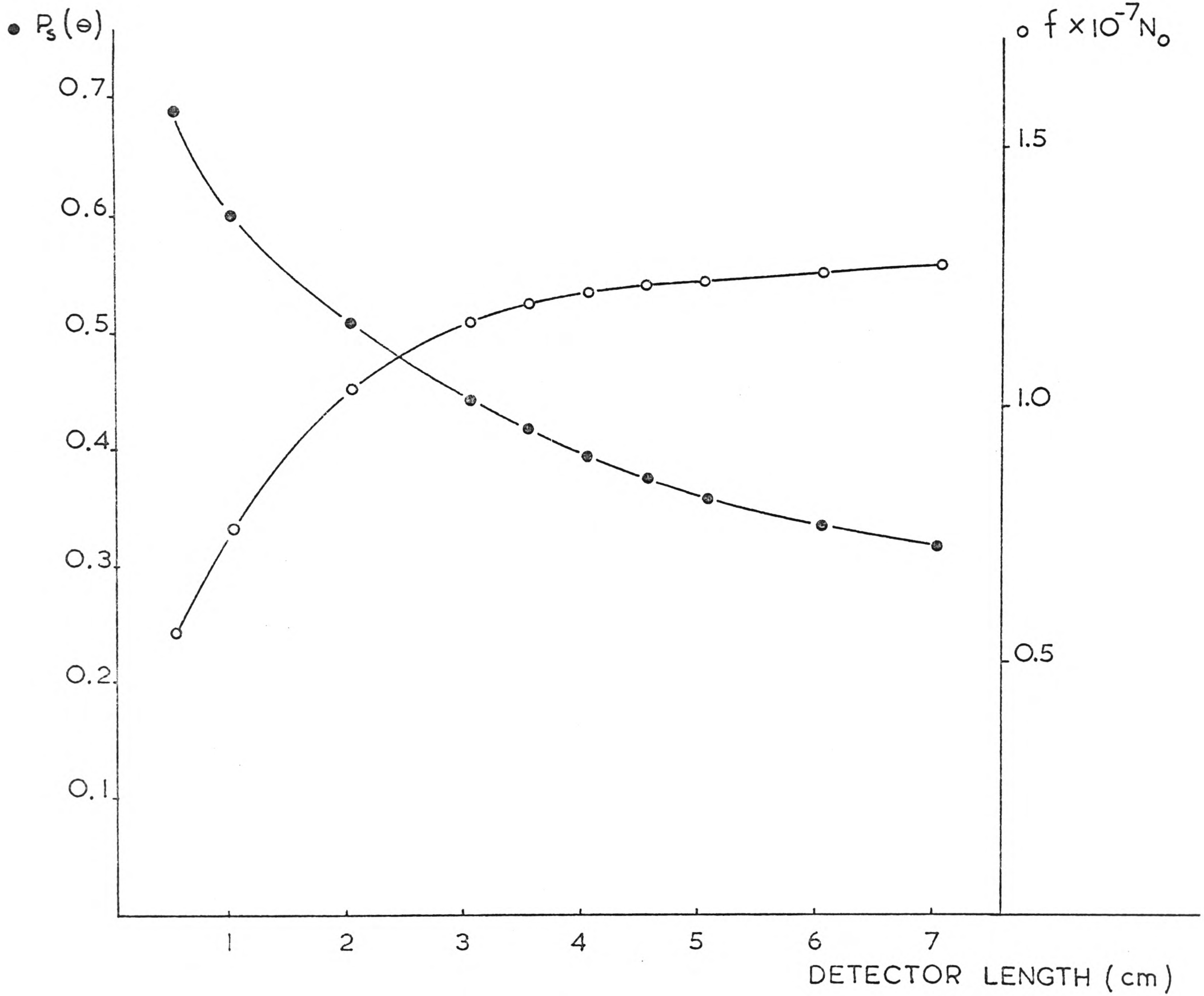

Fig.8. Analysing power $P_s(\theta)$ and figure of merit f for several side detector lengths.

dimensions of the side detectors will permit collection of all the polarization information in the angular interval from 1.8° to 5.5° in one measurement.

2.2.6 Comparison with a Typical He^4 Scattering Polarimeter.

Once all the geometrical parameters for a more efficient small angle Mott-Schwinger scattering polarimeter were determined, the analysing power and figure of merit for the selected experimental arrangement were calculated with the computer program described above and compared with those of a recent Mott-Schwinger[46] and a typical He^4 scattering [66] fast neutron polarimeter. Table 2.1 shows the comparison.

From this comparison it is concluded that a small angle Mott-Schwinger scattering fast neutron polarimeter employing the geometry described should take 1.5 times as long to obtain a polarization value with the same statistical accuracy as the He^4 scattering polarimeter.

This comparison has been made assuming that the side detectors in these three different systems have the same efficiency and that the neutron background is negligible. However, this latter assumption is far from the real situation, as far as the Mott-Schwinger polarimeter is concerned, since the neutron background in small angle experiments is rather high. Therefore, the measurements in this experiment will be carried out with and

Table 2.1. Comparison of figure of merit of a recent Mott - Schwinger and a typical He^4 scattering polarimeter with that of the present experimental arrangement.

Parameter	Mott-Schwinger	He^4	Present experimental geometry.
Ω_1 (sr)	9×10^{-5}	3×10^{-3}	2.3×10^{-4}
Ω_2 (sr)	3×10^{-4}	5×10^{-2}	3.7×10^{-3}
n(nuclei/cm^3)	3.3×10^{22}	1.8×10^{21}	3.3×10^{22}
t (cm)	2.6	5	2.6
$\sigma_o(\theta)$ (b/sr)	6.1 at 2^o	8×10^{-2} at 120^o	6.1 at 2^o; 5.8 at 5^o
$P_s(\theta)$	0.5 at 2^o	1 at 120^o	0.4
f	3.5×10^{15}	1.1×10^{17}	7.2×10^{16}
Relative figure of merit	1	31	20

without scattering sample, doubling the time taken for the Mott-Schwinger measurements; that is, it is expected that the present Mott-Schwinger scattering polarimeter should take at least three times as long to obtain a polarization value with the same statistical accuracy as the He^4 scattering polarimeter [66] based on a helium gas scintillator operating at a pressure of 70 atmospheres.

2.3 The Experimental Arrangement.

Due to the critical requirements imposed by the small angle experiments, particular attention was paid to the precise design, construction and assembling of all the different parts of the present Mott-Schwinger fast neutron polarimeter. A detailed description of the construction of the system is given in this section.

2.3.1 Target Assembly.

The target used is a TiD copper backed rectangular strip which can be soft soldered to the target holder. The target assembly consists of a brass target holder vacuum sealed into a quartz beam tube at its base with an 'O' ring; cooling water circulates within the interior of the target holder thus cooling the target and preventing the thermal outgassing of deuterium.

Two different target holders were used in the present investigation. One of them, hereafter called angled target, permits the target surface to be placed at 45° relative to the accelerator beam in such a way that the length of the rectangular target strip is in the reaction plane and its width is along the vertical axis of the collimator. Thus beam spot movement takes place along the collimator axis and the target-scatterer geometry is preserved. Further, this type of target holder provides a good visual indication of the position of the target surface, producing therefore, an easier alignment of the system, as explained later. The second target holder, hereafter called straight target, permits the target surface to be placed at 90° relative to the accelerator beam, so that the length of the rectangular target strip is normal to the reaction plane.

In order to renew the target material, the target holder in use can be removed and replaced in its original position without altering the alignment of the whole target assembly which can be accurately positioned, mechanically, relative to both the accelerator beam and the polarimeter. Figure 9 shows a photograph of the angled target and the whole target assembly with the straight target in position.

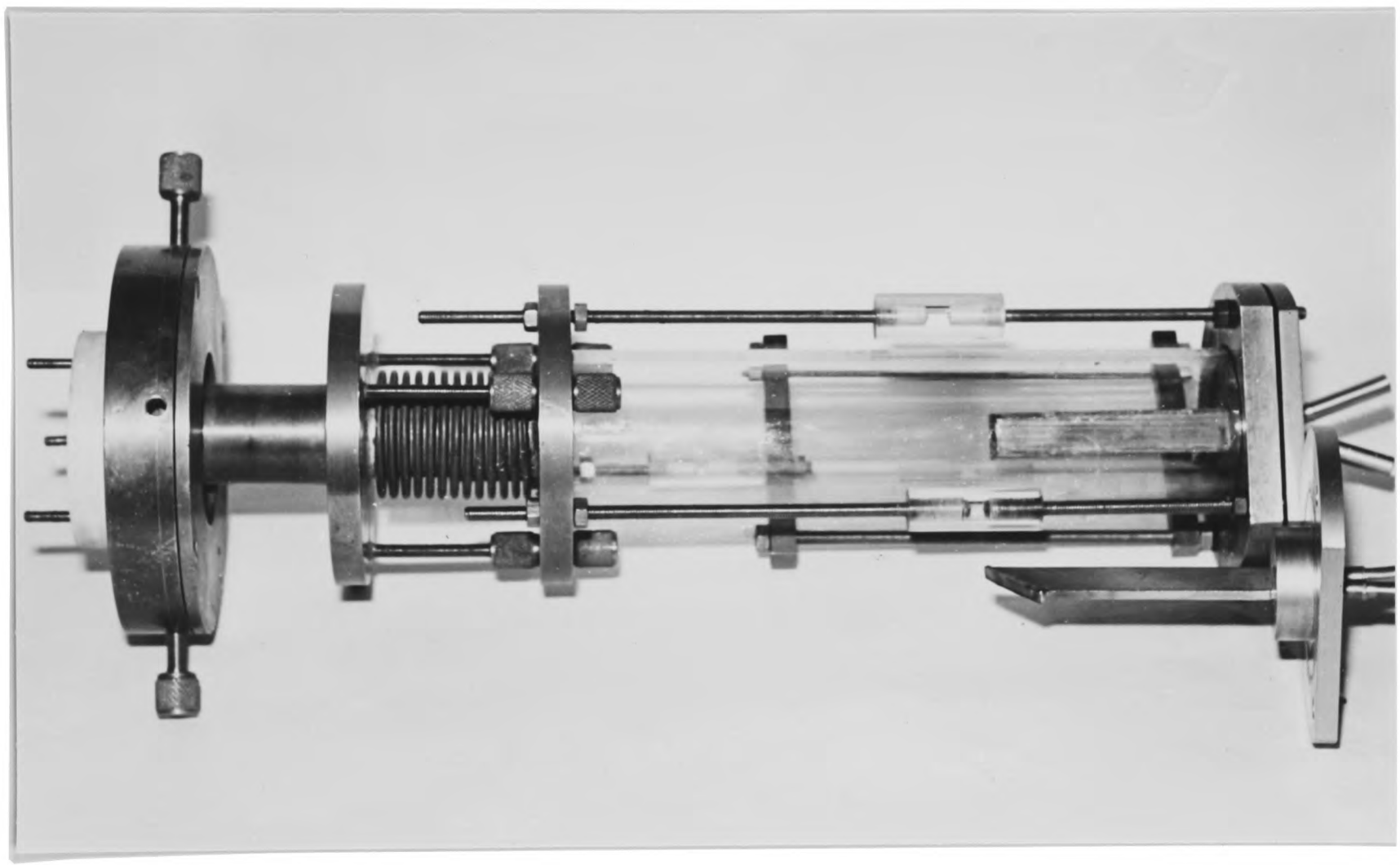

Fig.9. Photograph of the target assembly and target holders.

2.3.2 The Collimator.

The purpose of the collimator is to produce a well defined neutron beam with as small a halo as possible and to provide primary shielding for the side neutron detectors from the neutrons produced at the target.

The collimator, 46 cm long, is fabricated of a mild steel body narrower at the front than the back, and with the end faces perpendicular to an axial 5 cm internal diameter longitudinal tube. A ring of lead, 20 cm exterior diameter and 20 cm long, is placed around the axial tube just after the front face. The purpose of this lead piece, which is close to the target, is to produce attenuation of the undesired neutrons by inelastic scattering. A second piece of lead, 5 cm thick, covering the whole back face of the collimator is used to reduce the gamma ray flux produced by neutron capture in the paraffin wax filling the bulk of the collimator. The axial neutron beam tube accepts polythene inserts to provide the collimator aperture or throat required.

For the present experiment, polythene inserts, 5 cm diameter, with a 1 cm side square axial hole were assembled so that the square holes in the whole assembly are well aligned. This insert assembly has a small square cross section throated portion in a position dictated by the target-scatterer geometry. The objective

of this throated portion is to prevent the target from directly irradiating the aperture walls at the far end of the collimator, so reducing the contamination of the direct neutron beam due to scattering of neutrons in the aperture walls.

As mentioned earlier, the dimension of the collimated neutron beam at the position of the side detectors, defined by the collimator aperture, allows the side detectors to be positioned so that the minimum scattering angle is less than 2^{o}, where the differential scattering cross section due to the Mott-Schwinger interaction is comparable with the nuclear interaction.

2.3.3 The Scatterer Control System.

The lead scatterer, chosen according to the requirements mentioned in section 2.2.2, is placed at 11 cm from the collimator aperture exit with its length along the neutron beam direction. It is mounted on a specially designed motor controlled holder which enables measurements to be made with the scatterer accurately positioned in the neutron beam or with the scatterer out of the beam. To facilitate the posterior alignment, two lines were inscribed along the vertical and horizontal axis on the top end of the scatterer facing the side detectors. The scatterer holder frame was so constructed that it can be accurately positioned, horizontally and vertically, relative to both the back face of the collimator and the collimator aperture. This scatterer holder and its control circuit form the Scatterer Control

System. Figure 10 shows a photograph of the scatterer holder and Figure 11 shows the circuit associated with it. In the following description, reference is made to these figures.

Each middle vertical bar in the scatterer holder frame has a push-button switch Sw1, which opens the motor circuit when the plate holding the lead scatterer has reached the position selected by a double pole, double throw switch Sw2. A polarized single pole, double throw switch Sw3, placed at the rear of each middle vertical bar, is connected to a pair of TTL NAND gates across coupled as a latch to form a contact bounce eliminator, the output of which is connected to both a light emitting diode, through a resistor, and to one input of a TTL NOR gate. When the scatterer has reached one of its two positions, the plate holding the scatterer depresses the corresponding switch Sw3, the output of the contact bounce eliminator produces a high TTL logic level and the respective light emitting diode indicator turns on.

In addition to this manually operated mode, the Scatterer Control System can be operated in automatic mode as follows. The switch Sw2 is left in its central position and the switch Sw4 is closed to connect the mains to the poles of a double pole, double throw relay, R, connected in parallel with the switch Sw2. The state of the relay is controlled by the inverted output of a JK flip-flop. This is a two state logic element which can be set in either of its two states and will remain in that state providing a continuous output until some other input down-going transition

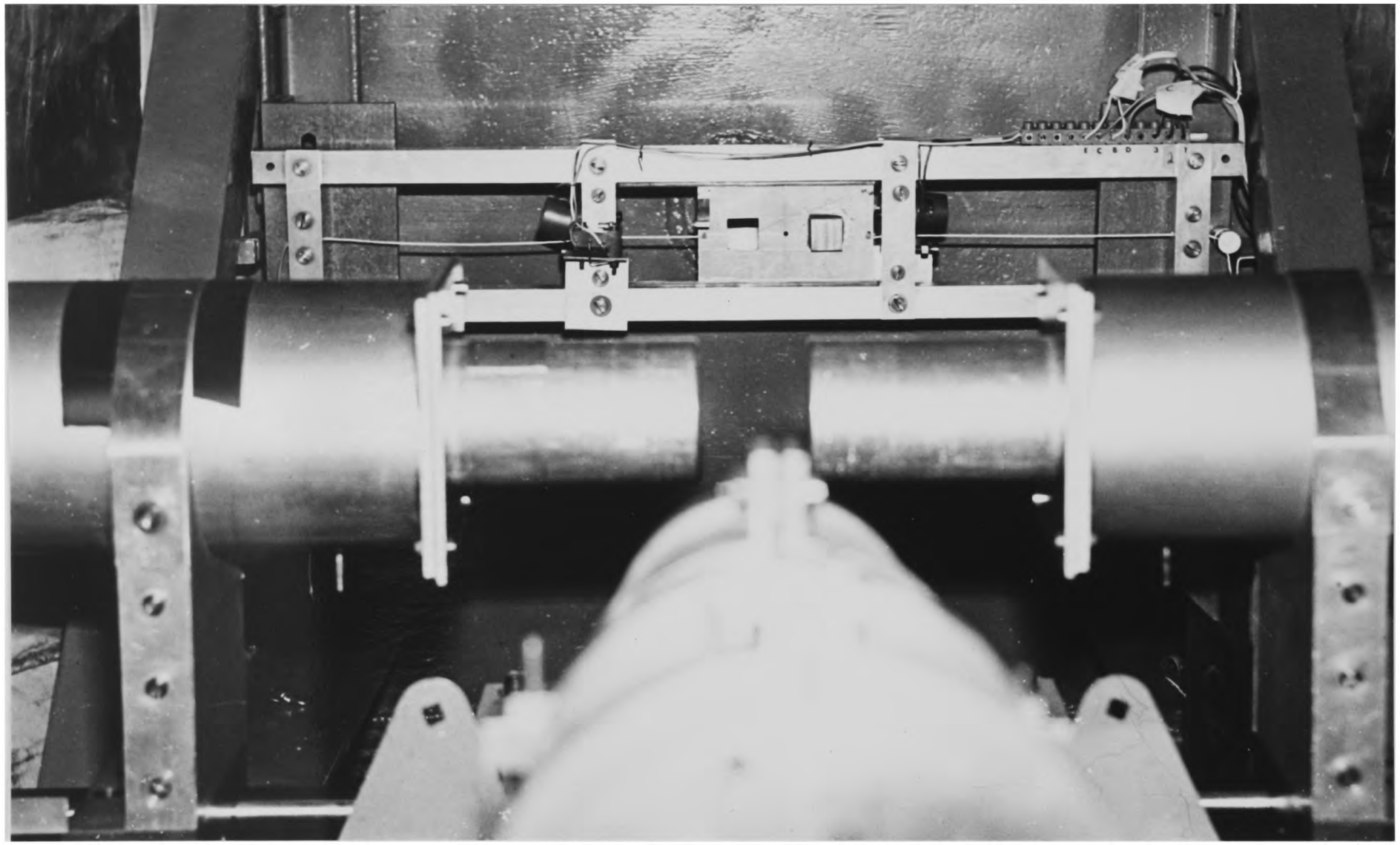

Fig.10. Photograph of the scatterer holder.

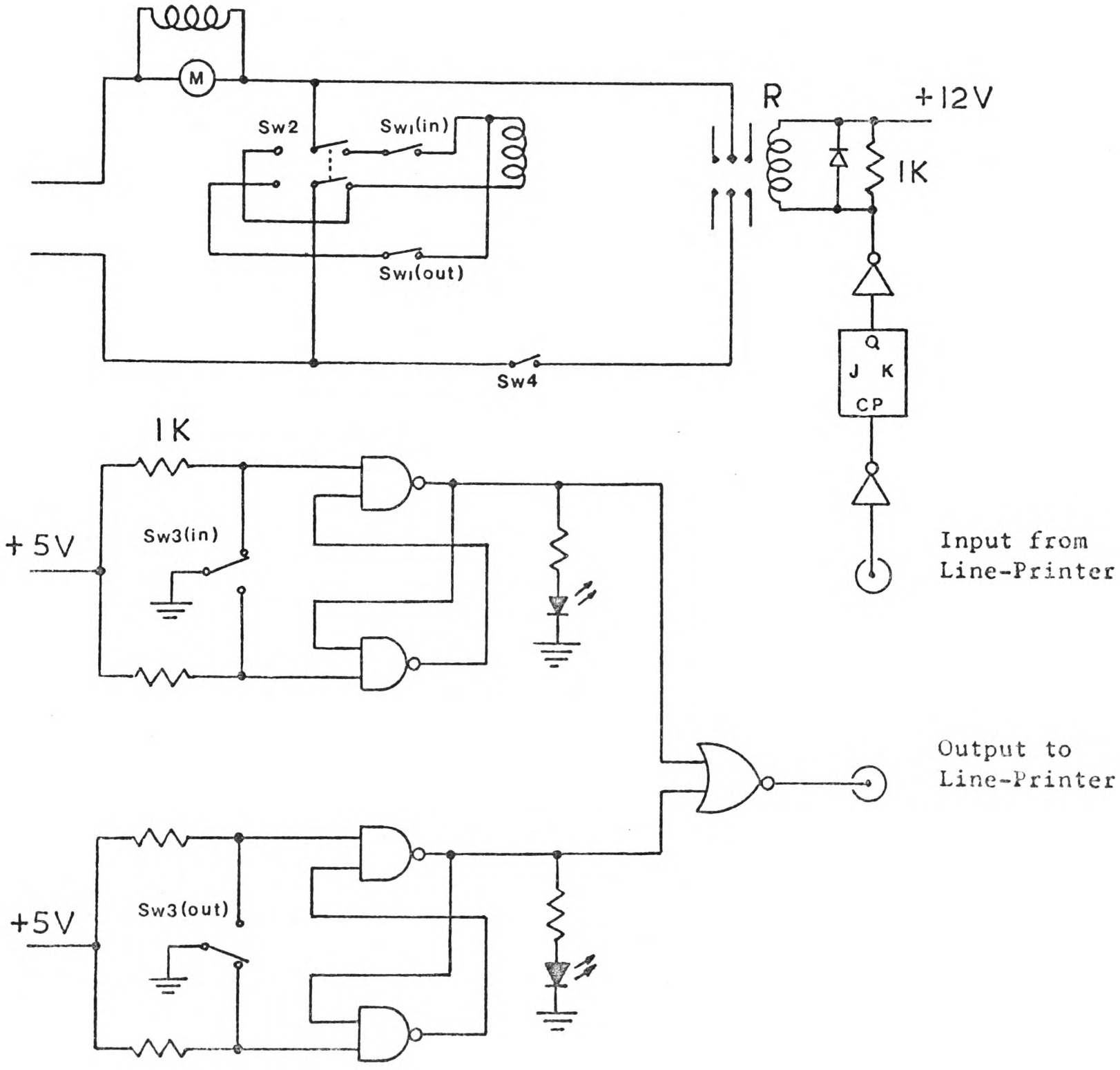

Fig.11. Circuit to control the position of the scatterer.

is applied to change the state.

The stop/start of a Line Printer-Scaler System [19], used in conjunction with the Scatterer Control System, provides a TTL up-going transition which is inverted in the input stage of the scatterer control circuit and then applied to the clock input of the JK flip-flop which in turn operates the relay and the scatterer changes position. The up-going transition is produced by an internal timer (range 10 to 9×10^4 secs) at the end of the preset time. The timer of the Line Printer requires a TTL down-going transition to be started, this transition is produced at the output of the TTL NOR gate when the scatterer has reached one position, that is, when the output of one of the bounce eliminators goes high and the respective light emitting diode turns on.

2.3.4 The Side Neutron Detectors and Collimated Beam Monitor Assemblies.

As mentioned in section 2.2.5, a cylindrical stilbene crystal was selected for each side neutron detector for the present polarimeter. Stilbene scintillators offer an efficient means of detecting fast neutrons, but have the inconvenient feature that they are sensitive to mechanical and thermal shock; consequently the present stilbene detection assembly was so designed that it does not rely on the crystal to be a structural member of the finished detector assembly. Although at this stage a description

of the entire side detectors arrangement is given, the actual mounting of the crystals was done after the photomultiplier and associated preamplifiers were tested, so reducing to a minimum the handling of the stilbene crystals.

The physical arrangement for the stilbene crystal and its incorporation with the photomultiplier are important design considerations. The diagram of figure 12 represents a complete stilbene neutron detection unit as used in the present polarimeter. A primary factor is the efficient transfer of light from the point of origin in the crystal to the photocathode; to achieve this, a diffuse reflector coating, 0.5 mm thick, was applied to all the crystal surfaces except one end face which was coupled to the photocathode of the photomultiplier by using an optical contact grease.

A cylindrical aluminium can of thickness 0.5 mm, internal diameter 55 mm and length 95 mm with its open end mounted in the central hole of a square aluminium plate, 10 cm side and 2 mm thick, provides mechanical protection and light tight cover for each crystal which is located accurately with its axis along the aluminium can major axis with a 'C' shaped piece of perspex fixed on the bottom of the can. For alignment purposes again, each aluminium can was marked with a line along its longitudinal axis and two transversal lines indicating the position of the geometrica centre of the stilbene crystal and its end face coupled to the photocathode of the photomultiplier.

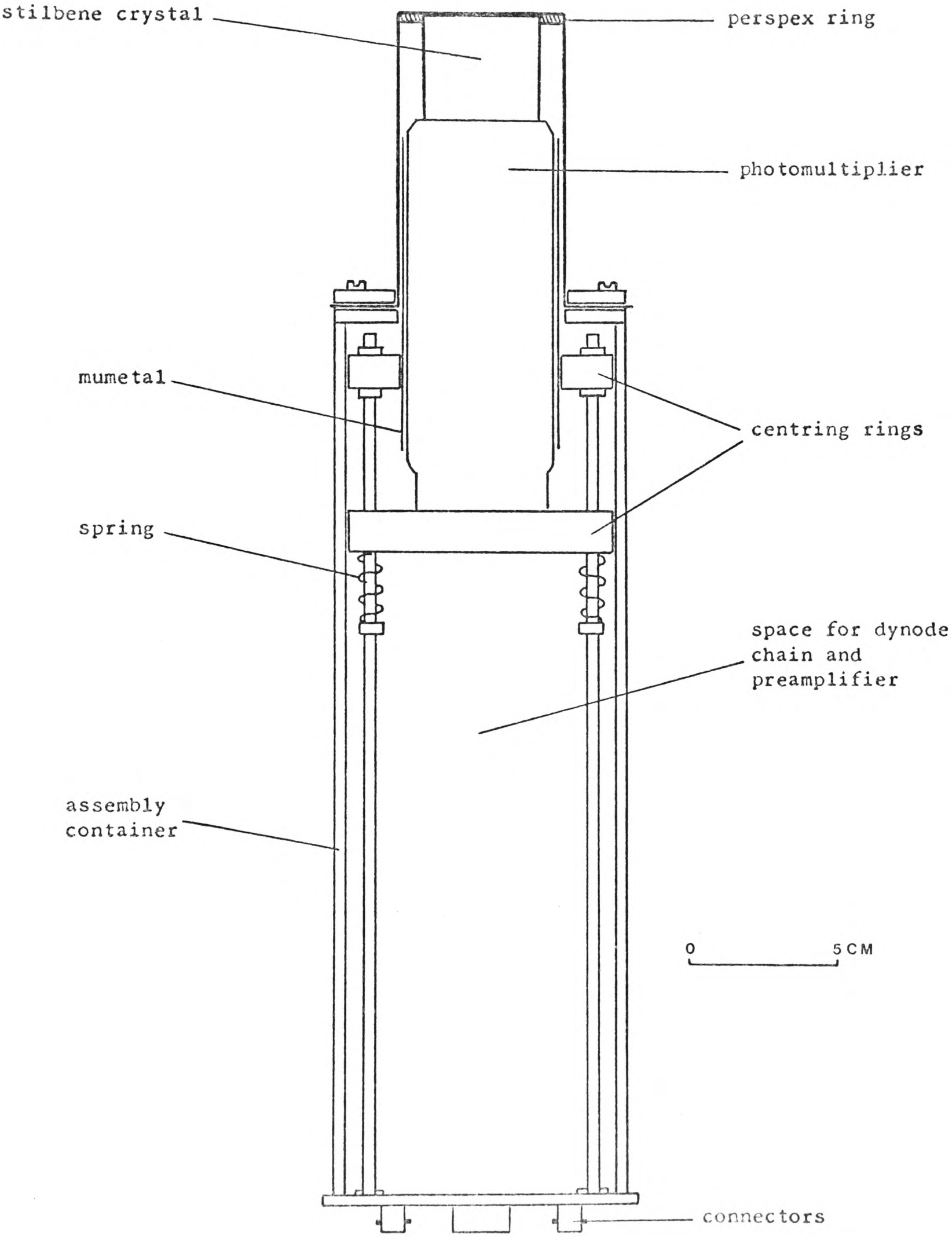

Fig.12. Sketch of a stilbene neutron detector.

The photomultiplier, protected by a Mumetal shield to reduce interference by either the Earth's magnetic field or stray magnetic fields from other equipment, is located with its major axis along the housing tube axis by a bakelite ring. The voltage divider network and the preamplifier are also inside the housing tube. Each entire detection unit is mounted on two supports which can move on a track perpendicular to the collimated neutron beam so that each stilbene crystal can be conveniently moved into the direct beam or into the beam scattered at various angles. This track, shown in figure 13, was so constructed that it can be accurately positioned relative to the neutron beam. The distance between the scatterer and the centre of the track is 61 cm.

The collimated neutron beam monitor is based on a NE213 liquid scintillator encapsulated in a bubble free cylindrical cell of 5 cm length and 5 cm diameter. The liquid NE213 was chosen for its high efficiency for fast neutron detection and pulse shape discrimination properties. The collimated beam monitor assembly is similar to those of the side neutron detectors, except that the preamplifier is not included in the housing tube. This assembly can be removed from its stand, for alignment purposes, and replaced accurately in its original position. The distance from the collimated beam monitor to the scatterer is 90 cm.

The collimated beam monitor stand and the track for the side detectors are mounted on an angle iron frame attached to the back

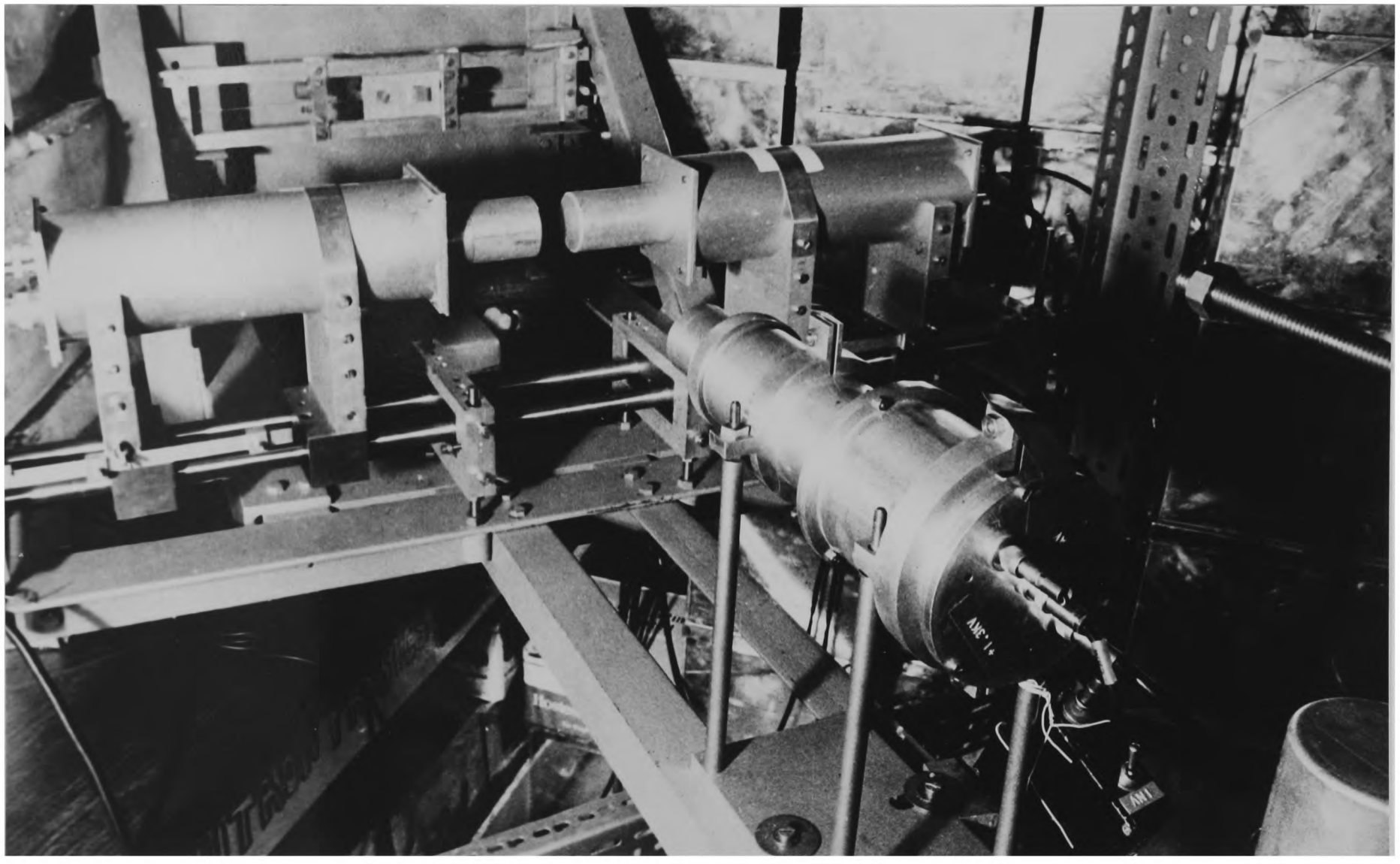

Fig.13. Photograph of the first polarimeter.

of the collimator. The photograph (figure 13) shows most of the parts forming the present Mott-Schwinger scattering polarimeter.

2.3.5 Alignment of the Polarimeter.

Once the polarimeter was completed and assembled, it was mounted with the collimator axis at a laboratory reaction angle of 45^{o}, this being close to the centre of a broad maximum in the polarization angular distribution from the $H^{2}(d,n)He^{3}$ reaction [59]. The alignment of the polarimeter, repeated before every experimental run, is made by means of a telescope located at the rear of the collimated beam monitor which has been previously removed from its stand and replaced by a plumb line passing by the top of the cylindrical detector. The polythene inserts assembly and scatterer holder frame are also removed and a cylindrical alignment insert with a 3 mm diameter axial hole is fitted into each end of the collimator beam tube.

The telescope is focussed, in turn, on the target, on the entrance and exit alignment inserts of the collimator, on the horizontal reference lines of the aluminium cans of the side detectors and on the plumb line which serves to align the crosswires of the telescope and determine the position of the collimated beam monitor. Once this procedure is completed, the polythene insert assembly and scatterer holder frame are placed in position and then aligned, checking that the scatterer repeats its aligned position after it has been moved several times between its two positions.

2.3.6 Shielding of the Polarimeter.

Because the neutron background was expected to be considerable, substantial shielding, at least 50 cm thick, consisting of paraffin wax and borated water contained in polythene bags inside tin cans, was built around the polarimeter to reduce the neutron background. A detailed investigation of the neutron background found during the present measurements will be presented in chapter four.

2.4 The Second Mott-Schwinger Polarimeter.

At this stage it is worthwhile emphasizing the symmetry property of the $H^2(d,n)He^3$ reaction in the centre of mass system. Because the incident particle and target are identical, the polarization $P_n(E_d,\varrho)$ of neutrons emitted from the $H^2(d,n)He^3$ reaction at a centre of mass angle ϱ is equal in magnitude and opposite in sign to that for centre of mass angle $(\pi-\varrho)$: that is, $P_n(E_d,\varrho) = -P_n(E_d,\pi-\varrho)$, although the neutron energies E_1, E_2 of these neutron beams will differ in the laboratory system.

This property can be exploited to further reduce the time of data collection by arranging a system consisting of two polarimeters mounted at centre of mass angles of ϱ and $\pi-\varrho$ respectively. Besides, such a system could be used to investigate the angular dependence of polarization in various neutron producing reactions.

The complete present experimental set-up consists of two Mott-Schwinger scattering polarimeters mounted at laboratory reaction angles of 45° and 130° respectively. The second polarimeter was planned after the first one was extensively tested and proved to be reliable. Actually, the second polarimeter was constructed in the late stage of this work and was used simultaneously with the first polarimeter in only the last two measurements (those with the lowest neutron yield) reported in this thesis. However, a description of the second polarimeter is given in this section.

Originally, the geometry of the second polarimeter was planned to be identical to that of the first one. However, the distance from the target to the collimator entrance was not 20 cm, as in the first polarimeter, but 23 cm. This reduces by 8% the solid angle subtended by the scatterer at target and therefore the figure of merit of the second polarimeter. The rest of the experimental geometry is identical to that of the first polarimeter, as well as the standard of construction. The collimator, polythene insert assembly, scatterer and scatterer control system are also identical to those described in the previous section.

The NE213 liquid scintillator side detectors, specially designed and constructed for the second polarimeter, have a cubic shape to maximise the scintillator volume, but each presents a solid angle at the scatterer similar to that presented by a stilbene side detector in the first polarimeter. The collimated

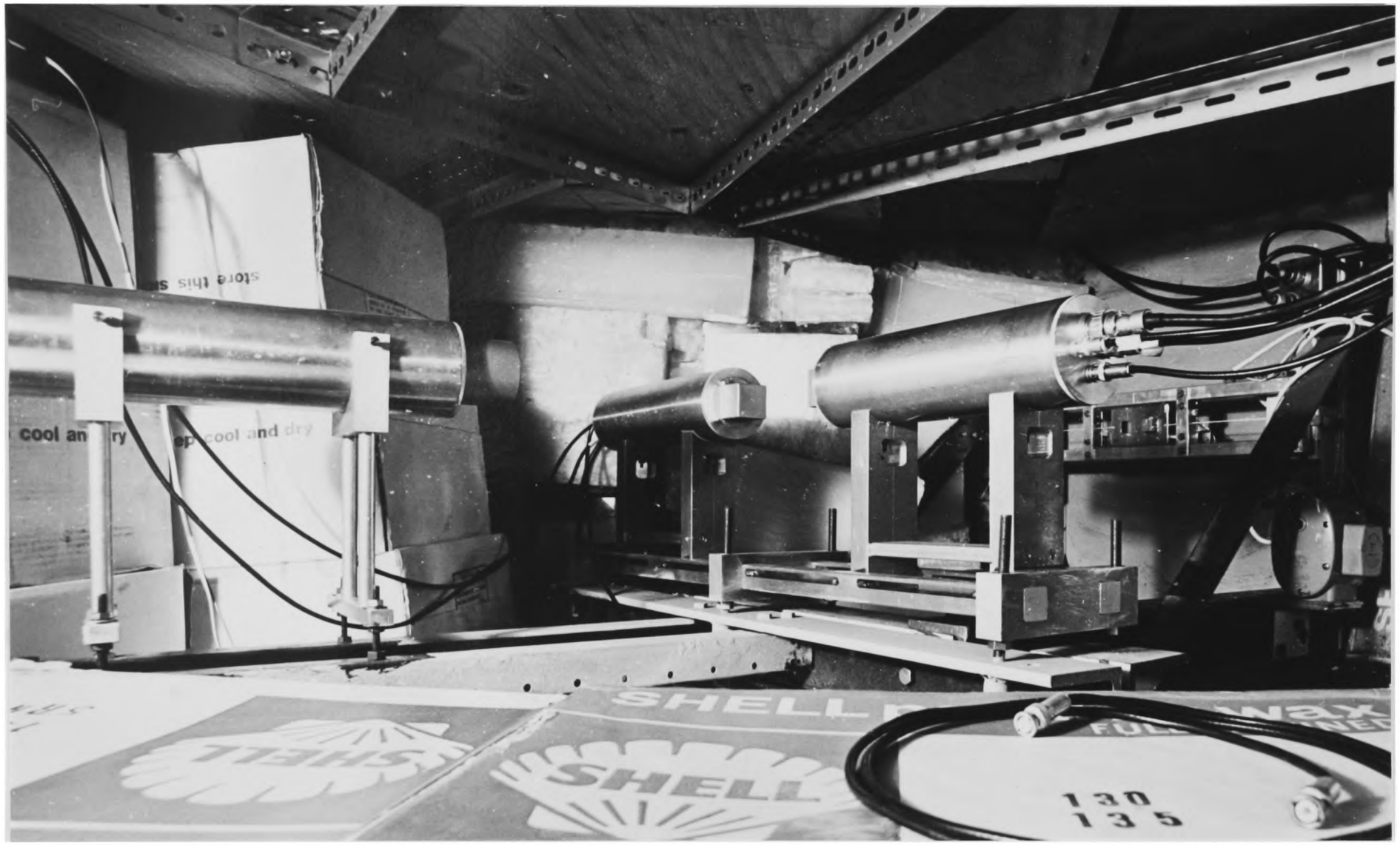

Fig. 14. Photograph of the second polarimeter.

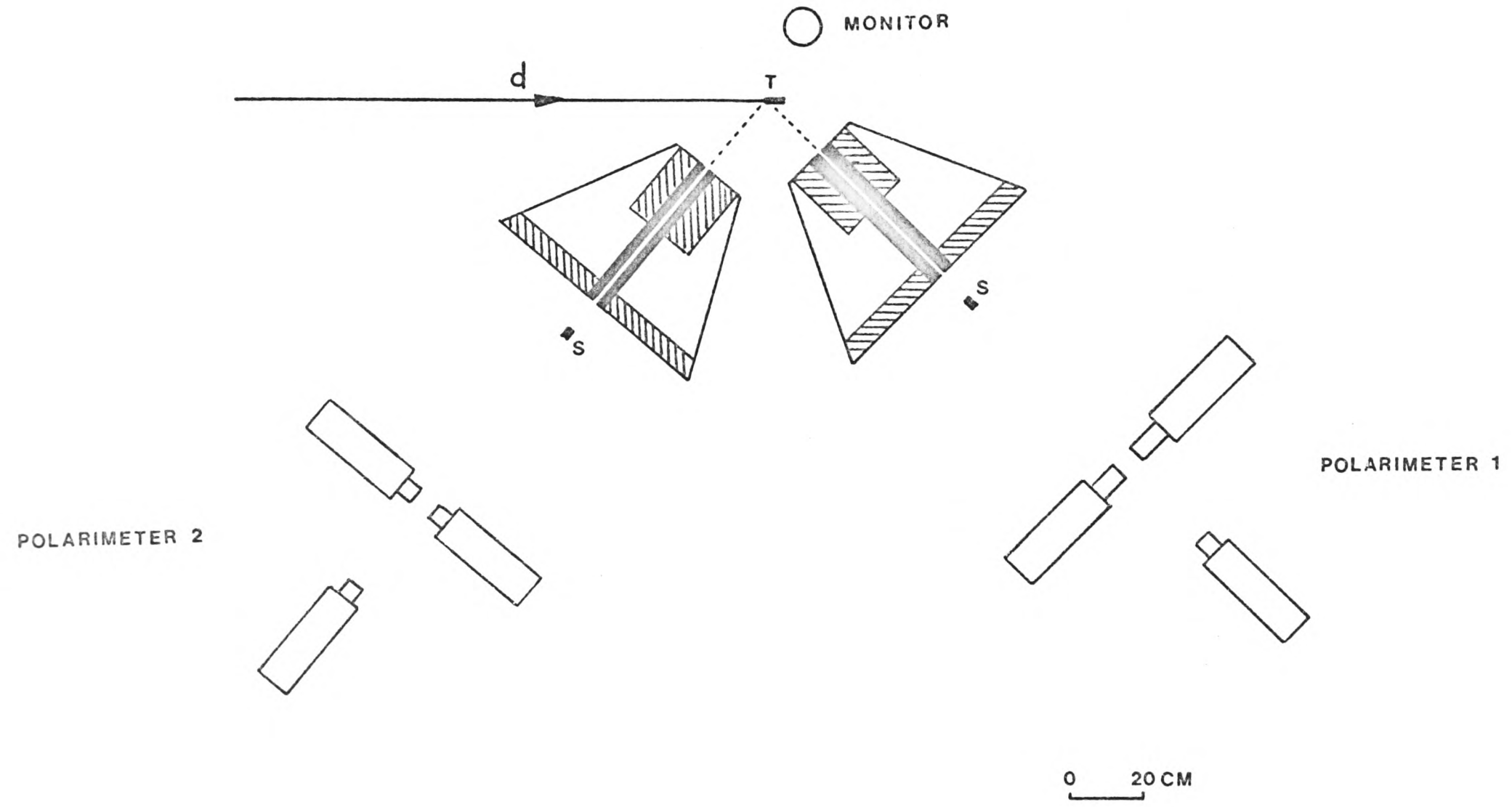

Fig.15. The experimental arrangement (shielding is not shown).

beam monitor is based on NE213 liquid scintillator encapsulated in a bubble free cylindrical cell of 5 cm length and 5 cm diameter, also designed and constructed for the present experiment. The side neutron detectors and collimated beam monitor assemblies are similar to those of the first polarimeter. Figure 14 shows a photograph of the second Mott-Schwinger scattering polarimeter, in which most of its parts are shown.

This second polarimeter was also surrounded with substantial shielding consisting of paraffin wax. An investigation of the neutron background found during the measurements with this polarimeter will be presented in chapter four.

The complete experimental set-up consisting of the two Mott-Schwinger scattering polarimeters is shown, without shielding, diagramatically in figure 15.

CHAPTER 3.

CHAPTER 3.

THE ASSOCIATED ELECTRONIC EQUIPMENT.

It is desirable that every experiment involving neutron detection should have some kind of discrimination against the inherent gamma ray background. For this reason, the choice of scintillators for the present experiment was governed by two requirements, namely, high fast neutron detection efficiency and good pulse shape discrimination properties. Stilbene and NE213 liquid scintillators were chosen since they meet both requirements. This chapter describes the two different pulse shape discrimination techniques employed in this work, their performance and the preliminary tests of the electronics set-up used with each technique.

3.1 Pulse Shape Discrimination in Organic Scintillators.

Pulse shape discrimination is a method which relies on the fact that the light pulse emitted from certain scintillators has a time dependence which is different for particles of different specific ionisation [75]. This property makes these organic scintillators a valuable tool for selecting neutron - induced recoil protons in the presence of recoil electrons from gamma ray interactions.

The shape of the scintillation light pulse is generally described as the sum of two exponential decay curves, although other components are known to exist [76,77]. The time constants of the two main exponentials differ by at least one order of magnitude. In the case of a scintillator with pulse shape discrimination properties, the intensity ratio of light emitted in these two main components depends of the mass and charge of the different particle types. For organic scintillators it is found that the slow component of the scintillation pulse is more strongly excited by heavily ionising particles than by electrons [75,76,78,79,80], while the decay constant of the fast component is independent of the type of exciting particle. For the particular case of neutrons (i.e. by recoil protons), the ratio of intensity of the slow component to that of the fast component is larger than for gamma rays (i.e. by electrons), both for stilbene and NE213 scintillators.

Techniques for pulse shape discrimination in scintillators described before 1962 have been reviewed by Varga [77] and Owen [81]. More recently progress has been reviewed by McBeth et al [82] and Hall [83]. Usually the authors of the different pulse shape discrimination systems report their results in different ways, so that it is useful to define a figure of merit M [84] in order to compare the performances of the different pulse shape discrimination systems. Figure 16 illustrates the definition of a pulse shape discrimination figure of merit. M is

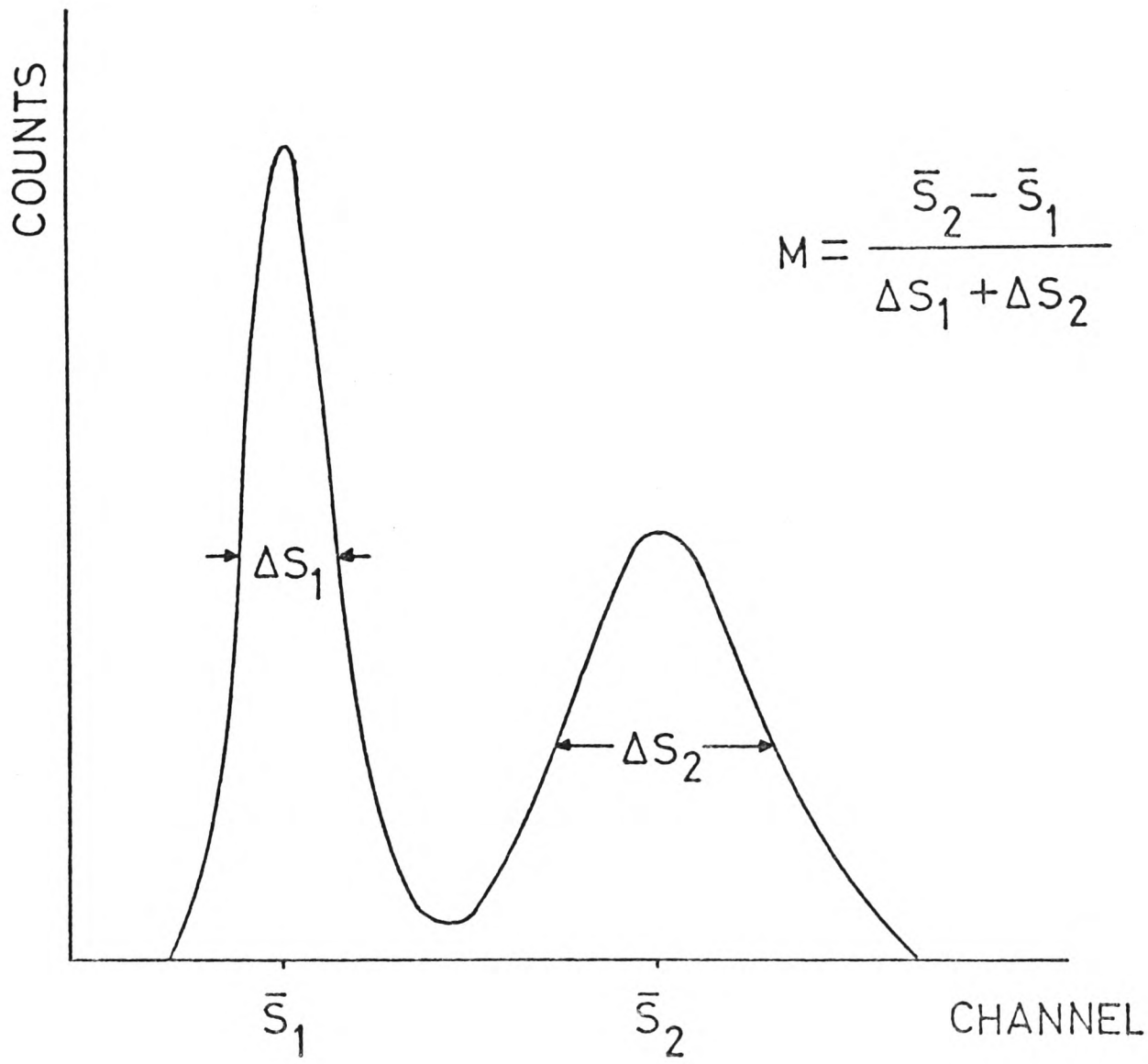

Fig.16. Definition of figure of merit.

defined as:

$$M = \frac{\bar{S}_2 - \bar{S}_1}{\Delta S_1 + \Delta S_2} \qquad (3.1.1)$$

where $\bar{S}_2 - \bar{S}_1$ is the difference between the mean peak positions, and ΔS_1 and ΔS_2 are the fwhm's of the peaks for gamma rays and neutrons. This figure of merit has been used to evaluate the performance of the two different pulse shape discrimination techniques employed in the present work.

3.2 Zero Crossing Method of Pulse Shape Discrimination.

This technique was originated by Alexander and Goulding [85] and there have been a large number of reports describing systems based on the same principle. For a detailed theoretical analysis of this technique see the report by Roush et al [86].

In this type of pulse shape discrimination in organic scintillators a dynode signal is integrated and then double differentiated so as to produce a base line crossover. The time at which this double differentiated pulse crosses zero, relative to the start of the pulse, is determined by the slow component of the scintillation decay and thus by the ionisation density of the charged particle absorbed in the scintillator. This time interval is in principle independent of the energy of the event and depends only on the dynode pulse shape, and so it is the parameter on whose value the pulse shape discrimination is based.

Typically, the difference in zero crossing times for protons and electrons interacting with an organic scintillator is of the order of some tens of nanoseconds.

Figure 17 shows the different pulse shapes in a zero crossing pulse shape discrimination system and figure 18 shows its general principle. The instant of the starting of the pulse is sensed by a leading edge discriminator (LED), while the zero crossing discriminator (ZCD) estimates the instant of the zero cross-over point. The time difference between the output pulses from these two discriminators is converted into a proportional voltage pulse in the time to amplitude converter (TAC). The amplitude of the resulting pulse thus depends upon the rise time of the integrated dynode signal and a discriminator can reject the pulses corresponding to gamma rays.

Since the leading edge discriminator has a finite threshold for triggering, there will be a slight dependency of the triggering instant on the amplitude of the pulse. However, this difficulty is overcome by measuring the time between the leading edges of the positive and negative pulse parts. Thus it is possible to adjust experimentally the threshold of the zero crossing discriminator to give a minimum variation of the measured time interval with the pulse amplitude.

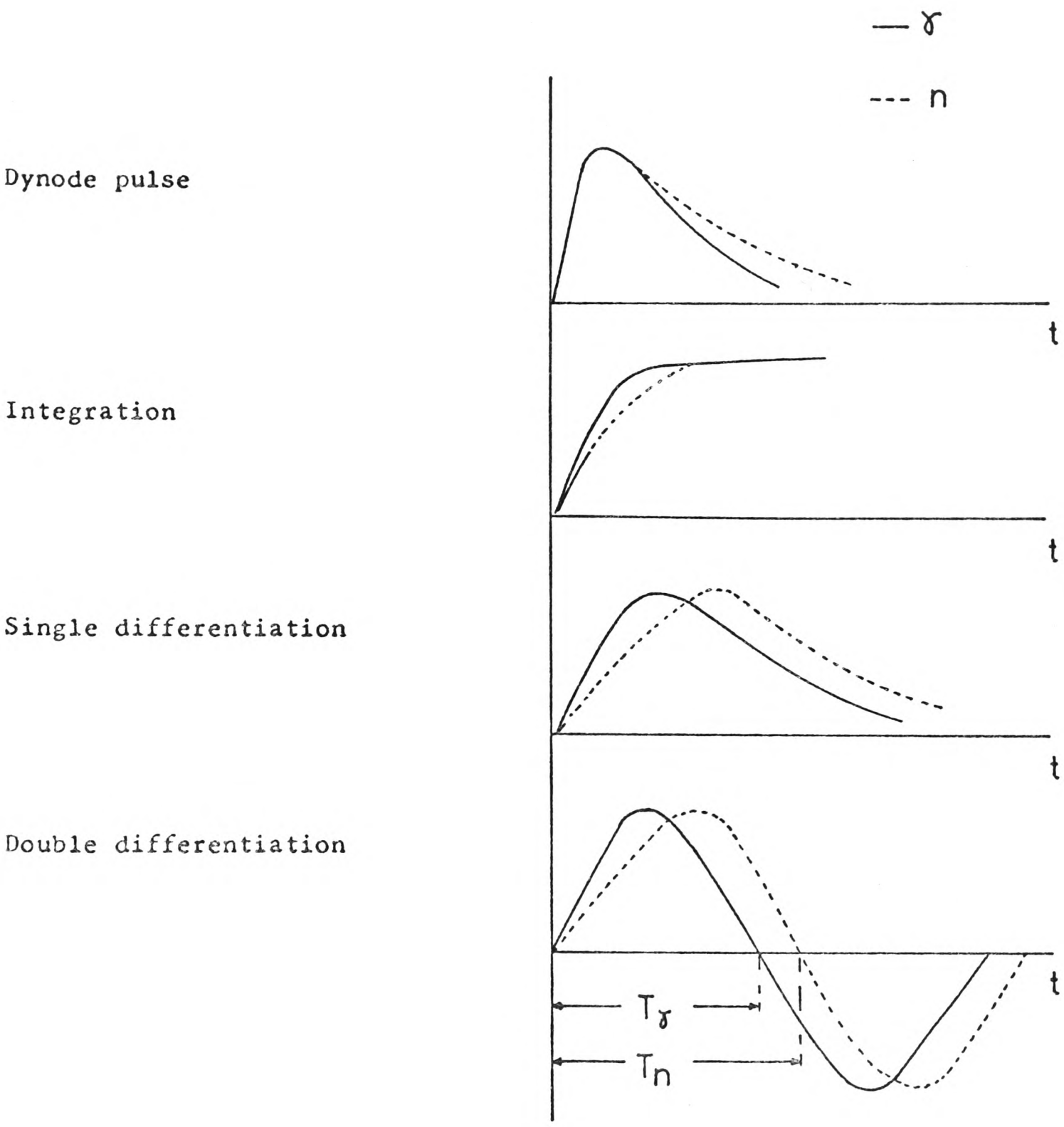

Fig.17. Dynode pulse shapes due to gamma ray and neutron events in the zero crossing time pulse shape discrimination method.

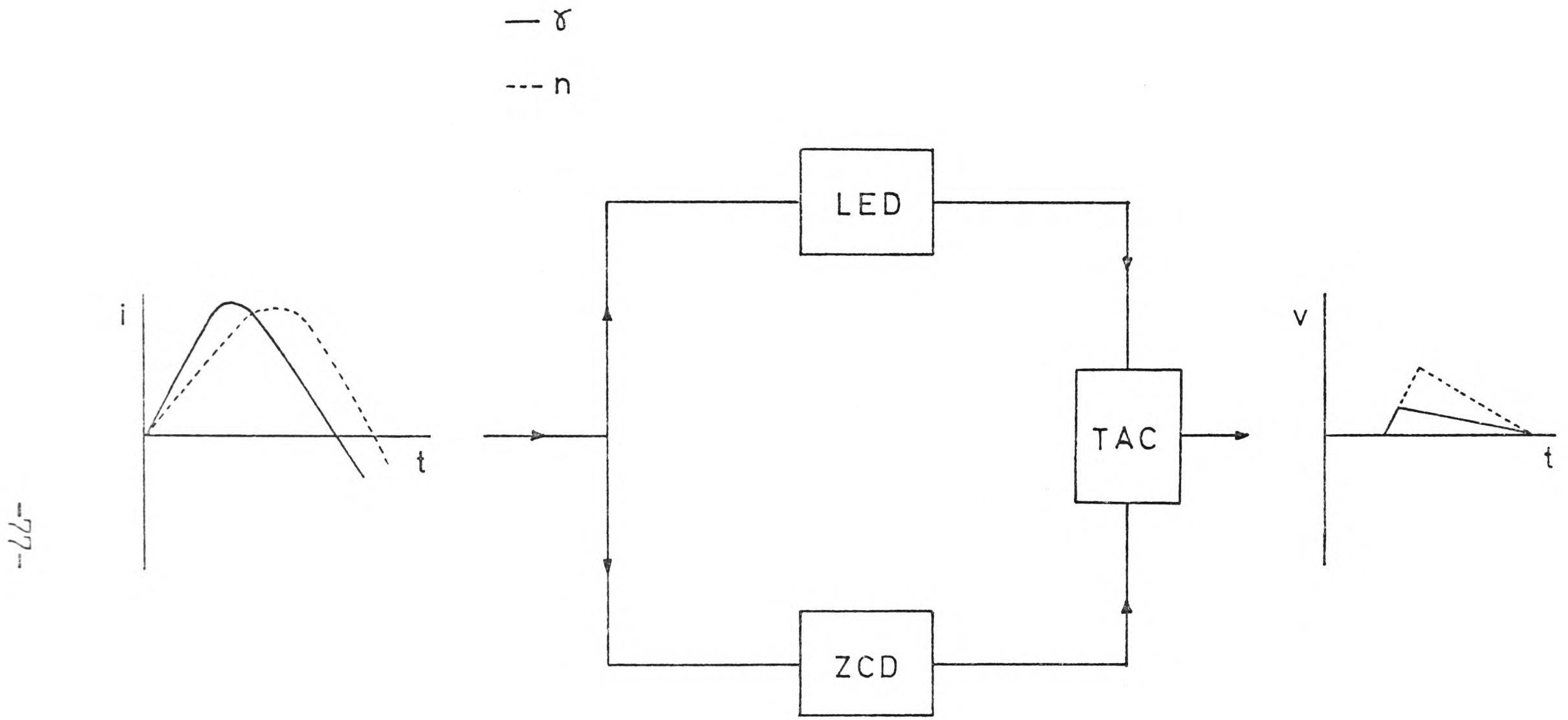

Fig.18. Principle of the zero crossing pulse shape discrimination method.

This zero crossing timing technique was applied to the three neutron detectors forming the first polarimeter of the present experiment, the actual pulse shape discrimination circuits employed are based on a design by Davie [87]. Before describing the performance of these circuits, the preliminary tests of the associated electronics are presented.

3.2.1 Preliminary Tests.

The preliminary tests described in this section were made before the final mounting of the stilbene crystals on the photomultipliers, so reducing their handling to a minimum.

The two stilbene detectors chosen for the first polarimeter employed an EMI type 9814B photomultiplier, whose dynode chain, given in figure 19, was constructed according to EMI directives[88]. The NE213 liquid scintillator used as collimated beam detector was coupled to a 56 AVP photomultiplier tube, whose dynode chain is given in figure 20.

The first test performed was of the linearity of the photomultiplier - preamplifier systems. The conditions for linear performance were obtained with a 2" x 2" NaI(Tl) crystal coupled onto the photomultiplier and standard gamma sources (Na^{22}, Cs^{137}, Mn^{54}, Co^{60}). The linear pulses from the last dynode were fed to a suitable preamplifier kept inside the detector assembly container. These pulses, after amplification, were analysed in a

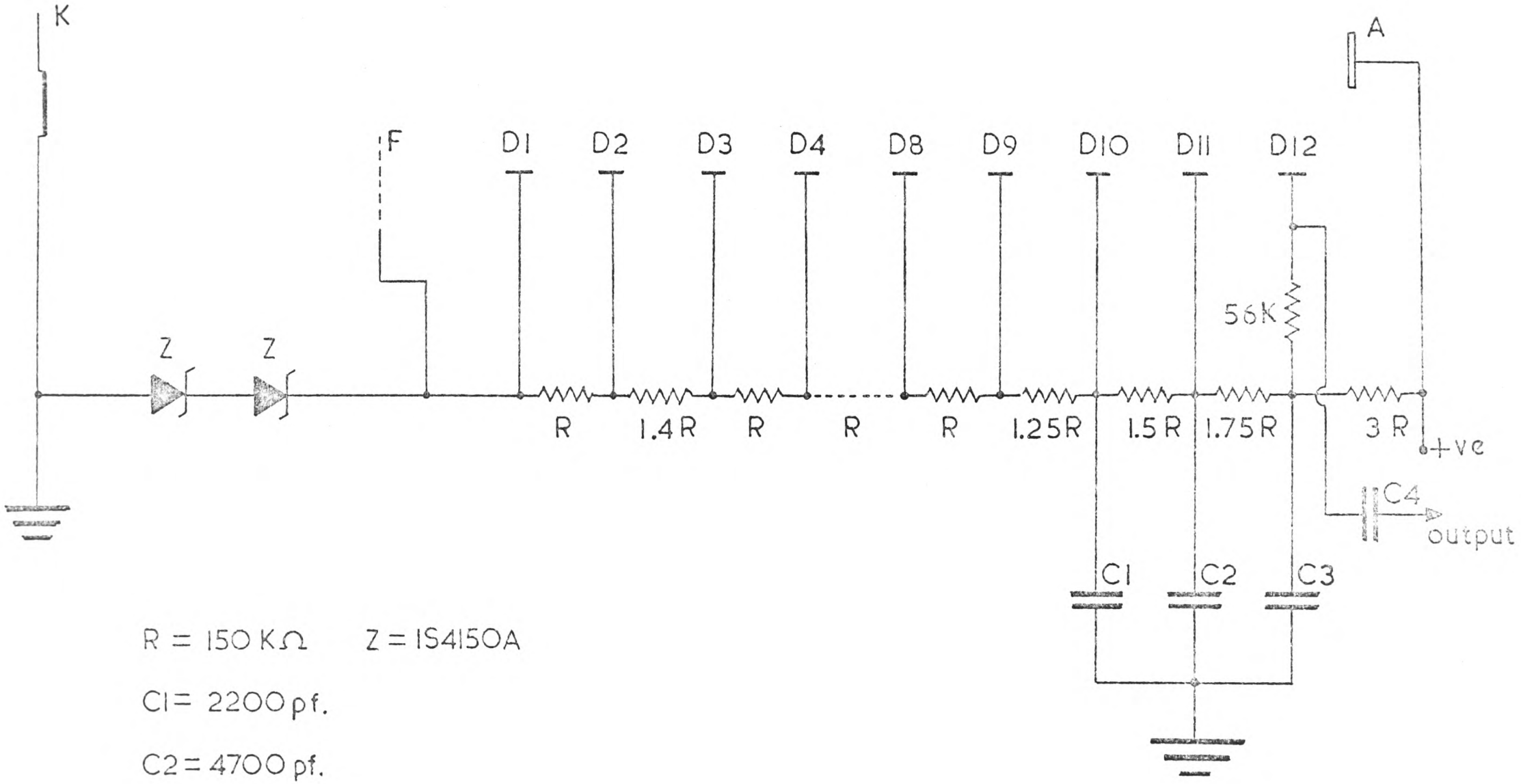

R = 150 KΩ Z = IS4150A

C1 = 2200 pf.

C2 = 4700 pf.

C3 = 10000 pf.

C4 = 10000 pf.

Fig.19. Dynode chain of the 9814B photomultiplier.

Fig.20. Dynode chain of the 56AVP photomultiplier.

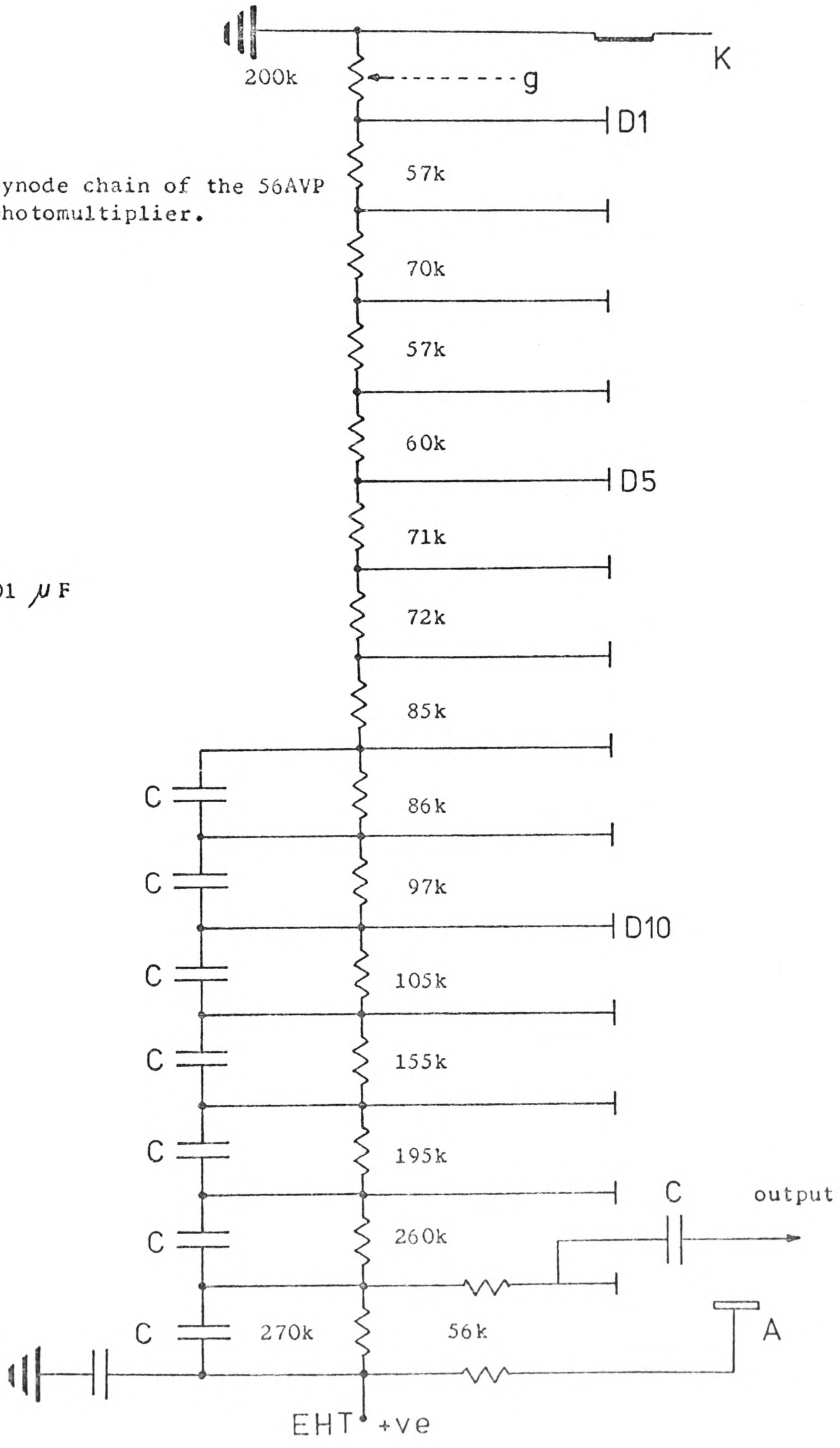

Laben 512 channels pulse height analyser. The energy calibration shown in figure 21, obtained with the photomultiplier arrangement assigned to one of the stilbene detectors, indicates good linearity at the 12th dynode of the 9814B photomultiplier up to an anode-to-cathode voltage of 1500v. Similar results were obtained with the other two photomultiplier arrangements.

The resolution of the photomultiplier arrangement was determined from the peak-to-valley ratio taken from the Co^{60} spectrum. A reasonably good peak-to-valley ratio (≈ 2) was obtained with the photomultiplier arrangement whose calibration curve is given in figure 21. Similar ratios were obtained with the other two photomultiplier arrangements.

The gain stability of the photomultipliers was also investigated. The time gain stability test was performed with the 2" x 2" NaI(Tl) crystal coupled onto the photomultipliers in turn, and a Cs^{137} gamma source. After the photomultiplier system warmed up, the pulse height spectra were recorded at one hour intervals for a period of thirteen hours. The mean gain deviation measured with this procedure was less than 1% for each of the three photomultiplier arrangements. The count rate stability test was performed with the same NaI(Tl) crystal and Cs^{137} source. In this test, the photomultiplier was operated, alternatively, at approximately 10^3 and 10 counts per second and the corresponding spectra were recorded. The gain shift due to this effect was under 1% for each photomultiplier arrangement.

Fig.21. Linearity test of a 9814B photomultiplier performed with a NaI crystal.

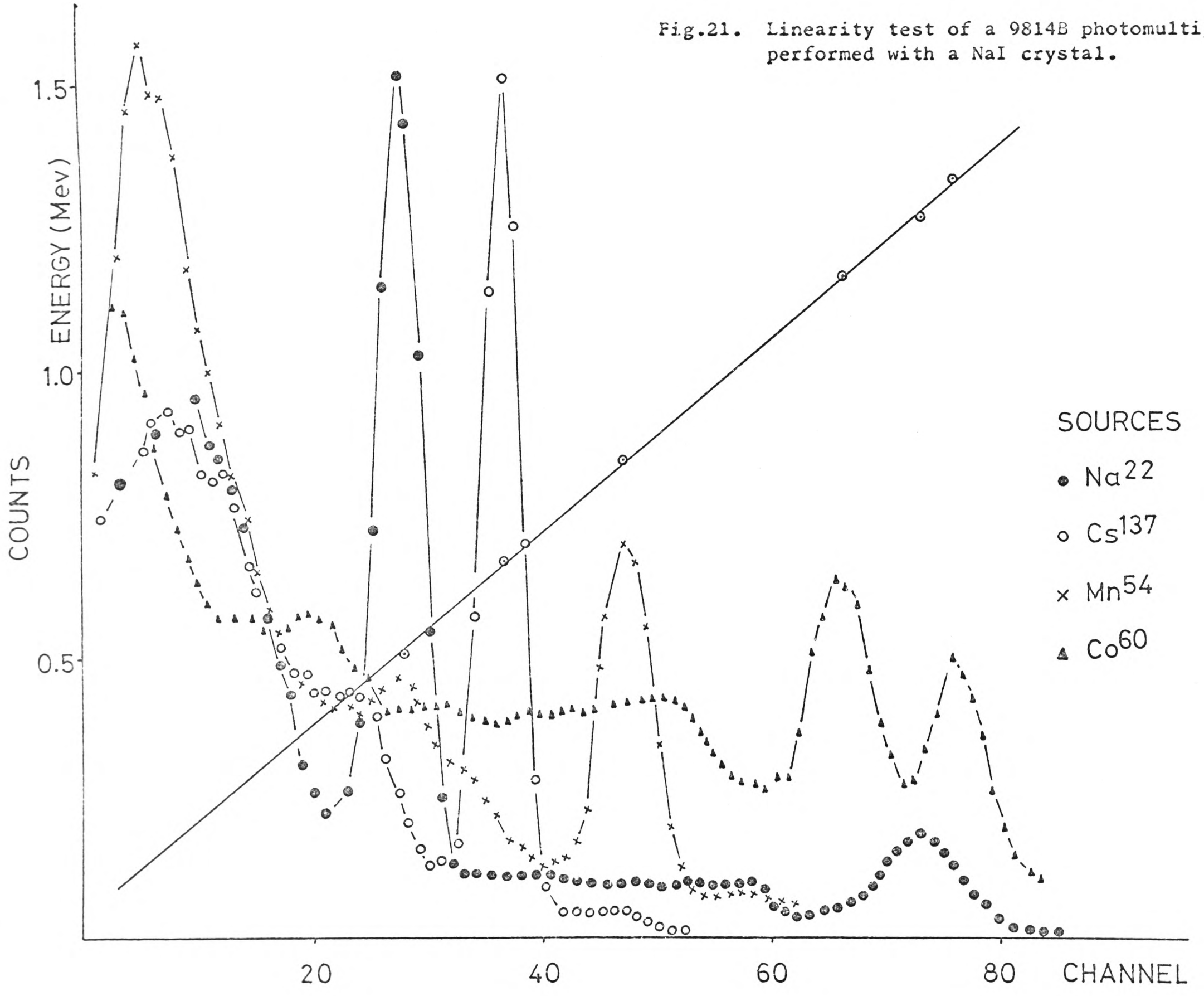

3.2.2 Performance of the zero crossing pulse shape discrimination method.

In order to check the performance of the pulse shape discrimination circuits and the electronics associated with each stilbene crystal, a standard cylindrical 2" x 2" NE213 liquid scintillator was employed. The equipment associated with the collimated beam monitor was tested directly with its NE213 liquid scintillator.

The electronic system associated with each scintillation detector is shown in figure 22. The linear pulses from the last dynode of the photomultiplier, after passing through the preamplifier, were used for both a linear amplifier and a pulse shape discrimination unit. The output pulses from this latter unit were fed simultaneously to a discriminator (P.S.D. discriminator) and to a Laben 512 channels pulse height analyser. The output pulses from the linear amplifier were fed to another discriminator, (linear discriminator). Both linear and PSD discriminators contained variable delays up to 3 μsec so that the optimum time relation between linear and PSD pulses could be obtained for the coincidence circuit. The resultant coincidence pulses were shaped by a pulse driver to meet the characteristics required by the coincidence input of the multichannel pulse height analyser.

P/A - preamplifier AMP - amplifier DISC - discriminator

PSD - pulse shape discrimination circuit

AND - coincidence circuit

DRIV - pulse shaper

PHA - pulse height analyser

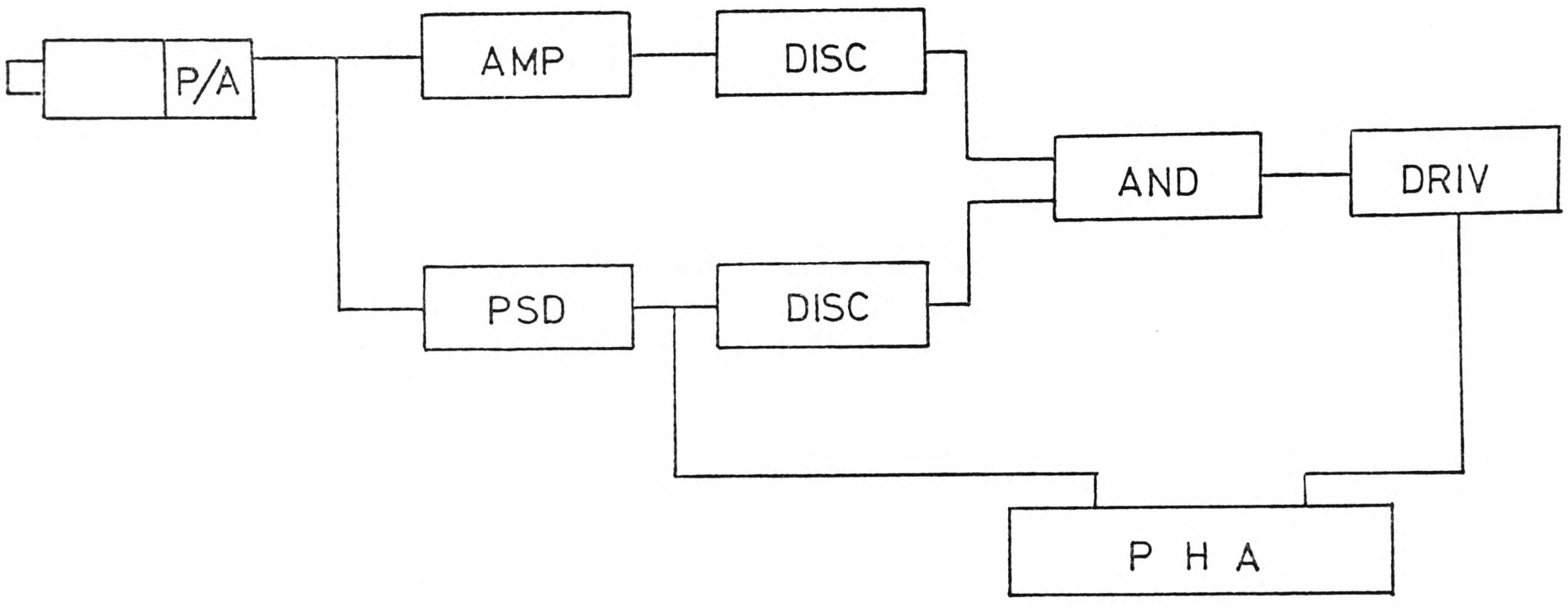

Fig.22. Block diagram of the zero crossing time pulse shape discrimination system.

The spectrum of the PSD pulses, using an Am^{241} - Be source, was displayed on the pulse height analyser being gated by the coincidence pulses. The linear discriminator threshold was set at the first Compton edge of a Na^{22} spectrum obtained with a EHT photomultiplier voltage of 1500 v. The EHT voltage was varied until the optimum separation between neutron and gamma peaks was obtained, readjusting then the linear discriminator threshold to the 340 kev Compton edge of the Na^{22} spectrum. Figure 23 shows the spectrum obtained with the photomultiplier and electronics system assigned to one of the stilbene crystals.

The final step was to set the PSD discriminator threshold to the valley between the two peaks to reject pulses due to gamma rays, observing that the settings of the discriminator delays were not inhibiting pulses due to neutrons. The former condition was checked using a Na^{22} gamma source and it was observed that the PSD spectrum did not show any gamma peak. The last condition was checked by comparing the number of counts under the neutron peak in the PSD spectra gated, respectively, by shaped linear pulses and coincidence pulses.

From figure 23, the figure of merit for that particular system was M = 1.33, which according to McBeth et al [82] gives a theoretical gamma rejection ratio better than 750 : 1, assuming 100% neutron detection efficiency. Similar figures of merit were obtained for the systems of the other two scintillators.

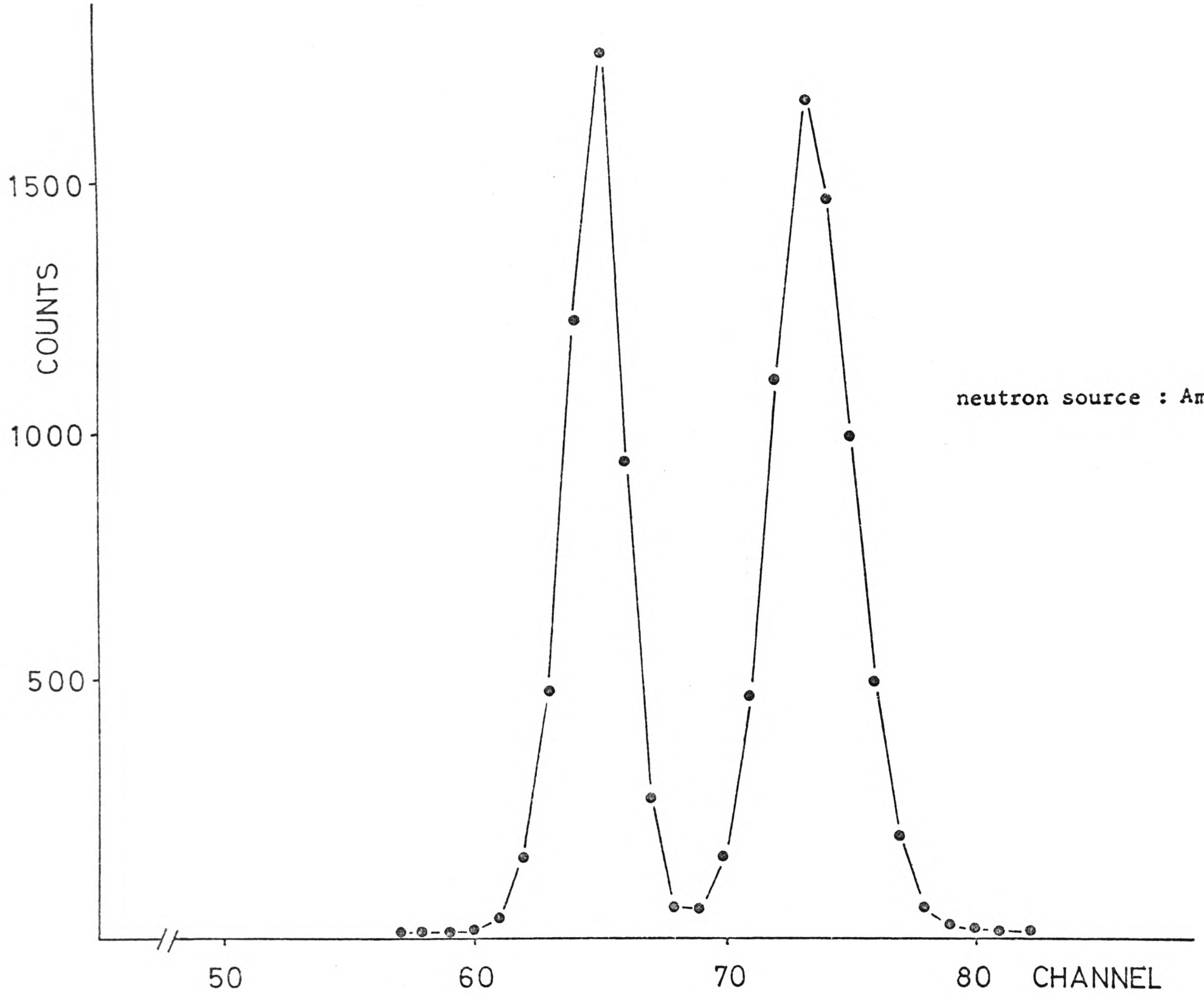

Fig.23. PSD spectrum obtained with a 9814B photomultiplier coupled to a NE213 liquid scintillator

Once the linearity, stability and PSD performance of the system associated with each stilbene crystal were tested, the crystals were mounted on the photomultipliers and all the tests described were repeated, with similar results, for the three detectors. Finally, the possible energy dependence of the pulse shape discrimination systems was investigated by observing, separately, the PSD spectra due to gamma rays emitted from Na^{22}, Cs^{137} and Mn^{54}. The different PSD spectra obtained with the different gamma sources did not show any shift nor change in shape in the normalised gamma peak.

3.2.3 The electronic set-up of the first polarimeter.

As mentioned before, the first polarimeter is based on four detectors. Two of them are for detecting neutrons scattered from the lead sample and the other two are used for monitoring purposes; one is used to monitor neutrons coming through the collimator and the other one is for monitoring the neutron yield from the target.

The target yield monitor, common to both polarimeters, was a slow neutron detector, insensitive to gamma rays. This detector was based on a NE400 scintillator consisting of a grooved disc of Boron polyester, with ZnS as scintillator, of 25 mm diameter and 1.2 mm active layer. This detector was coupled to a EMI 6097B and then surrounded by 10 cm of paraffin wax to moderate fast neutrons.

A simplified block diagram of the electronics set-up of the first polarimeter of the present work is shown in figure 24. The two stilbene detectors and the collimated beam monitor have identical circuitry. The pulses from these three detectors were fed to the Laben 512 channel pulse height analyser, through its mixer, and collected simultaneously in three of the four sections of the pulse height analyser memory. To get the optimum time relationship between the PSD pulses and the gating pulses to be analysed a delay of about 3 μsec was required in series with the input to the pulse height analyser. The pulses from the target yield monitor were not fed to the pulse height analyser, but to one of the seven scalers forming part of the Line - Printer System mentioned in section 2.3.3 and extensively described in reference 19.

The coincidence pulses from the stilbene detectors and collimated beam monitor were also fed to scalers in the Line - Printer System, which controlled the "stop start" of the scalers and printed the numbers registered in the scalers at the end of the present time. Thus it was possible to check at any time the PSD spectra in the pulse height analyser without altering the preset running time. The coincidence pulses from the collimated beam monitor were also fed to a ratemeter to provide a continuous sampling mode to help in the setting up and readjusting of the accelerator.

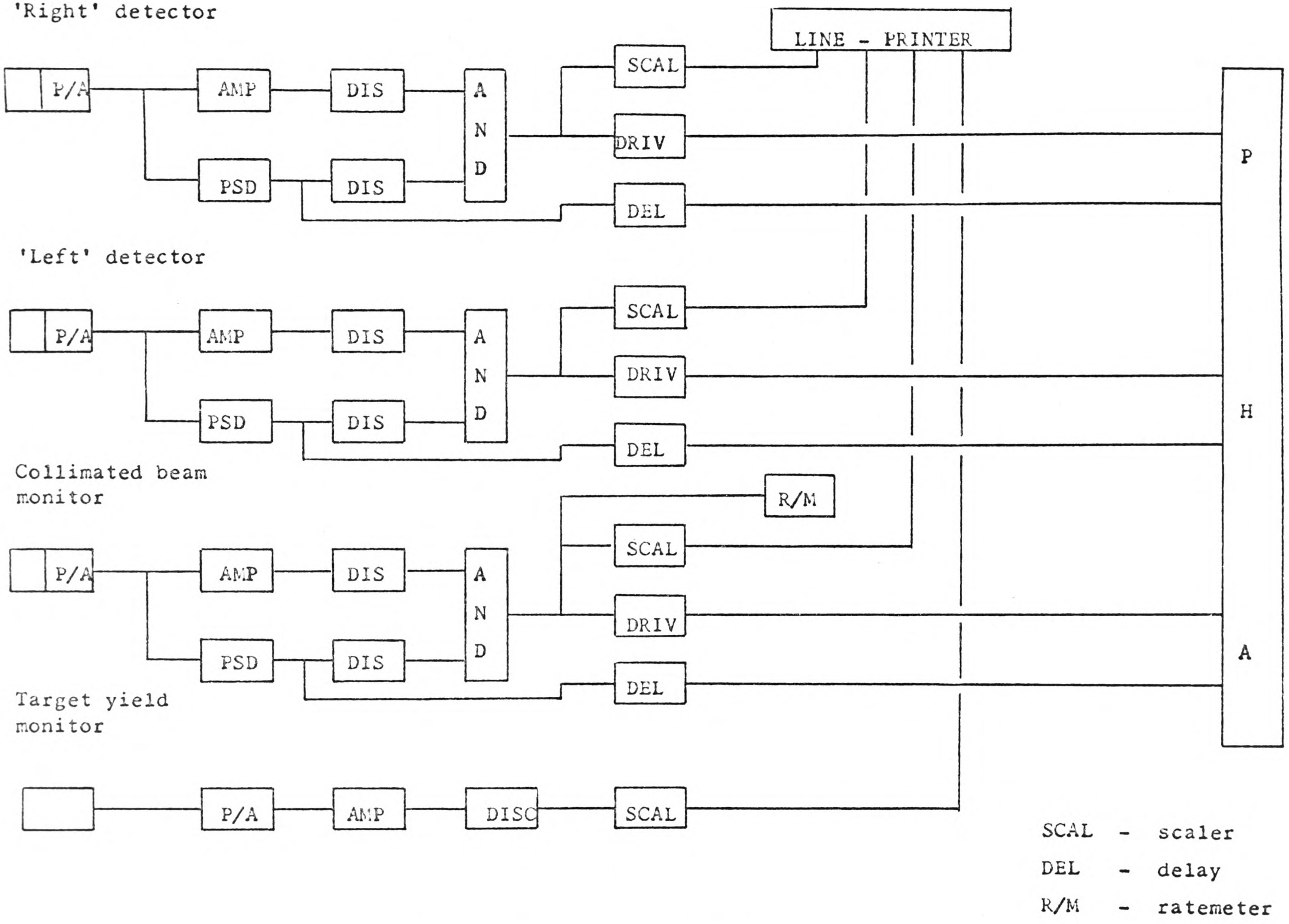

Fig.24. The electronic system associated with the first polarimeter.

Some of the electronic units used in the present work, in both polarimeters, are based on Davie's designs. These units proved throughout the experiment to be reliable. A description of the various units used and of the different tests performed on them can be found in Davie's thesis [87].

3.3 Owen method of pulse shape discrimination.

Owen [89] developed the first pulse shape discrimination method for use with organic scintillators. This method was later modified by Batchelor et al [90] and so it is commonly referred to as the Owen - Batchelor method. The principle of this technique is based on the fact that in organic scintillators, the ratio of the slow component of the light output to the total light output is different for protons and electrons.

In this technique, the anode of the photomultiplier is maintained only a few volts positive with respect to the last dynode, on which a pulse, hereafter called the saturated pulse, is developed. The arrival of the photomultiplier current pulse at the last dynode produces a space charge saturation condition in the region between this dynode and the anode. During the initial fast component of a pulse, due to an exciting electron, a limitation on the current passing from the last dynode to anode occurs due to space charge saturation effect, and so a large proportion of the multiplied charge cannot leave the last

dynode, which is driven to a negative potential. Later, during the lower intensity part of the slow component, the electron current arriving at the last dynode is small and the current to the anode is no longer saturated, so that the last dynode has only a small positive swing due to the loss of its secondary electrons. In the case of a pulse due to an exciting proton, the much less intense fast component does not drive the last dynode so far to the space charge saturation point and as a result a large positive swing due to the secondary electron emission is produced.

The pulse shapes at the last dynode corresponding to the two cases discussed above are illustrated in figure 25, where it is clear that a discriminator threshold set on this positive part of the last dynode signal permits a distinction to be made between the pulses due to neutrons (i.e. recoil protons) and gamma rays (i.e. recoil electrons).

Pulse shape discrimination based on the Owen technique was applied to the three neutron detectors forming the second polarimeter of the present experiment. The preliminary tests performed on the electronics associated with each neutron detector are presented below before describing the performance of the pulse shape discrimination system.

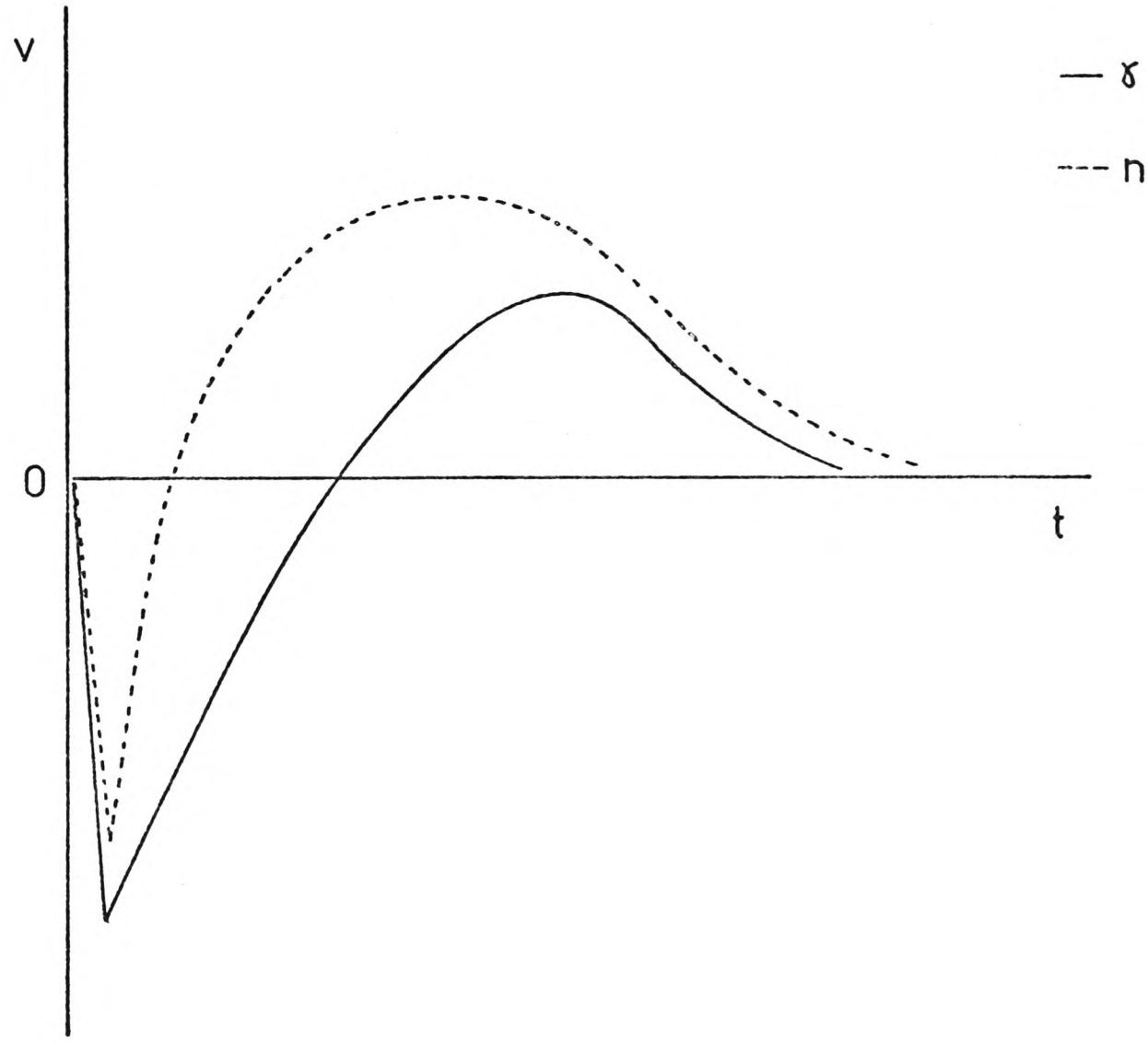

Fig.25. Last dynode pulse shapes due to gamma ray and neutron events in the Owen pulse shape discrimination method.

3.3.1 Preliminary tests.

The three NE213 liquid scintillators, constructed specially for the second polarimeter, employed EMI 6097B photomultipliers and the dynode chain used is shown in figure 26.

The linearity of the photomultiplier - preamplifier arrangements was tested in a similar manner to that described in section 3.2.1. For this purpose, the pulses from the second last dynode, hereafter called linear pulses, were fed to a preamplifier kept inside the detector assembly container. These pulses, after passing through the amplifier, were analysed in a Laben 512 channels pulse height analyser. The energy calibration curve (Fig. 27) obtained with the photomultiplier arrangement assigned to one of the side detectors indicated good linearity at the 10th dynode of the photomultiplier up to an anode-to-cathode voltage of 1100 v. Similar results were obtained with the other two photomultiplier arrangements.

The gain stability test of the three photomultiplier arrangements was performed as described in section 3.2.1. A mean gain deviation less than 1% was obtained, in each case, from the time gain stability test. Similarly, the gain shift due to count rate effect was less than 1% for each photomultiplier arrangement.

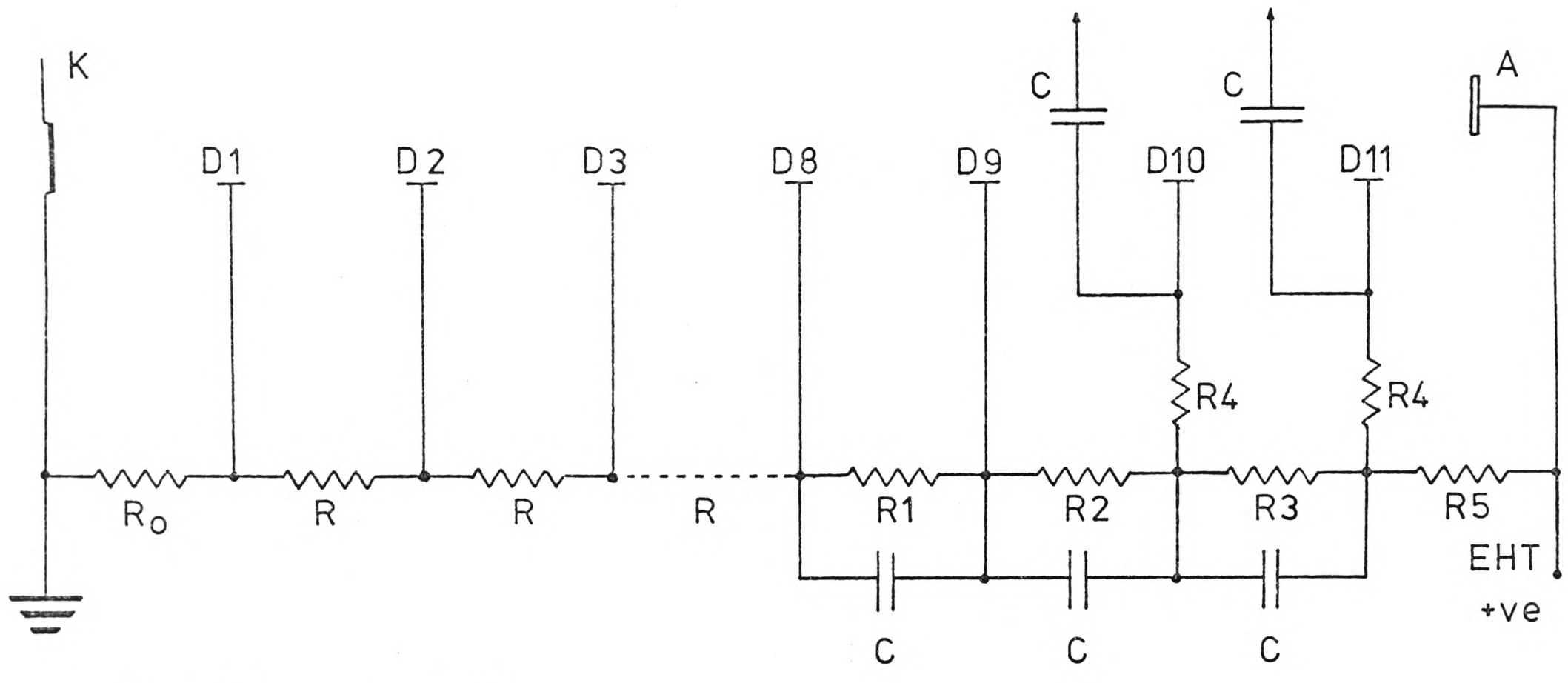

R_o	= 150k	R_3	= 180k
R	= 82k	R_4	= 56k
R_1	= 120k	R_5	= 1.5k
R_2	= 150k	C	= 0.01μF

Fig.26. Dynode chain of the 6097B photomultiplier.

Fig.27. Linearity test of a 6097B photomultiplier performed with a NaI crystal.

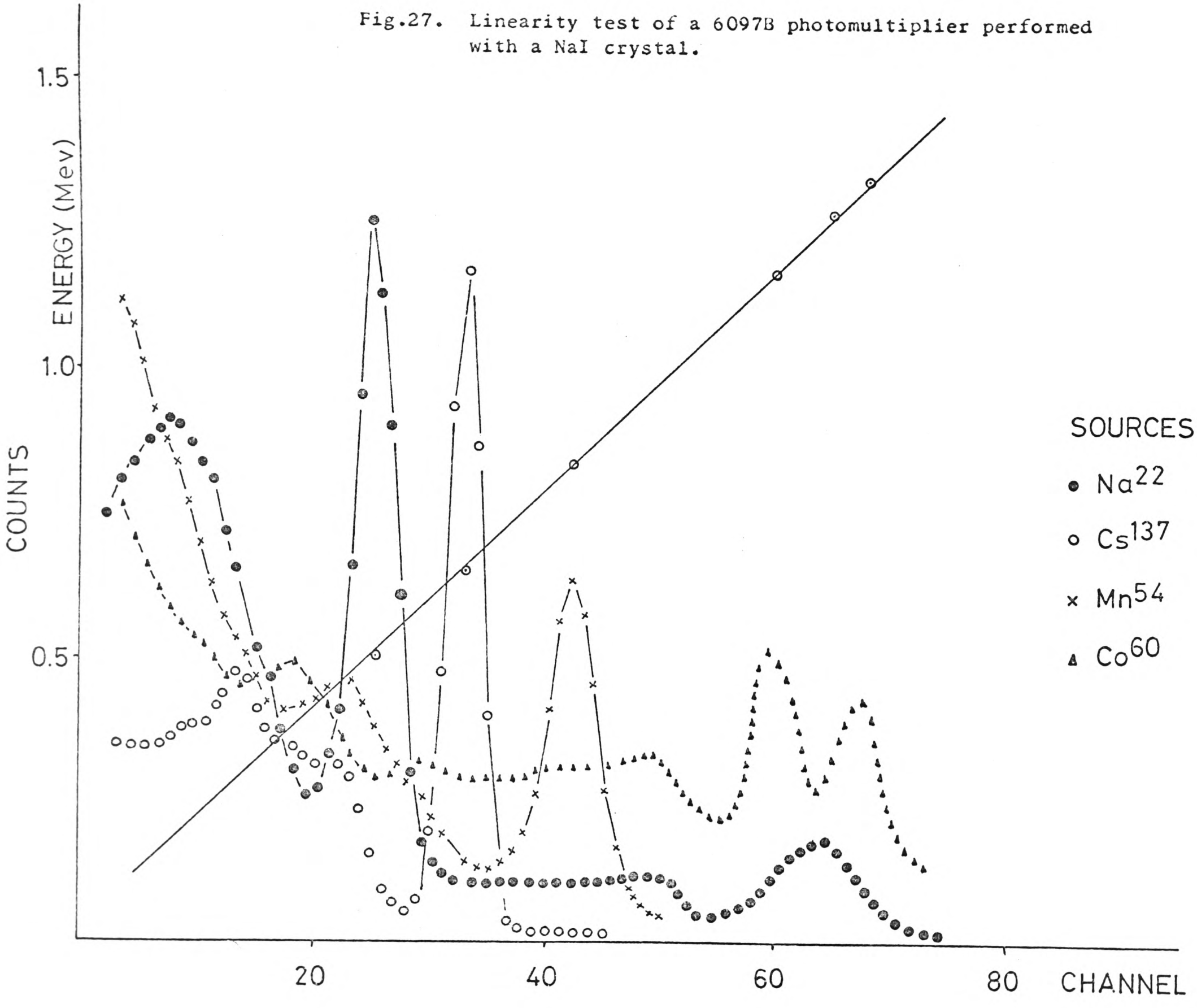

3.3.2 Performance of the Owen pulse shape discrimination method.

The tests on the performance of the pulse shape discrimination systems were made with the final liquid scintillators mounted on their respective photomultiplier assemblies, so that the performance of each liquid scintillator, in itself, could be investigated.

The procedure of these tests was similar to that described in section 3.2.2. The electronic system associated with each liquid scintillator detector is represented in figure 28. Two outputs, linear and saturated, were taken from the dynode chain and coupled to their respective preamplifiers kept inside the photomultiplier assembly container. These preamplifier pulses, after amplification, were fed to the linear and saturated discriminators respectively. These discriminators, as mentioned before, contained variable delays up to 3 μsec so that the optimum time relation between linear and saturated pulses could be obtained for the coincidence circuit. The coincidence pulses were shaped to meet the requirements of the coincidence input of the pulse height analyser.

The spectrum of the saturated pulses, using a Cf^{252} neutron source, was displayed on the pulse height analyser gated by the shaped coincidence pulses. The linear discriminator threshold was previously set at the first Compton edge of a Na^{22} linear spectrum obtained with a photomultiplier voltage (PMT) of 1050 v.

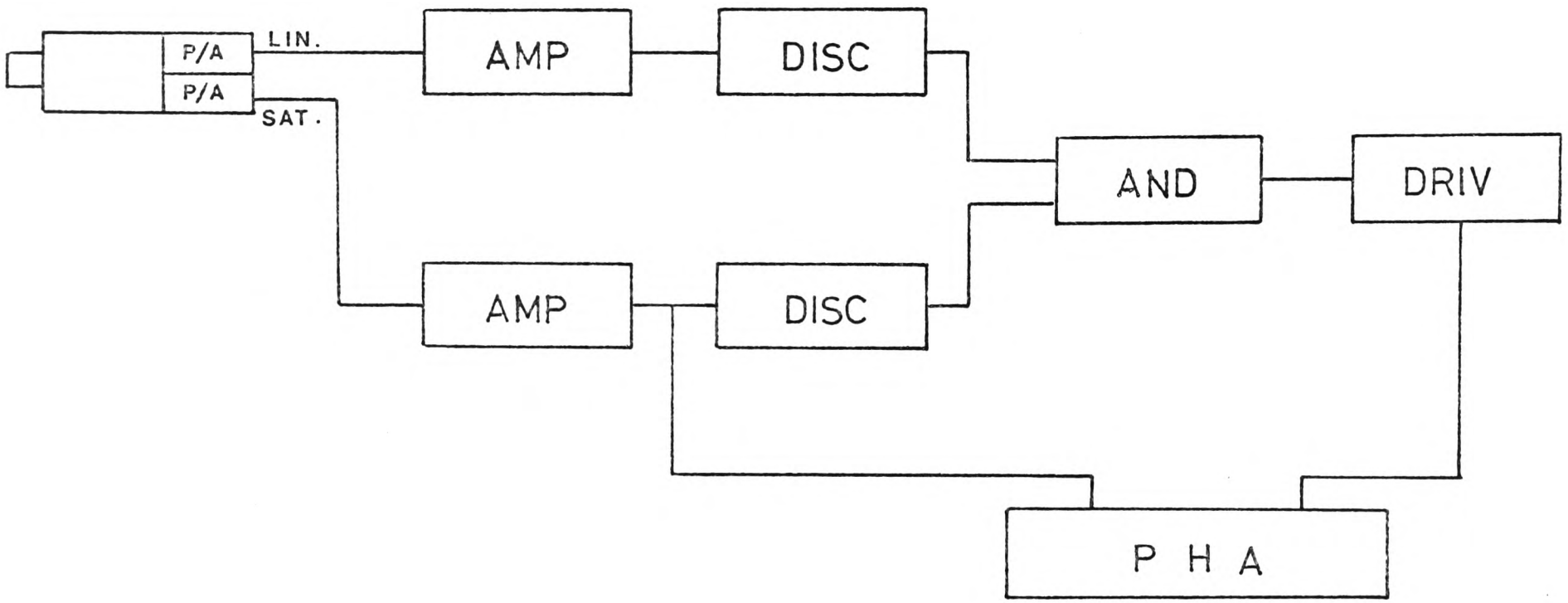

Fig.28. Block diagram of Owen pulse shape discrimination system.

This EHT voltage was varied until the optimum separation between gamma and neutron peaks was obtained, readjusting then the linear discriminator threshold to the 340 kev Compton edge of a linear Na^{22} spectrum. Figure 29 shows the spectrum obtained with the photomultiplier and electronic system assigned to one of the side detectors. Finally, the saturated discriminator threshold was set to the valley between gamma and neutron peaks, observing that the relative delays on the discriminator were not inhibiting pulses due to neutrons. These two last conditions were checked as described in section 3.2.2.

From fig. 29, the measured figure of merit for that particular system was M = 1.30, which represents a theoretical gamma rejection ratio better than 750 : 1. The other two systems produced a similar figure of merit.

Here, too, the possible energy dependence of the pulse shape discrimination systems was investigated in a similar manner as that described in section 3.2.2. The results of these tests indicated that the three pulse shape discrimination systems based on the Owen technique were not energy dependent in the energy region investigated.

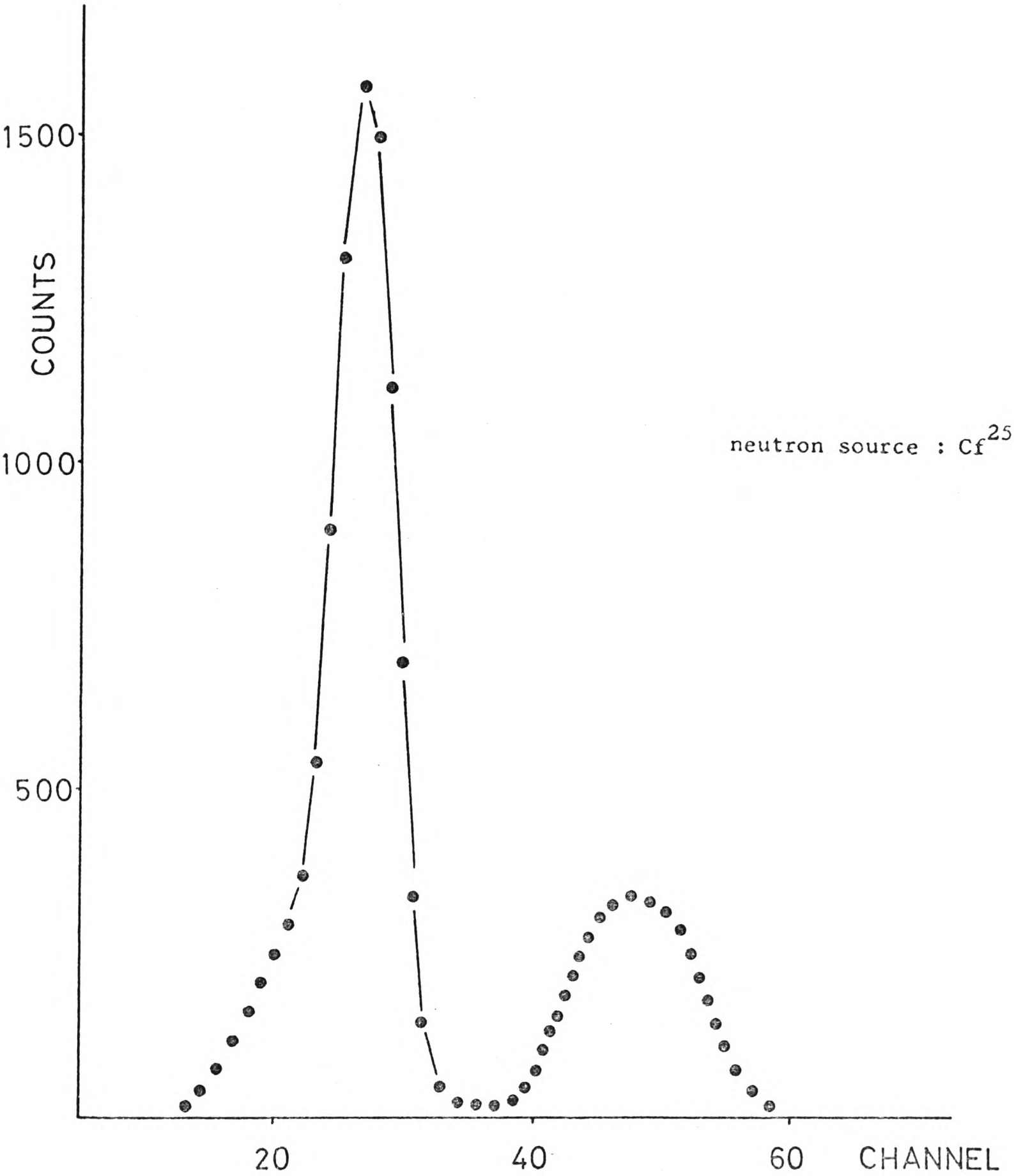

Fig.29. Owen PSD spectrum obtained with a 6097B photomultiplier coupled to a NE213 liquid scintillator and a Cf^{252}.

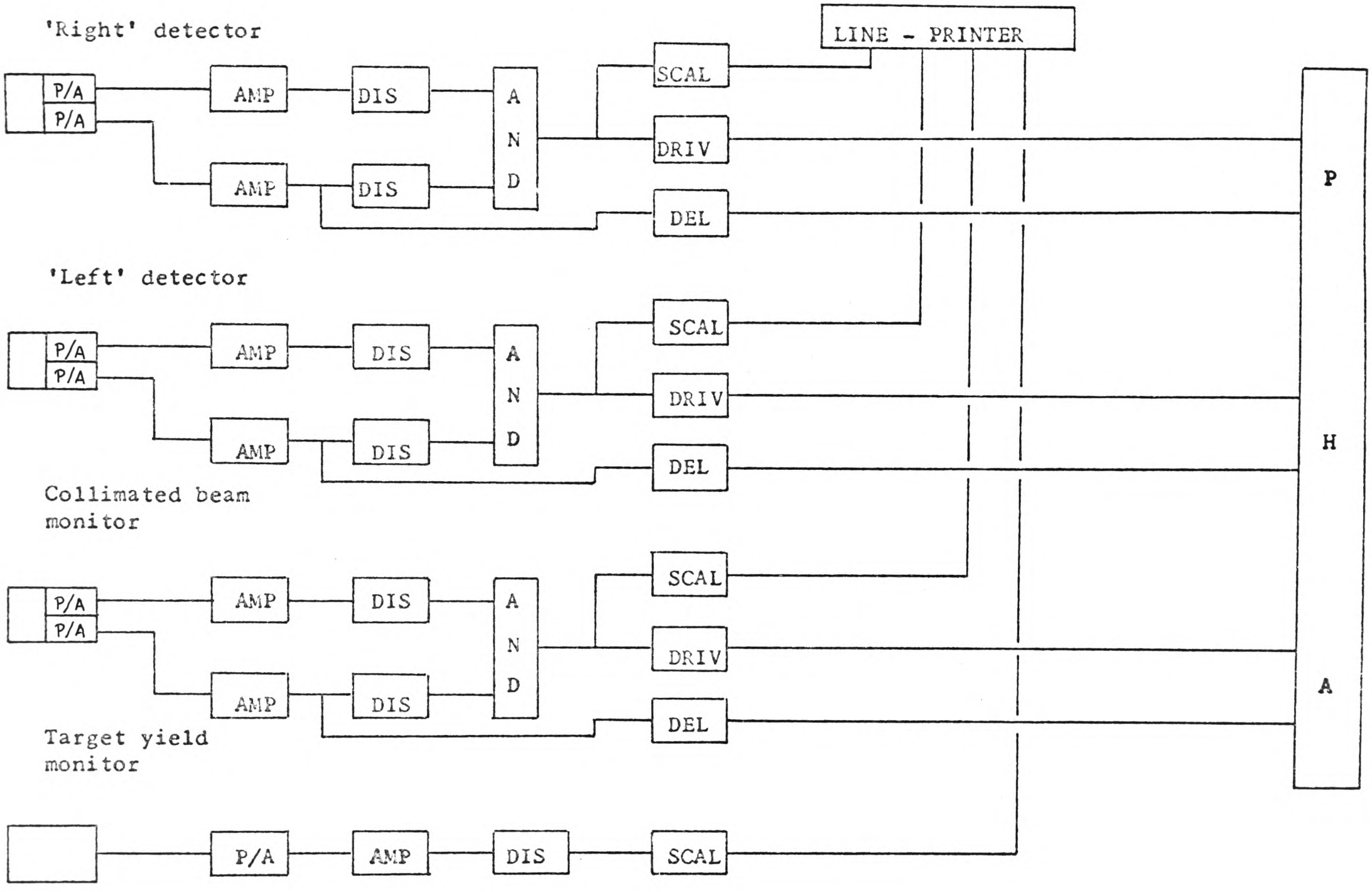

Fig.30. The electronic system associated with the second polarimeter.

3.3.3 The electronic set-up of the second polarimeter.

The block diagram in figure 30, which is self explanatory, shows the associated electronic equipment used with the second polarimeter of the present work. The setting up and checking of the electronics were made with the Laben 512 channels pulse height analyser used for the first polarimeter. Each scaler, coupled to the output of each coincidence circuit, belonged to the Line-Printer System, which controlled the stop start of the scalers and printed the numbers registered in them at the end of the preset running time.

CHAPTER 4.

CHAPTER 4.

DETERMINATION OF THE NEUTRON BACKGROUND AND THE EXPERIMENTAL PROCEDURE.

Small angle scattering systems used in the determination of the polarization of fast neutrons require the side detectors to be placed close to the fine neutron beam and have, therefore, a severe neutron background. The nearest position of the side detectors to the collimated neutron beam axis is determined by the neutron beam profile, which also defines the effectiveness of the geometrical shielding of the collimator. This chapter describes the beam profile measurements performed on both polarimeters, a detailed investigation of the neutron background found during the actual experiment and some preliminary polarization measurements on neutrons from the $H^2(d,n)He^3$ reaction.

4.1 Measurement of the beam profile.

4.1.1 Horizontal beam profile.

A description of the beam profile measurements performed on the first polarimeter is given in this section. A similar procedure was followed for the second polarimeter.

Before proceeding with the beam profile measurements, the alignment of the polarimeter was checked as described in section 2.3.5. During this alignment the centre of each stilbene crystal, indicated by the crossed lines inscribed on each aluminium can, was aligned with the collimator axis and the corresponding position of the support of the detector in turn, relative to the track, was recorded.

The experimental arrangement for the determination of the horizontal beam profile was the same as that for the detection of scattered neutrons, but the lead sample was out of the beam. At this stage the electronic system associated with each detector of the polarimeter was checked as described in chapter 3 and a final check on PSD settings was made using the neutron beam from the $H^2(d,n)He^3$ reaction.

The beam profile was measured, twice, by scanning the beam by each of the two stilbene detectors in turn. This measurement was made by moving the stilbene detector in 2.5 mm steps across the beam, while the other was placed at a distance of 12 cm from the centre of the beam in order to avoid scattering from it into the detector scanning the beam. The time for each measurement was 256 sec at the end of which the readings of the scalers for the target yield monitor and stilbene detector measuring the beam were recorded. The number of counts recorded in the scaler for this stilbene detector were normalised with respect to the number of counts registered by the target yield monitor. The

normalised relative counting rate as a function of the detector distance from the centre of the beam is plotted in figure 31 for the two stilbene detectors.

The beam profile obtained with the right detector shows a lower slope on the right hand side of the curve due to neutrons scattered into the stilbene crystal from the photomultiplier and material in the detector assembly when they intercept the direct neutron beam. This is also shown in the other side of the beam profile obtained with the left detector. Excluding this effect, the good agreement of the two curves proved that the polarimeter was horizontally well aligned as required for the experiment. The position on the track of each stilbene detector in which the counting rate was a maximum was compared with the position of the same detector recorded when the centre of the stilbene crystal was optically aligned with the collimator axis. A difference of no more than 1 mm was found between these two positions for each stilbene detector.

Due to the length of the stilbene crystal, 3.5 cm, and to the finite size of the beam, the curves given in fig. 31 do not represent the real dimension of the beam at the side detectors position. In order to obtain the real dimension of the beam the length of the stilbene crystal was subtracted from the total width of the curve. Figure 32 clarifies this argument; B represents the beam profile at the side detectors position and S represents the stilbene crystal moving from left to right.

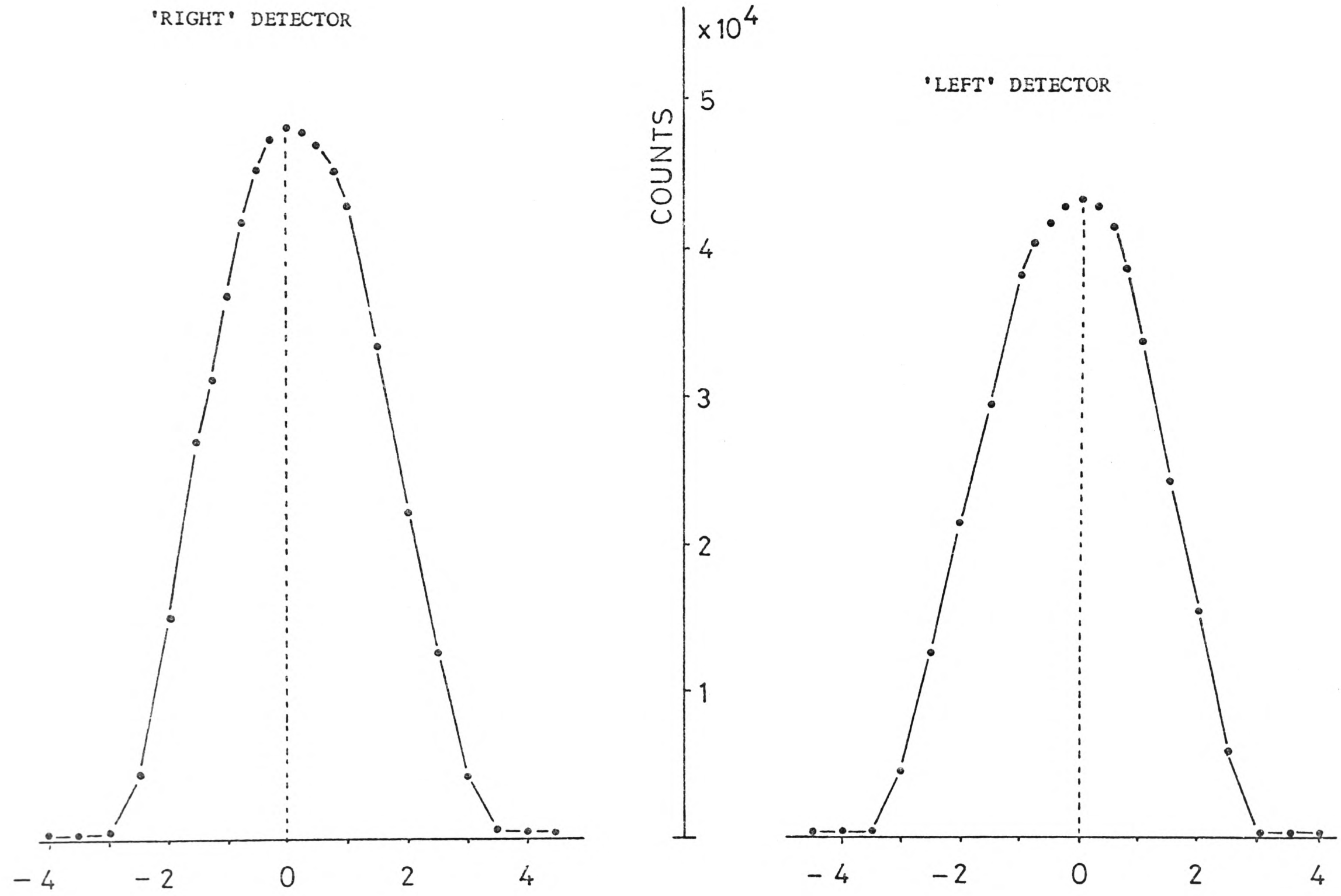

Fig.31. The horizontal beam profile in the first polarimeter as measured by each stilbene detector.

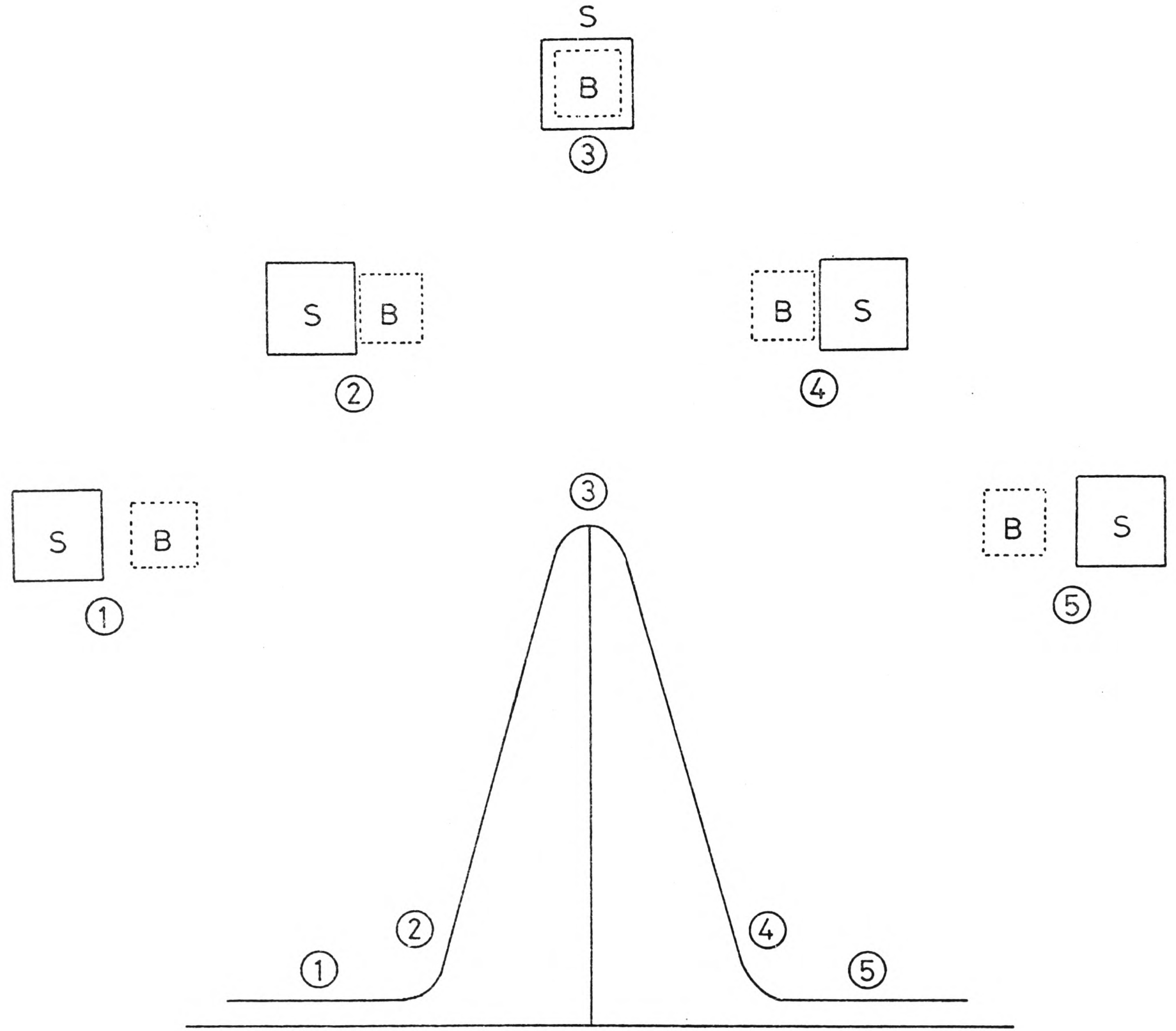

Fig.32. Beam profile measurements.

In position (1) the counting rate is due only to background; in position (2), when the stilbene crystal and beam just touch, the counting rate starts to increase linearly according to the overlapped areas of beam and crystal up to position (3) where the maximum counting rate occurs. As the movement of the crystal continues the counting rate decreases, passing by position (4) where crystal and beam just touch and the counting rate is near to background position (5). From position (2) to position (4) the crystal was moved a distance equal to the sum of the beam dimension and detector length. Therefore, it was concluded that the beam dimension at the side detectors position was 3.1 cm. A half of this width determined the closest position of the stilbene crystal to the beam axis.

Thus, the spread in the neutron beam at the side detectors position was $\pm$ 15.5 mm, which corresponds to an angle of 1.46° measured from the position of the scattering sample. The position of both side detectors for the experiment was chosen so as to have a minimum scattering angle of 1.8° which corresponds to a distance of 20 mm between the beam axis and the nearest point of each stilbene crystal to the beam axis.

An evaluation of the effectiveness of the shielding employed was made by taking the ratio of the counting rate at the position corresponding to 1.8° (i.e. background) to the counting rate at the beam centre (peak). This ratio was 1.6×10^{-3} for both side detectors.

As mentioned before, the second polarimeter was constructed in the late part of the present work, however, a brief description of the beam profile measurements performed on this polarimeter is given here. A similar procedure to that described above was followed. Preliminary beam profile measurements performed on this polarimeter produced a ratio of the background to peak counting rates of 3.9×10^{-3}, indicating that the shielding surrounding the polarimeter was rather poor. Further investigation on this neutron background problem indicated that the shielding at the side of the collimator near to the accelerator line was weak. The shielding in general was improved giving special attention to that particular region. Beam profile measurements made after the shielding was improved gave a ratio of background to peak counting rates of 2×10^{-3}, indicating that although the neutron background was higher than that found in the first polarimeter, it was still reasonable. The beam profile curves obtained with the two NE213 liquid detectors are shown in figure 33. These curves, too, present a lack of symmetry due to the effect described above.

From fig. 33 the dimension of the beam, after correction for the finite dimension of the NE213 liquid scintillator, turned out to be 29.4 mm. Hence, the spread in the neutron beam was $\pm$ 14.7 mm, which corresponds to an angle of 1.39° measured from the position of the scattering sample. The small difference in the beam dimension for the two polarimeters was due to the different distances between target and collimator in the two systems.

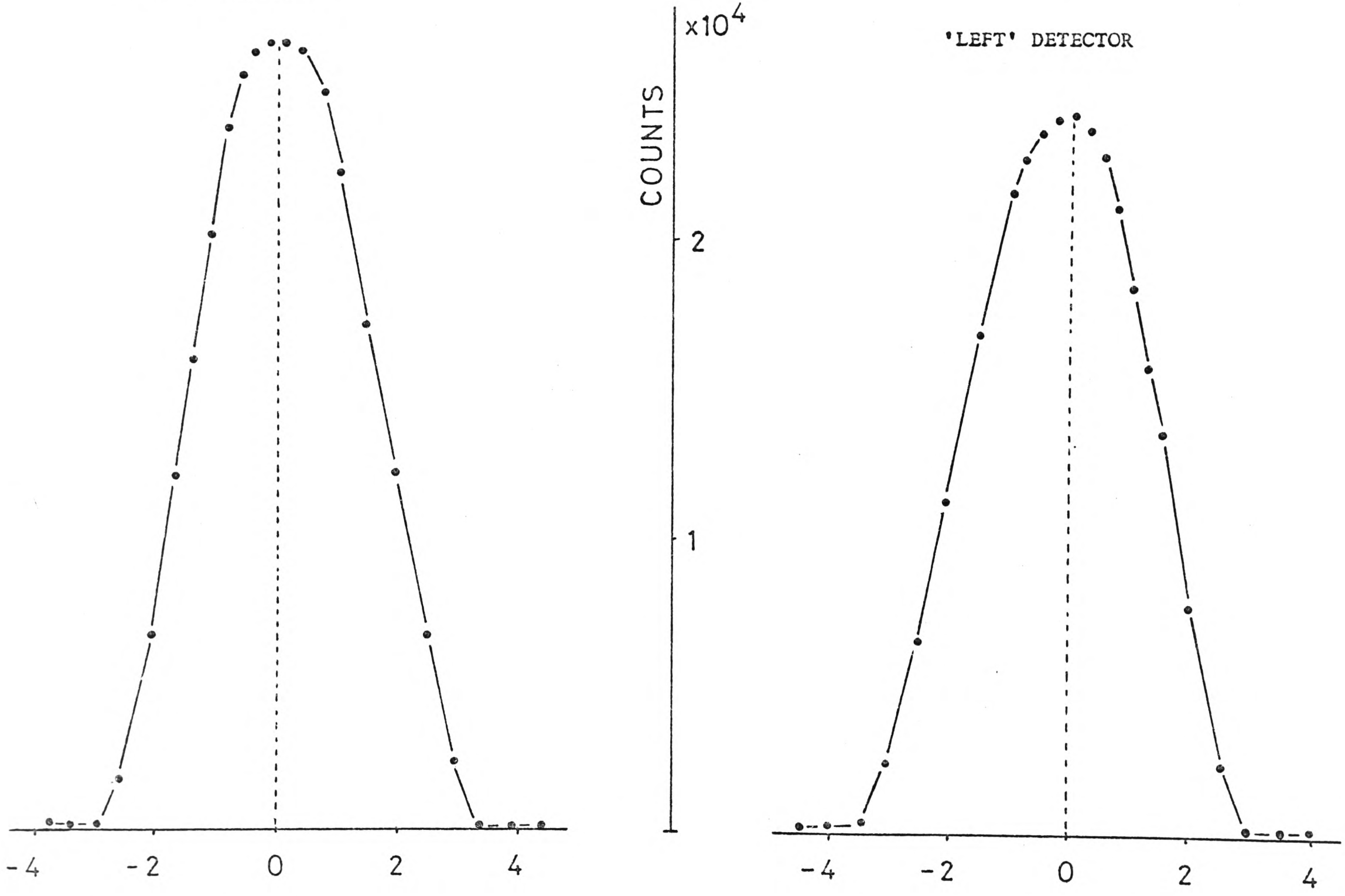

Fig.33. The horizontal beam profile in the second polarimeter as measured by each side detector.

The position of both side detectors for the experiment was chosen so as to match the corresponding geometry of the first polarimeter, that is, to have the same angular interval of scattering angles. Thus, a minimum scattering angle of 1.8^{o} was also chosen for the second polarimeter.

4.1.2 Vertical beam profile.

In order to have a better knowledge of the beam behaviour, the vertical beam profile for the first polarimeter was also measured. The experimental arrangement used for this purpose was based on a 3 mm x 20 mm x 30 mm stilbene crystal with a 20 mm x 30 mm face in optical contact with the photocathode of a 56 AVP photomultiplier and the other faces of the crystal coated with titanium dioxide paint as diffuse reflector. An aluminium can of 0.5 mm thickness provided mechanical protection and a light tight cover for the crystal, which was accurately located on the photocathode of the photomultiplier by means of a piece of perspex fixed in the bottom of the can. For alignment purposes a line indicating the longitudinal axis of the photomultiplier and the longest axis of the crystal was inscribed on the aluminium can.

The entire detection unit including stilbene crystal, photomultiplier and voltage divider was encased in a detector assembly similar to that described in section 2.3.4. This detector assembly could move on accurately machined rails with a

screw drive to set the position of the stilbene crystal relative to the beam axis.

The rails were mounted vertically at the rear of the polarimeter so as to have a distance of 153 cm between the exit of the collimator and the stilbene detector assembly. For this operation the collimated beam monitor was removed from its stand and the rails were accurately aligned relative to the collimator axis by means of a telescope. This alignment was checked by observing that the reference line inscribed on the aluminium can containing the stilbene crystal remained aligned with the vertical collimator axis along its travel. Figure 34 shows a photograph of the experimental arrangement used for the vertical beam profile measurements.

Gamma ray discrimination based on the Owen technique was applied to this detector and the final check on the pulse shape discrimination settings was made using the neutron beam.

The vertical beam profile measured at a distance of 153 cm from the exit of the collimator is represented in figure 35. The spread in the neutron beam and the full width at half maximum (FWHM), as measured from the beam profile curve, were $\pm$ 37 mm and 46 mm respectively. Such a spread in the neutron beam corresponded to an angle of 1.49^{o} measured from the position of the scattering sample which is in very good agreement with the

Fig.34. Photograph of the experimental arrangement used to measure the vertical beam profile in the first polarimeter.

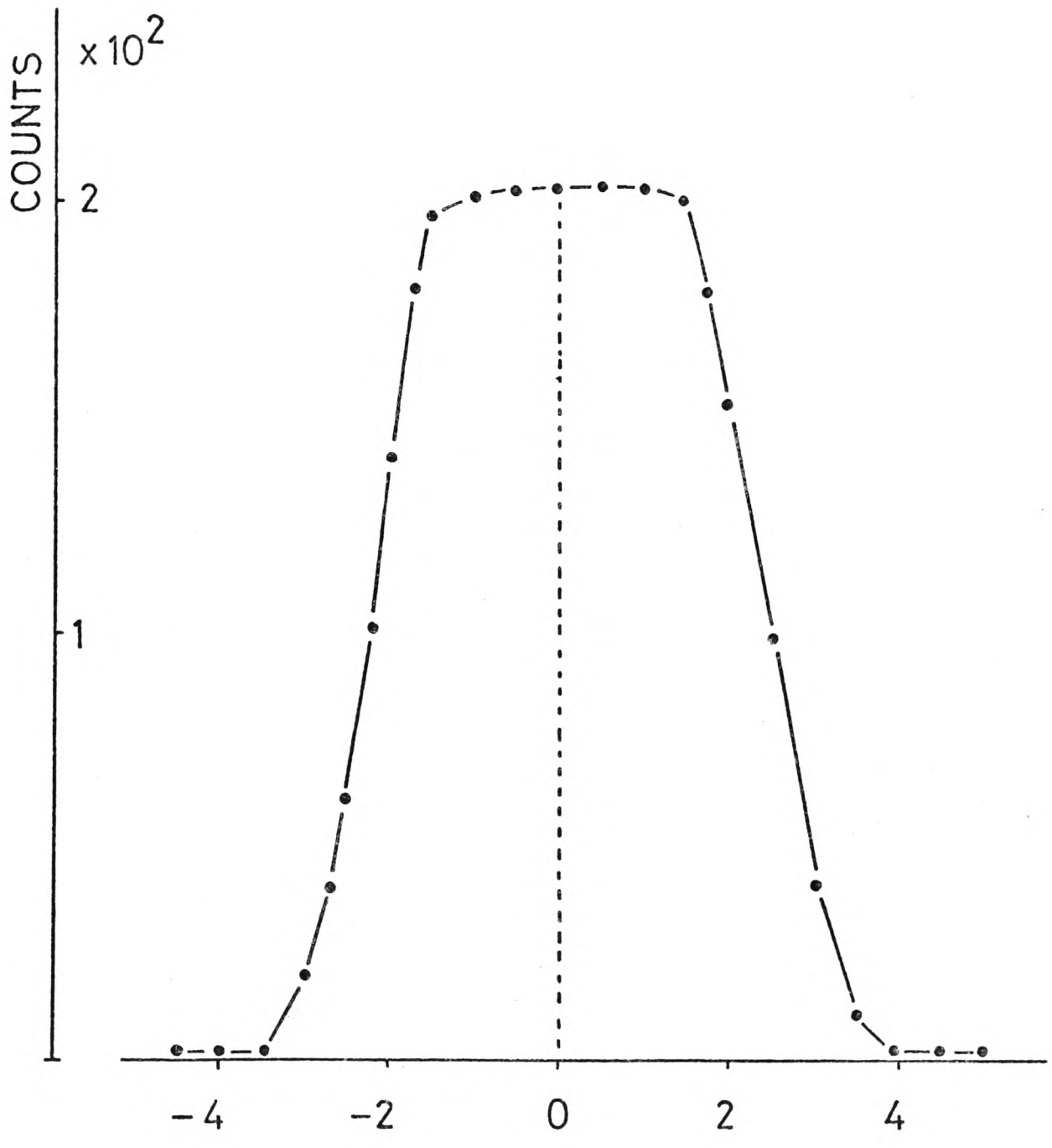

Fig.35. The vertical beam profile in the first polarimeter.

angle of 1.46° obtained from the horizontal beam profile. The FWHM corresponded to an angular divergence of the neutron beam of ± 0.45° which agrees with the solid angle defined by the exit of the collimator.

Thus, it was concluded that the optical alignment as carried out on the first polarimeter was reliable and that it would satisfy the requirements of the experiment. Hence, a similar alignment procedure was followed in the second polarimeter and there was no need to measure the vertical beam profile in this second polarimeter.

4.2 Determination of the neutron background.

As mentioned before, the neutron polarization in Mott - Schwinger systems can be calculated directly from the experimental total cross section and differential cross section values, which, in turn, depend on the precise determination of the neutron background. For this reason, a detailed investigation was carried out in order to measure the neutron background found in the first polarimeter during the actual experiment and draw from there a procedure to follow in this and in the second polarimeter.

For this investigation, the polarimeter was usually prepared so as to measure the polarization of neutrons from the $H^2(d,n)He^3$ reaction. Most of the tests were made for 340 kev deuterons incident on a thick Ti - D target, but different incident energies

below 500 kev were also employed. It was observed that the results of the tests reported here are generally applicable in the deuteron energy range of interest.

Because the origin of the neutron background at this stage was still uncertain, the measurements made involved equal counting times, usually 2000 sec., with the following conditions:

i) background sample

ii) scattering sample

iii) without any sample

The background sample was a lead sample with the same thickness (i.e. transmission) as the scatterer sample and which could be placed in and removed from the entrance of the collimator. The central idea of the use of this background sample is that because the possibility of an appreciable background contribution due to neutron scattering from the walls of the collimator and the air between the collimator exit and the side detectors, a determination of the counting rate with the scatterer sample removed could not give a true neutron background measurement. However, with the scattering sample removed and the background sample placed in the entrance of the collimator, the neutron flux incident on the air column between the collimator exit and the side detectors was subject to about the same attenuation as when the background sample was removed and the scattering sample put into place.

The three different measurements (i), (ii) and (iii) were usually repeated, sequentially, for a period of 40 hours, at the end of which an intercalibration of the detection efficiencies of the collimated beam monitor and the stilbene side detectors was made by placing each side detector in turn in the direct beam and removing it when the corresponding measurement for the collimated beam monitor was to be made. These intercalibration measurements, each of 200 sec. duration, were repeated until ten measurements with each of the three different detectors were completed.

At the end of each run with one of the three different conditions (i), (ii) or (iii), the number of counts registered in each scaler were printed out by the Line - Printer. The readings corresponding to the side detectors were normalised with respect to the collimated beam monitor, since it provided a true measure of the neutron flux passing through the collimator. Normalisation with respect to the target yield could not give accurate measurements because it monitored the flux from the target irrespective of the neutron flux passing through the collimator. In the case of the efficiency intercalibration measurements, the collimated beam monitor could not be used for normalisation because the flux incident on it was altered by the detector placed in the direct beam. During the experiment and the intercalibration measurements the PSD spectra were checked several times in the multichannel pulse height analyser.

The measurements gave, throughout the tests, a transmission of about 50% for both background and scattering samples. Typical ratios of the counting rates in the side detectors for condition (iii) to those for conditions (i) and (ii) were ≈ 1 and ≈ 0.7 respectively. The former ratio could possibly indicate that the background contribution due to neutron scattering by air, mainly in the region near the side detectors, was not appreciable, or that the decrease in counting rate in the side detectors due to the reduction of the neutron flux incident on the air column between the collimator exit and the side detectors was offset by neutron scattering in the background sample giving a diffuse beam into the collimator. At this stage it was decided that further tests should be made in order to determine the origin of the neutron background.

One of these tests consisted in the determination of the possible background contribution due to neutron scattering from one side detector into another. This test was made keeping one side detector in its experimental position, while the other was placed, alternately, in its experimental position and at a distance of 12 cm from the centre of the beam. The ratio of the normalised counting rates from the first detector for the two different conditions indicated that the background contribution due to this effect was negligible. Similarly, the possible neutron backscattering from the collimated beam monitor assembly into the stilbene side detectors turned out to be sufficiently small.

In order to determine the room-scattered neutron background, the polythene insert assembly was removed and the collimator was blocked with blank polythene inserts. The side detectors were placed in their experimental position. With this arrangement, several runs, each of 2000 sec duration were made. The readings in the scalers corresponding to the collimated beam monitor and stilbene side detectors were normalised with respect to the target yield monitor readings. From this test, it was found that the room-scattered neutron background was approximately 73% of the total background measured with condition (iii). Thus it was concluded that the combined effect of neutron scattering in the collimator walls, from the air near the detectors and from the materials forming and surrounding the polarimeter was responsible for the remaining 27% of the total background.

An experimental comparison of the straight square collimator used in the present work and a double-truncated conical collimator was made in order to estimate the background contribution due to scattering in the walls of the straight square collimator. The double-truncated conical collimator, specially constructed for this test, consisted of a series of polythene inserts having a combined length of 46 cm. The taper angle on the cone nearest to the target was chosen so that the scattering sample did not view any of its surface; the taper angle on the cone nearest to the scattering sample was chosen so that the target did not bombard this part of the collimator. These taper angles were 5° and 2° respectively. The diameter at the throat position was 5 mm.

The first test performed on both collimators consisted in comparing the beam profiles obtained in similar conditions with the straight square and the double-truncated conical collimator, respectively. For this, the position of the throat was adjusted until the spread of the neutron beam, corresponding to the tapered collimator, was similar to that of the straight collimator. Figure 36 shows the beam profiles obtained with one stilbene side detector under similar accelerator conditions. In this figure, the symbols □ and ○ represent the beam profile corresponding to the straight square and tapered conical collimators respectively.

As can be seen from the curves, the background in the vicinity of the beam turned out to be essentially the same in both measurements. The background to peak ratio for the straight collimator was 1.6×10^{-3} and 2.1×10^{-3} for the tapered conical collimator. The ratio of these two figures gave just a 3% difference with respect to the ratio of the corresponding solid angles. Thus, it was concluded that the performance of the straight square collimator was comparable to that of the double-truncated conical collimator and that the calculations of beam contaminations made for tapered collimators can be applied to the particular straight square collimator employed in this work. This conclusion is supported by the analysis of Simon and Clifford [91] in which they have shown that the wall scattered neutron flux in a straight long duct is small compared with the direct neutron flux travelling directly in air from one end of the duct to the other.

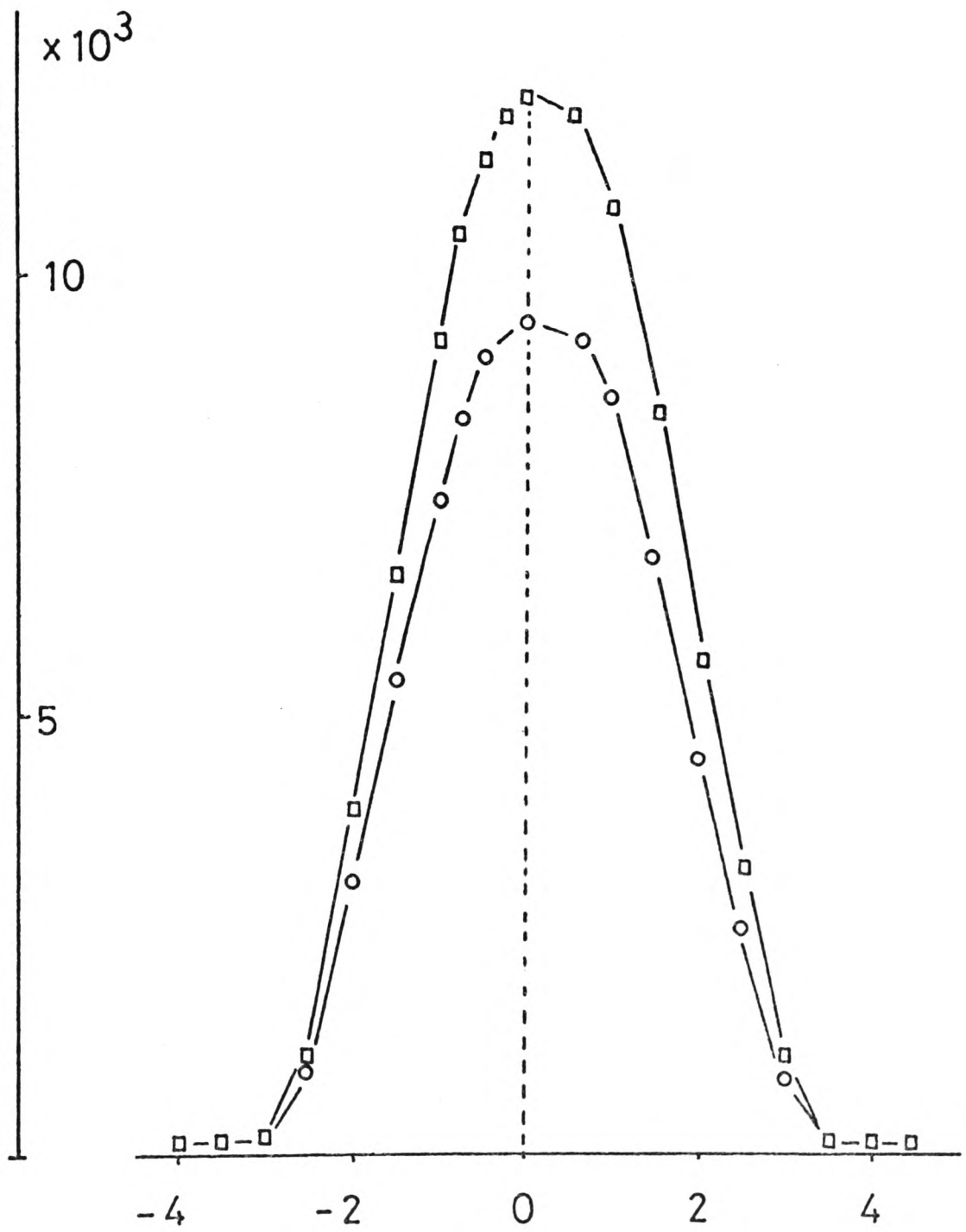

Fig.36. Beam profiles obtained with a straight square collimator (□) and a double-truncated conical collimator (○).

Applying the analysis of Glasgow et al [92] for a cylindrical collimator to the present straight square collimator, it was estimated that the ratio R_c of single scattered neutron flux from the collimator walls to the direct neutron flux at the stilbene side detectors position on the axis of the beam had a value of $R_c = 0.00024$. Because of the proximity of the stilbene side detectors to the direct beam, it was possible to assume that the scattered flux from the collimator walls reaching the side detectors was approximately R_c. With this value and the beam profiles of figure 31, the background contribution due to this effect was about 15% of the total background.

An estimate of the background contribution due to neutron scattering by air along the path of the collimated beam was made applying the analysis of Langsdorf [93]. According to this analysis, the ratio R_a of single scattered to primary flux at a point on the axis of the beam at a distance x from the target is $R_a = (x/2\lambda)(\pi\Omega)^{1/2}$, where Ω is the solid angle defined by the far end of the collimator aperture and λ is the length of a mean free path of neutrons in the air. The beam radius r outside the collimator at the distance x is $r \approx x(\Omega/\pi)^{1/2}$, These parameters evaluated for the present experimental geometry at the side detectors position were $R_a = 0.00015$ and $r = 1.2$ cm, respectively. Since the air scattered neutron flux throughout the area of the beam is nearly constant at its central value and because the side detectors are placed very near to the collimated beam, it was possible to assume that the scattered neutron flux reaching the

side detectors was nearly R_a. With this value and the beam profiles of figure 31, the background contribution due to air scattering along the path of the collimated beam was about 10% of the total background. The beam radius r = 1.2 cm, calculated assuming that only air scattering is present, was in agreement with the value r = 1.53 cm determined experimentally from the beam profile measurements.

It should be emphasized at this time that the calculated background contributions due to neutron scattering from the collimator walls and by air along the beam path were not considered as a precise but as a rough estimate of the effects. However, it was possible to draw an important conclusion from this estimate.

As mentioned earlier, the background sample placed at the entrance of the collimator could reduce the neutron flux incident on the air column between the collimator exit and the stilbene side detectors to about the same level as when the scattering sample was in position, but at the same time it reduced the neutron flux incident on the collimator walls, so reducing the background caused by neutron scattering from the collimator walls. Since the background due to air scattering was not considerable and because the reduction in the background counting rate in the side detectors when the background sample was in position was not observed, it was concluded that the use of the background sample was not essential, and, therefore, that the background measured with condition (iii) represented the true background.

Since the second polarimeter was constructed with the same design as the first one, it was not considered necessary to repeat all the tests described above but only the background measurements required for correction of total and differential cross sections, i.e., room-scattered neutron and total background. These measurements, made during the actual experiment, are presented in the next chapter. However, to complete this section it is enough to say that the room-scattered neutron background found in the second polarimeter amounted to ~80% of the total background, which indicated that its shielding was not as good as that of the first polarimeter.

Finally, it was concluded that the neutron background found in both polarimeters, though appreciable, could be tolerated and it did not interfere considerably with the primary objective of the experiment.

4.3 Preliminary neutron polarization measurements.

This chapter is concluded with the description of several other tests performed on the first polarimeter, including some preliminary polarization measurements on neutrons from the $H^2(d,n)He^3$ reaction for 340 keV deuterons incident on a thick Ti-D target.

As a final and conclusive test concerning the performance of the first polarimeter in general and the straight square collimator in particular, the polarimeter was used to measure the polarization of neutrons from the reaction and with the conditions mentioned above. These results were compared, respectively, with published values and with the experimental values obtained with the same polarimeter under the same accelerator conditions but using the double-truncated conical collimator.

These preliminary polarization measurements, as well as the rest of the measurements carried out with both polarimeters, were made following the procedure described here. After the alignment and the associated electronics of the polarimeter were checked, a number of runs, each of 2000 sec duration, were taken with the scattering sample alternately in and out of the beam. At frequent intervals an intercalibration of detection efficiencies of the collimated beam monitor and the stilbene side detectors was made by placing each detector in turn in the direct beam. Just before the end of the booked running time, two runs, each of 2000 sec duration, were made with the collimator blocked, so that the general room-scattered neutron background could be determined for correction purposes.

Following this procedure, the polarization of the neutrons from the reaction and with the conditions described above, measured with the first polarimeter with the straight square

collimator was $P_n = -(16.1 \pm 2.7)\%$ in a time of 20 hours. In these measurements, the scattering to background ratio was 0.4, the room-scattered neutron background was 72% of the total background and the average counting rate in the collimated beam monitor with the sample out was 267 c/sec. Although this polarization value had a poor statistical accuracy, it indicated good agreement with the value $P_n = -(15.2 \pm 0.9)\%$ obtained in a time of 55 hours with a He^4 scattering polarimeter based on a gas scintillator [94]. However, at this stage the main concern of these preliminary tests was not to attain a good statistical accuracy but to evaluate the general performance of the polarimeter. Thus, from here it was concluded that the first polarimeter was working reliably.

After this test, the straight square collimator was replaced by the double-truncated conical collimator and the throat position was adjusted so as to have the same spread in the neutron beam at the side detectors position. With this arrangement and with similar accelerator conditions a polarization value of $P_n = -(15.0 \pm 2.9)\%$ was obtained in a time of 24.5 hours. In this case, the scattering to background ratio was 0.41, the room-scattered neutron background was 72% of the total background and the average counting rate in the collimated beam monitor with the sample out was 217 c/sec. Comparing this polarization value with that obtained with the straight square collimator, it was observed that the difference in the standard errors corresponded to the difference in running time and neutron flux passing through the collimator.

Thus, it was concluded that the performance of the straight square collimator was comparable with that offered by the double-truncated conical collimator and had at the same time the advantage of larger solid angle, so accepting a larger neutron flux through it and therefore reducing the time of data collection.

The last test performed on the first polarimeter with the straight square collimator in place, consisted in measuring the polarization of the neutrons from the $H^2(d,n)He^3$ reaction for 340 keV deuterons incident on a thick Ti-D target, with both side detectors placed, alternately, at symmetrical minimum scattering angles of 1.8° and 3°. With the first condition, a polarization value of $P_n = -(14.7 \pm 2.5)\%$ was obtained in a running time of 22 hours. In the second case, the corresponding polarization value was $P_n = -(15.0 \pm 3.7)\%$. The comparison between these two values indicated that the measured polarization is independent of the angle of measurement, as expected from Schwinger's theory. The rate of data collection attained with the side detectors placed at a minimum scattering angle of 1.8° turned out to be 2.2 times larger than that corresponding to a minimum scattering angle of 3°, so proving that Schwinger scattering process increases rapidly with diminishing angle.

For the purpose of the tests, the polarization values were quoted without any comment concerning the treatment of the experimental data, however, a complete description of such treatment is given in the next chapter.

CHAPTER 5.

CHAPTER 5.

TREATMENT OF THE EXPERIMENTAL DATA, RESULTS AND CONCLUSIONS.

As already mentioned, the main objective of the present work was to develop an efficient Mott-Schwinger fast neutron polarimeter and assess its performance with the $H^2(d,n)He^3$ reaction for deuteron energies below 500 keV. The actual experimental measurements carried out with the first polarimeter involved incident deuteron energies of 340, 400 and 500 keV using thin targets and a measurement for 340 keV deuteron incident on a thick target. The second polarimeter was used in combination with the first one to measure the $H^2(d,n)He^3$ polarization for incident deuteron energies of 150 and 250 keV using thin targets.

As pointed out in section 1.7, accurate total and differential cross sections are needed for reliable calculation of neutron polarization in a Mott-Schwinger scattering polarimeter. Since the present experimental geometry involved a comparatively large scattering sample and a rather large spread in scattering angles, the measured finite geometry total and differential cross sections had to be corrected before they could be compared with nuclear theory.

The present chapter describes the different corrections applied to the experimental total and differential cross section data, and a comparison of the corrected cross sections with published data. The polarization measurements on neutrons from the $H^2(d,n)He^3$ reaction at different deuteron energies below 500 keV are also presented and compared with those obtained with a typical He^4 polarimeter and the new technique based on a helium filled proportional chamber [72]. Finally, the chapter concludes with the comparison of the efficiency of data collection attainable with the present system and with a typical He^4 scattering polarimeter, and some suggestions to improve further the present system.

5.1 Determination of the Total Cross Section.

The total cross section of lead for neutrons from the $H^2(d,n)He^3$ reaction for different incident deuteron energies below 500 keV were measured by the conventional transmission technique. From the transmission T of the lead sample, the total cross section σ_T was determined from the expression:

$$T = \frac{I}{I_o} = \exp(-\sigma_T nt) \qquad (5.1.1)$$

where I and I_o represent, respectively, the flux at the collimated beam monitor with the lead scattering sample in and out of the neutron beam; n is the number of nuclei per cm^3 in

the sample and t is its thickness. The measured transmission T was corrected, when required, for neutron background and single and double inscattering effects, which represent the principal corrections. These corrections are described in the following sections.

5.1.1 Neutron background correction.

This correction had to be applied to the measured transmission since some of the neutrons detected with the collimated beam monitor, both with lead sample in and out, generally did not come directly from the target but from scattering into that detector from the floor, walls and materials forming and surrounding the polarimeter, that is, room-scattered neutrons. The procedure to determine the room-scattered neutron background consisted, as described in chapter 4, in blocking the collimator with blank polythene inserts and recording the number of counts registered by the collimated beam monitor during a time equal to that taken by each measurement with or without scattering sample. The transmission corrected for room-scattered neutron background is given by:

$$T_B = \frac{I - I_B}{I_o - I_B} \qquad (5.1.2)$$

where I_B is the number of counts in the collimated beam monitor

obtained with the collimator blocked and I/I_o is the measured transmission. In all the measurements carried out with both polarimeters it was found that the counting rate due to room-scattered neutron background was always less than 0.2% of the counting rate obtained with the sample out of the beam. With this figure, the measured transmission was approximately 1.003 times the transmission corrected for room-scattered neutron background.

5.1.2 Inscattering correction.

Because of the finite size of the present transmission geometry, it was necessary to include a correction for neutrons scattered forward in the sample and counted by the collimated beam monitor as if no interaction had occurred. As pointed out in chapter 2, this inscattering correction was minimized by using a scattering sample just large enough to overlap completely the neutron beam.

Due to this inscattering effect, the measured transmission of the scattering sample after background correction was considered equal to

$$T = T_o + T_1 + T_2 \qquad (5.1.3)$$

where T_o is the true transmission of unscattered neutrons, T_1 is the ratio of counting rate of neutrons singly scattered by the sample reaching the detector to the counting rate without sample,

T_2 is a similar ratio of counting rate of neutrons doubly scattered in the sample into the detector.

Following a similar procedure to that given in reference 95, the expression derived for T_1 was :

$$T_1 = \frac{I_1}{I_o} = \left(\frac{A}{L_1}\right)^2 \left(\frac{L}{L_2}\right)^2 n t \sigma_e(0°) \exp(-n t \sigma_T) \qquad (5.1.4)$$

where $(A/L_1)^2$ is the solid angle subtended by the scatterer at the target, L and L_2 are the target-detector and sample-detector distances, respectively; $\sigma_e(0°)$ is the differential elastic scattering cross section for forward scattering, and σ_T is the measured total cross section.

For correction purposes, the elastic differential scattering cross section $\sigma_e(0°)$ was evaluated using the result of the diffraction theory based on a continuum model developed by Feld et al [96]. According to this theory, $\sigma_e(0°)$ is given by :

$$\sigma_e(0°) = \frac{(kR+1)^4}{4k^2} \qquad (5.1.5)$$

where k is the wave number of the incident neutron and R is the radius of the bombarded nucleus.

The term T_1 for single inscattering evaluated for the present experimental geometry for 3 MeV neutrons turned out to be about

1.001 times the corrected transmission. Since the correction for single inscattering is larger than that for double inscattering, this latter correction was not estimated.

Taking into account the corrections to the transmission due to room-scattered neutron background and single inscattering, the measured total cross section had an apparent decrease no greater than 0.7% from its true value. Other sources of error were those associated with the determination of the number of nuclei per cm^3 in the sample (n), the thickness of the sample (t), and the counting statistics. The errors associated with these quantities were estimated to be $\pm$ 0.1%, $\pm$ 0.05% and $\pm$ 0.03%, respectively. These errors combined with those associated with the transmission, produced a total error of about $\pm$ 0.8% to the total cross section values.

5.1.3 Total Cross Section Values.

The total cross section values obtained with both polarimeters for the different experimental conditions are given in table 5.1. The first column indicates the incident deuteron energies, the next column indicates the type of target employed and its thickness, while column three contains the mean deuteron energies. The neutron energies are contained in column four, and the measured total cross section values are contained in column five. Published[74] total cross sections of lead at the

Polarimeter	Incident deuteron energy (keV)	Target type * and thickness (keV)	Mean deuteron energy (keV)	Neutron energy (MeV)	Measured total cross section (barns)	Published total cross sections (barns)
1	150	(st) 88	106	2.74	7.3 ± 0.06	7.2
2	150	(st) 88	106	2.26	6.7 ± 0.06	6.2
1	250	(st) 108	196	2.86	7.4 ± 0.06	7.4
2	250	(st) 108	196	2.20	6.6 ± 0.06	6.2
1	340	(at) thick	243	2.93	7.4 ± 0.06	7.5
1	340	(at) 148	266	2.95	7.5 ± 0.06	7.5
1	400	(at) 140	330	3.02	7.5 ± 0.06	7.6
1	500	(at) 128	436	3.14	7.6 ± 0.06	7.6

* (st) : straight target, (at) : angled target

Table 5.1 Total neutron cross sections results.

same neutron energies are listed in the final column of the table.

The total cross section values listed in column five were calculated using the accumulated readings of the collimated beam monitor obtained, respectively, with the scattering sample in and out of the neutron beam and normalised to the target yield monitor readings. The errors associated with the present total cross sections represent the total error calculated as described in the previous section, and which can be taken as the upper limit of the total probable error. From table 5.1, it can be seen that the present total cross sections are in excellent agreement with those of reference 74.

5.2 Determination of the Differential Elastic Scattering Cross Section.

As described in section 2.2.5, the dimensions of the side detectors in both polarimeters were chosen so as to collect all the polarization information in the angular interval from 1.8° to 5.5° in one measurement. This angular interval, measured in the reaction plane containing the neutron beam axis and the centroids of the two detectors, was determined by the nearest and farthest points of the side detector to the beam axis.

The differential elastic scattering cross section, $\sigma(\theta)$, for scattering into unit solid angle at scattering angle θ, was calculated for each side detector, separately, from the equation [97] :

$$\sigma(\theta) = \frac{F_s r^2}{F_{in} N} \qquad (5.2.1)$$

where F_s is the scattered neutron flux (neutrons/cm^2sec) appropriately corrected for background, F_{in} is the neutron flux incident on the scattering sample, r is the distance between the scattering sample and the side detector, and N is the number of nuclei in the sample.

F_s was determined as the difference in the normalised counting rates of the same side detector for the two different conditions, namely, sample in and out of the beam, respectively. F_{in} was measured with the collimated beam monitor with the sample out of the beam. Since F_s and F_{in} were determined with a different detector, it was necessary to make some intercalibration measurements of the collimated beam monitor and the side detectors, as described in section 4.3. The distance r from the centre of the scattering sample to the centre of the active volume of the detector was measured directly.

The differential elastic cross sections so obtained were corrected, when required, for double scattering of neutrons in the scattering sample, finite size of scatterer and side detector,

attenuation of the incident and scattered neutron beams in the scatterer, difference in sensitivity of the detector over the whole volume, possible systematic error in the intercalibration measurements and finally for inelastic scattering. These corrections are described in the following sections.

5.2.1 Correction to the intercalibration measurements.

As already mentioned, the intercalibration of the detection efficiencies of the collimated beam monitor and the side detectors was made by placing each side detector in turn in the collimated neutron beam. With this condition, the direct neutron beam was observed mainly by the central portion of the scintillator while the scattered beam illuminated the entire scintillator. The correction to the intercalibration measurements consisted in calculating the intrinsic efficiency of the scintillator in its two different conditions. These calculations were made in the following way.

According to Schwarz and Zetterstrom [98], the intrinsic efficiency ϵ of a scintillator for neutrons of energy E_n, assuming only single scattering with hydrogen and carbon, is given by :

$$\epsilon(E_n, L) = n_H \sigma_H \left[1 - \exp(-\Sigma L)\right] / \Sigma \qquad (5.2.2)$$

where $\Sigma = n_H \sigma_H + n_C \sigma_C$, L is the effective length of path of a particular neutron within the scintillator, n_H and n_C are the number of hydrogen and carbon atoms per cm^3, and σ_H and σ_C are the neutron scattering cross section for hydrogen and carbon at energy E_n.

Figure 37 represents the coordinate system used to evaluate the intrinsic efficiency of a stilbene side detector of the first polarimeter in its position to measure the scattered neutron flux. The scatterer and effective area of the detector projected on plane yz were divided into differential volume and surface area elements respectively. The different parameters involved in this evaluation were calculated with the computer program produced for such purpose and described here.

The program calculated the scattering angle, θ, between the vector $\underline{l}_k$ and $\underline{l}_\ell$ which defined a scatterer and a surface area elements respectively. The energy E_n' of the scattered neutron was then calculated from the kinematics of the scattering, and the neutron scattering cross section for hydrogen was calculated from Wasson's [99] expression :

$$\sigma(E_n', H) = 5.603\pi/(1 + 7.417 E_n' + 0.11 E_n'^2) + \qquad (5.2.3)$$

$$+ 0.865\pi/(1 + 0.243 E_n' + 0.003 E_n'^2) \text{ barns/atom}$$

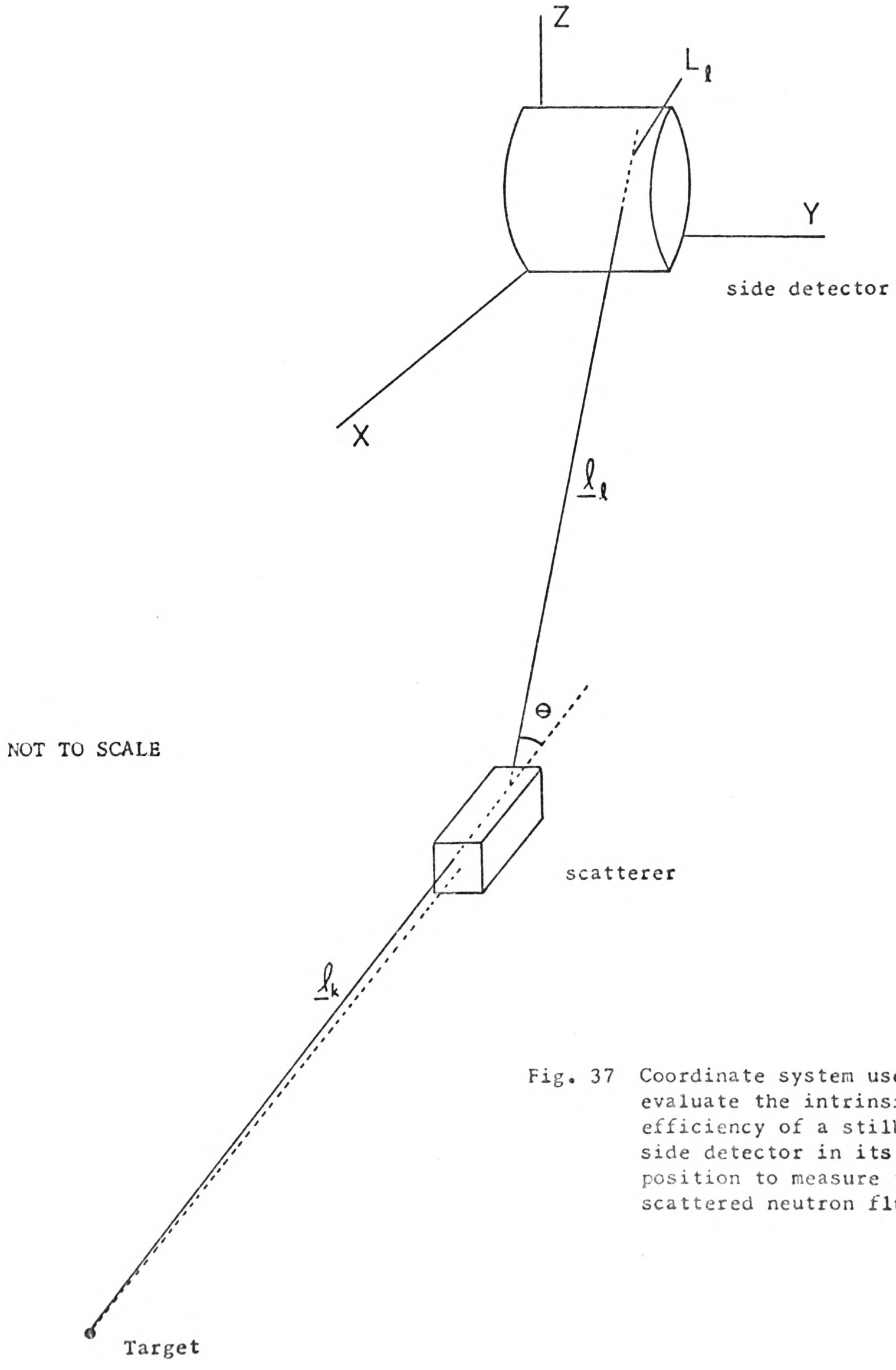

Fig. 37 Coordinate system used to evaluate the intrinsic efficiency of a stilbene side detector in its position to measure the scattered neutron flux.

The corresponding macroscopic cross section Σ was chosen from the values reported in reference 100. Finally, after calculating the effective length, L_ℓ, of path of a particular neutron within the scintillator, the program calculated the corresponding intrinsic efficiency ϵ_ℓ using equation (5.2.2). This process was repeated until the whole scatterer and detector geometry was covered. Thus, the program simulated the actual geometry of the experiment, tracing more than 20,000 neutron scattering histories and gave an estimate of the intrinsic efficiency of the side detector weighted over the experimental geometry.

The intrinsic efficiency of the side neutron detector placed in the direct collimated neutron beam was calculated in a similar manner to that just described. Figure 38 represents the coordinate system in which this calculation was made. For this calculation, the effective area presented by the detector to the direct neutron flux was taken from the beam profile measurements. In this case it was necessary to calculate only the effective length, L_j, of path of a neutron within the scintillator and the corresponding intrinsic efficiency, ϵ_j, over the effective volume of the scintillator. This was made with a computer program which traced more than 4,000 neutron histories and estimated the intrinsic efficiency of the detector in the direct neutron beam.

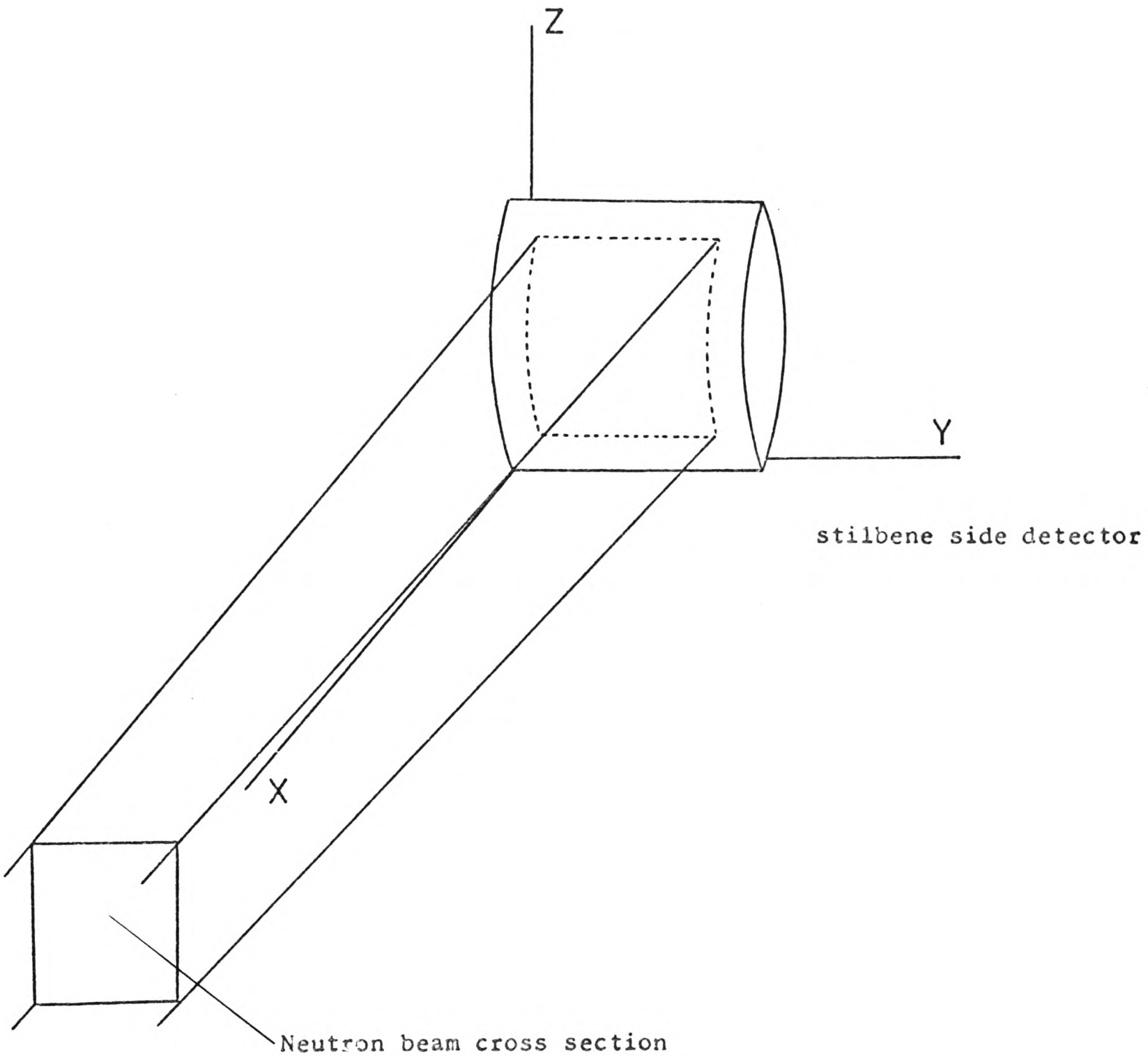

Fig. 38 Coordinate system to evaluate the intrinsic efficiency of a stilbene side detector in the direct neutron beam.

The results of these calculations for a neutron energy of 3 MeV, indicated that the intrinsic efficiency of the stilbene crystals in the scattered beam was 0.98 times the intrinsic efficiency in the direct beam. A similar result was obtained at a neutron energy of 2.7 MeV, which was the lowest neutron energy involved in the measurements carried out with the first polarimeter.

The counting rate sensitivity of the side detector was investigated by observing the contribution to the dead time of the multichannel analyser with the side detector in the direct beam. In this condition, the highest counting rate was about 4×10^2/sec which increased the dead time of the pulse height analyser by no more than 1% of that observed when the side detector was measuring the scattered beam.

Since the slightly higher intrinsic efficiency of the stilbene crystal in the direct beam was partially offset by the decrease in detection efficiency due to the higher counting rate in that condition, it was considered that the correction to the intercalibration factors due to these two effects was less than 1%.

In the case of the second polarimeter, it was not considered necessary to repeat all the detailed calculations given above because the side detectors in this polarimeter had the same sensitivity over the entire volume. This was investigated as follows. According to Curran [101], the intrinsic efficiency ϵ

of a scintillator for neutrons of energy E_n, considering the recoil of protons only, is given by :

$$\epsilon(E_n) = B\,\sigma_H \frac{V}{A} \qquad (5.2.4)$$

where B is a constant which depends on the particular scintillator, σ_H is the cross section of hydrogen for the scattering of neutrons of energy E_n , and V and A are the effective volume and area of the scintillator presented to the neutron flux. From the geometry of the side detectors of the second polarimeter, it could be considered that V/A represented the effective length of path of the neutrons within the scintillator, hence :

$$\epsilon(E_n) = B\,\sigma_H L \qquad (5.2.5)$$

The effective length L of path presented by the scintillator to the direct neutron beam was equal to its depth and that presented to the scattered beam was approximately :

$$L_1 = \frac{L}{\cos\bar{\theta}} \qquad (5.2.6)$$

$\bar{\theta}$ is the mean scattering angle. The computer program described above calculated the weighted mean scattering angle, which turned out to be 3.7°. With this value, L_1 was $L_1 = 1.002L$. Therefore, the intrinsic efficiency of the scintillator in its two different positions was essentially the same.

The counting rate in the direct beam in the second polarimeter did not exceed 2×10^2/sec, so that the contribution to the dead time of the pulse height analyser was sufficiently small ($< 1\%$). Here, too, it was concluded that the correction to the intercalibration factors was less than 1%.

5.2.2 Attenuation of the incident and scattered neutron beams.

The thickness (2.56 cm) of the lead scattering samples, in both polarimeters, was approximately 0.6 of one mean free path of the neutrons in the scatterer in the range of energy of interest. Therefore, it was necessary to apply the proper correction for attenuation of the incident and scattered neutron fluxes in the scatterer. In this effect, the incident neutron beam was attenuated by the scattering sample so that the scattering nuclei farthest from the target were not exposed to the full intensity, and the neutrons forward scattered, at any point in the scatterer, were attenuated by the rest of the sample.

Attenuation of the incident and scattered neutron beams was corrected for by replacing the ratio F_{in}/F_s in equation (5.2.1) by the quantity :

$$F' = \frac{F_{in}}{F_s} \frac{1}{V} \int_V \exp(-n\sigma_T r_1) \exp(-n\sigma_T r_2) \, dv \qquad (5.2.7)$$

where r_1 is the distance into the scattering sample the incident neutron had to pass to reach the volume element dv, r_2 is the distance between this volume element and the far end of the scatterer measured along the path of the scattered neutron, n is the number of nuclei per cm^3 in the sample and σ_T is the total cross section.

Figure 39 represents the geometry to evaluate this quantity. From this figure it is clear that F' is a function of the angles α and β. However, since α only varied from 0° to $\sim 0.5^\circ$ as determined from the beam profile measurements, little error and much simplification was introduced by making $\alpha = 0^\circ$, that is by making $r_1 = t_1$. The angle β was related to the corresponding scattering angle θ through the relation $\beta = \theta - \alpha$. In order to estimate the upper value of the angle β, the maximum finite geometry scattering angle involved in the experimental geometry was calculated with the computer program described in the previous section. This maximum scattering angle turned out to be 6.8°, which was in turn the upper value of the angle β. With this value it was possible to assume that $r_2 = t_2$ and, therefore, $r_2 + r_1 = t$. Thus, the integral F' could be evaluated in terms of elementary functions.

The result of the integration was :

$$F' = \frac{F_{in}}{F_s} \exp(-n\sigma_T t) \qquad (5.2.8)$$

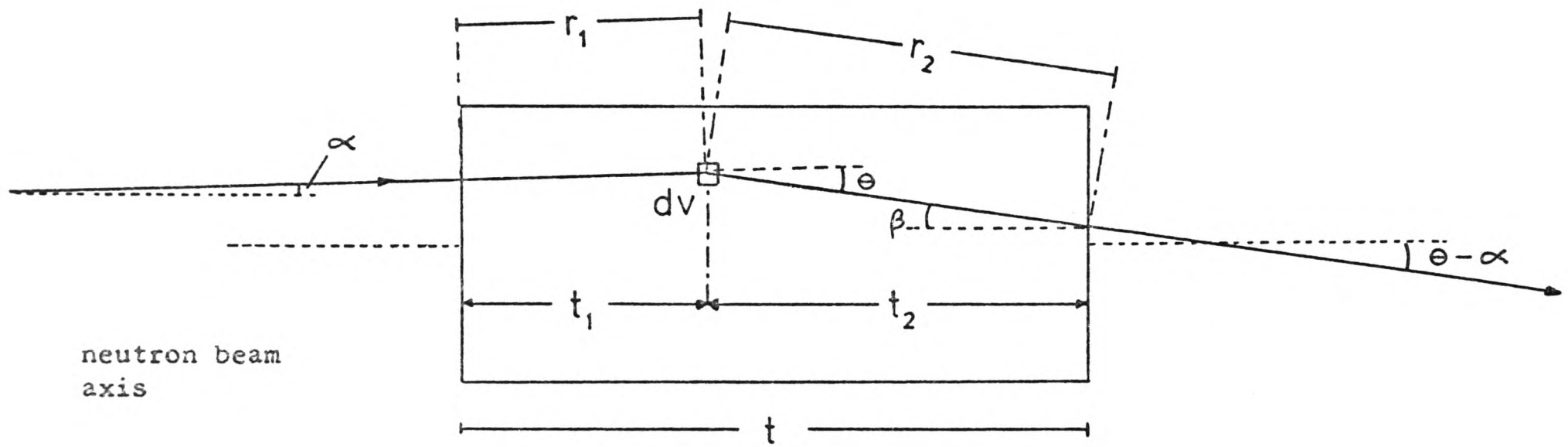

Fig. 39 Detail of single small angle scattering.

where $\exp(-n \sigma_T t)$ essentially measured the attenuation of the direct beam times the attenuation of the scattered beam into the scattering sample. This latter quantity is the well known formula of the transmission given by equation (5.1.1). Thus, the expression to calculate the differential cross section became :

$$\sigma(\theta) = \frac{F_s r^2}{T F_{in} N} \qquad (5.2.9)$$

The measured transmissions ranged from 52.6% in the first polarimeter at a neutron energy of 3.1 MeV to 57.2% in the second polarimeter at a neutron energy of 2.2 MeV. This indicated that the correction for attenuation of the direct and scattered neutron beams was quite considerable.

5.2.3 Multiple scattering correction.

Because of the thickness of the sample, the scattering ratio was considered as a sum of the terms :

$$S = S_1 + S_2 \qquad (5.2.10)$$

where S_1 and S_2 refer to the neutrons scattered in the sample into the side detector by single and double scattering respectively. In order to have an estimate of the effect of double scattering, the ratio S_2/S_1 was calculated by means of an analytic method presented here. Figure 40 represents the geometries for these calculations.

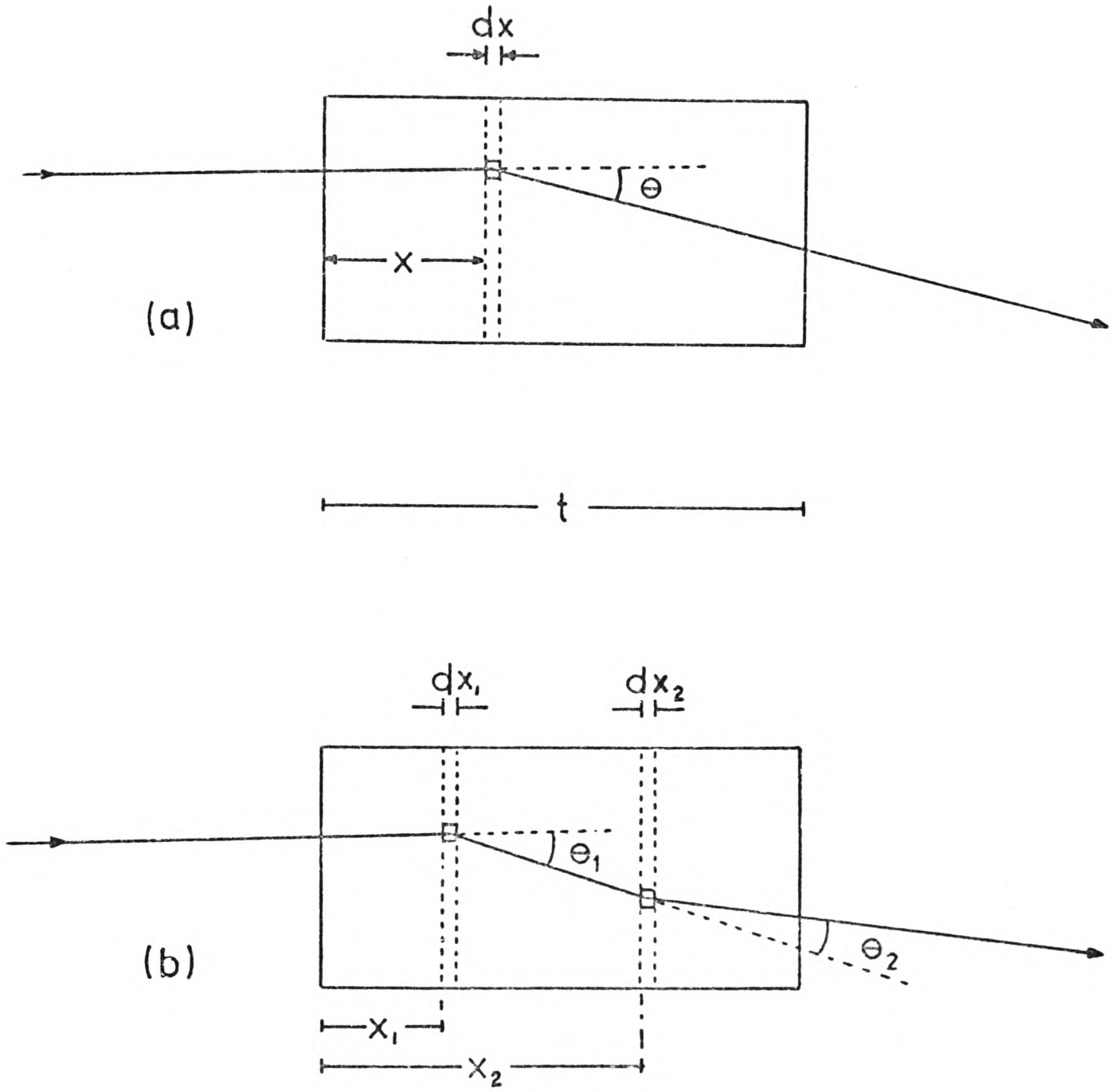

Fig. 40 Detail of scattering geometry :

(a) single scattering

(b) double scattering

The expression for S_1 was determined, using fig. 40a, by evaluating the integral :

$$S_1 = \int_o^t y\,\Omega_s \exp(-n\sigma_T x)\left[n\,dx\right]\sigma(\theta)\Omega_d \exp\left[-n\sigma_T (t-x)\right] \qquad (5.2.11)$$

in which y is the number of neutrons incident on the scatterer of thickness t, Ω_s is the solid angle subtended by the scatterer at the target, $\exp(-n\sigma_T x)$ is the probability that incident neutrons penetrate the distance x, ndx is the number of nuclei/cm^2 in the thickness dx, $\sigma(\theta)\Omega_d$ is the differential cross section for elastic scattering at the forward angle θ times the solid angle subtended by the side detector at the scatterer, and $\exp(-n\sigma_T(t-x))$ is the probability that neutrons scattered at x penetrate the rest of the scatterer. This simplified expression for S_1 was derived assuming suitable approximations similar to those mentioned in section 5.2.2.

Since $\sigma(\theta)$ is large only for small values of θ, an upper limit for S_1 was obtained by setting $\sigma(\theta) = \sigma(o°)$, that is

$$S_1 = y\,\Omega_s\Omega_d\, n\, t\,\sigma(o°)\exp(-n\sigma_T t) \qquad (5.2.12)$$

The number, S_2, of neutrons doubly scattered in the scattering sample and arriving to the side detector was calculated using fig. 40b and an extended expression from that given for single scattering.

This expression was :

$$S_2 = \int_0^{\theta_m} \int_{x_2}^{t} \int_0^{x_2} \left[y \Omega_s \exp(-n \sigma_T x_1) \right] \left[n \, dx_1 \right] \left[\sigma(\theta_1) 2\pi \sin\theta_1 \, d\theta_1 \right]$$

$$\times \left[\exp(-n\sigma_T (x_2 - x_1)/\cos\theta_1) \right] \left[n \, dx_2 \right] \left[\sigma(\theta_2) \Omega_d \right]$$

$$\times \left[\exp(-n\sigma_T (t - x_2)) \right] \qquad (5.2.13)$$

Where the factors in brackets represent the number of incident neutrons at a depth x_1 , the number of nuclei/cm^2 in the thickness dx_1 , the differential cross section for elastic scattering at the angle θ_1 times the appropriate solid angle increment, the probability that neutrons scattered at x_1 arrive at x_2 before having a second scattering, the number of nuclei per cm^2 in the thickness dx_2 , the differential cross section for a second elastic scattering at the angle θ_2 (towards the side detector) times the solid angle subtended by the side detector at the scatterer, and the probability that neutrons second scattered forward at x_2 penetrate the rest of the scatterer.

The integral S_2 was evaluated considering that because of the strong forward scattering, the main contribution to the correction was due to small values of θ_1 and θ_2 , and therefore, that $\theta_1 = \theta_2 = \theta$ if the neutrons were to have a chance of

entering the side detector; thus $\cos\theta$ could be replaced by unity and $\sin\theta$ by θ. Further, since $\sigma(\theta)$ is large only for small scattering angles, the upper limit of S_2 was obtained by setting $\sigma(\theta_1) = \sigma(\theta_2) = \sigma(0°)$ and integrating only up to a maximum angle θ_m which included the forward lobe of the scattering angular distribution. The upper limit for S_2 was :

$$S_2 = Y \pi \Omega_s \Omega_d (nt)^2 \sigma^2(0°) \exp(-n\sigma_T t) \frac{\theta_m^2}{2} \qquad (5.2.14)$$

An appropriate value of θ_m is [96] $1/kR$, where k is the wave number of the incident neutron and R is the nuclear radius. For these calculations, the value of $\sigma(0°)$ was obtained from the measured total cross section using Wick's limit [102]:

$$\sigma(0°) = \left(\frac{k\sigma_T}{4\pi}\right)^2 \qquad (5.2.15)$$

The contribution to the observed scattering due to double scattering, calculated as the ratio S_2/S_1, had a value of 5.9% at a neutron energy of 2.2 MeV in the second polarimeter and 7.8% at a neutron energy of 3.1 MeV in the first polarimeter.

In order to verify the validity of the magnitude of the double scattering correction calculated as described, the number of neutrons doubly scattered in a solid angle Ω_d at an angle θ was also calculated with the expression developed by Dukarevich and Dyumin [103] :

$$S_2' = Y \Omega_s \Omega_d \exp(-\sigma_T n t)(nt)^2 \sigma^2(0°) \frac{\pi}{4k_1^2} \exp\left(-\frac{3}{2} k_1^2 \theta_o^2\right) \qquad (5.2.16)$$

where $k_1 = (R + \lambda)/2\lambda$. For this calculation, the angle θ_o was considered as the mean scattering angle of the present experimental geometry, which was calculated with the computer program described in section 5.2.1. The ratio S'_2/S_2 evaluated for a neutron energy of 3.1 MeV was 0.91, which indicated that the estimate of the double scattering correction made by any of the two expressions S or S' was essentially the same.

Since in both polarimeters the dimensions of the scattering sample were smaller than one mean free path of the neutrons, it was considered that triple scattering processes could be neglected. This assumption is supported by Cox [104], who has shown that the influence of triple scattering is one order of magnitude lower than that of double scattering, provided that the condition just mentioned is satisfied.

5.2.4 Correction for finite geometry.

As mentioned earlier, the geometry of the present experiment was designed so as to have a rather large spread in scattering angles, thus, the dimension of the side detectors permitted to collect, in one measurement, all the polarization information in the angular interval from 1.8° to 5.5° measured from the centre of the scatterer in the reaction plane containing the neutron beam axis and the centroids of the two side detectors. However, due to the finite size of the scatterer and side detector, scattering angles smaller than 1.8°and larger than 5.5° occurred.

In order to determine, precisely, the range of scattering angles involved, the minimum and maximum scattering angles present in the experimental geometry were calculated with the computer program described in section 5.2.1. These angles turned out to be 0.79° and 6.8°, respectively. Since the cross section associated with Schwinger scattering change rapidly over small angular regions, it was considered necessary to evaluate this cross section over the angular interval from 0.79° to 6.8° so that the proper correction could be applied.

This evaluation consisted in calculating the cross section for Schwinger scattering given by :

$$\sigma_{sc} = \gamma^2 \cot^2(\theta/2) \qquad (5.2.17)$$

in the three different intervals of scattering angles, namely 0.79° to 1.8°, 1.8° to 5.5° and 5.5° to 6.8°. However, since the sensitivity of the side detectors in the first polarimeter was not uniform over their entire volume, the term σ_{sc} was replaced by the quantity :

$$\sigma_{sc}' = \gamma^2 \frac{\sum (\epsilon_\ell/\epsilon_o) \cot^2(\theta_\ell/2)}{\sum (\epsilon_\ell/\epsilon_o)} \qquad (5.2.18)$$

where ϵ_ℓ is the intrinsic efficiency of the stilbene crystal associated with a particular neutron scattered through an angle θ_ℓ (see fig.37), and ϵ_o is the maximum intrinsic efficiency of the scintillator, which should occur along the diameter of the stilbene crystal. The quantities σ_{sc} and σ_{sc}' were calculated with the

computer program described in section 5.2.1 over the geometry of scatterer and side detector.

The results of these calculations indicated that 5.5% of the total number of scattering events were associated with scattering angles between 5.5° and 6.8° and produced an average Schwinger cross section of 0.06 barns/sr in that angular interval; 11% of the events were associated with scattering angles between 0.79° and 1.8° producing and average Schwinger cross section of 1.07 barns/sr in that angular interval; and the interval of scattering angles from 1.8° to 5.5° had 83.5% of the total number of scattering events and an average Schwinger scattering cross section of 0.178 barns/sr.

The difference between the nominal and weighted Schwinger scattering cross section in the angular interval from 1.8° to 5.5° was obtained by comparing the result of the previous calculation with that obtained by means of the expression :

$$\sigma_{sc}'' = \gamma^2 \frac{\int_{\theta_1}^{\theta_2} \cot^2(\theta/2)\, d\theta}{\int_{\theta_1}^{\theta_2} d\theta} \qquad (5.2.19)$$

evaluated in the same angular interval. This comparison indicated that the weighted Schwinger scattering cross section was 0.94 times the nominal one. Thus it was concluded that the lack of uniform sensitivity in the side detectors produced such a difference.

The average Schwinger cross section weighted over the whole range of scattering angles (0.79^{o} - 6.8^{o}) was 0.28 for the first polarimeter and 0.34 for the second polarimeter. These values had to be subtracted from the corresponding differential cross sections for the elastic scattering of unpolarized neutrons in order to obtain the differential cross sections for the nuclear interaction.

5.2.5 Correction for Inelastic Scattering.

In the present experiment, the lead scattering samples consisted of three isotopes Pb^{206}, Pb^{207} and Pb^{208} with relative abundancies of 24.1%, 22.6% and 52.3% respectively. The first polarimeter involved separate measurements with incident neutron energies of 2.74, 2.86, 2.93, 2.95, 3.02 and 3.14 MeV respectively, and the second polarimeter involved separate incident neutron energies of 2.2 and 2.26 MeV respectively. In both cases, the incident neutron energy exceeded several excitation levels of the lead nucleus, so giving rise to inelastic neutron scattering.

In order to minimise the contribution to the measured differential cross section from this effect, the bias of the detectors, in both polarimeters, was set at about 1.6 MeV neutron energy. For 2.74 MeV incident neutron energy, which was the lowest neutron energy involved in the first polarimeter, there

are several excitation levels [105] of less than 1.14 MeV which could contribute to the measured cross section. For 2.26 MeV incident neutron energy, the highest neutron energy involved in the second polarimeter, there is only one excitation level [105] (Pb^{207} at 0.57 MeV) which could contribute to the measured cross section.

The contribution from inelastically scattered neutrons was evaluated from the angular distribution of inelastically scattered neutrons, reported by Cranberg [105], corresponding to excitation in Pb^{206} and Pb^{207} for incident neutrons of 2.5 MeV. It was estimated that this effect contributed 0.11 and 0.06 b/sr to the differential cross sections measured with the first and second polarimeter, respectively. These contributions, although small, were also subtracted from the measured differential cross sections.

5.2.6 Differential Elastic Scattering Cross Section Values.

Table 5.2 contains the corrected differential elastic scattering cross sections of lead for the different energies of polarized neutrons involved in the present experiment. In the first column are listed the mean deuteron energies, the second column indicates which polarimeter was employed in the measurement. The neutron energies, calculated from the kinematics of the reaction are contained in the third column. The differential cross sections for polarized neutrons, measured by the 'right' and 'left' detectors of the respective polarimeter are listed in

$\bar{E}_d$ (keV)	Polarimeter	E_n (MeV)	$\sigma_R(\theta)$ (b/sr)	$\sigma_L(\theta)$ (b/sr)	$\sigma_o(\theta)$ (b/sr)
106	1	2.74	6.3 ± 0.046	5.7 ± 0.043	6.0 ± 0.03
106	2	2.26	5.1 ± 0.05	5.6 ± 0.052	5.4 ± 0.04
196	1	2.86	6.46 ± 0.043	5.8 ± 0.04	6.13 ± 0.03
196	2	2.2	4.92 ± 0.045	5.5 ± 0.05	5.21 ± 0.033
243	1	2.93	6.84 ± 0.032	6.11 ± 0.03	6.47 ± 0.021
266	1	2.95	6.6 ± 0.034	5.9 ± 0.031	6.21 ± 0.023
330	1	3.02	7.0 ± 0.034	6.25 ± 0.032	6.62 ± 0.023
436	1	3.14	7.13 ± 0.034	6.35 ± 0.031	6.74 ± 0.023

Table 5.2 Differential elastic scattering cross sections.

column four and five, respectively. The differential elastic scattering cross section $\sigma_o(\theta)$ for the unpolarized neutrons was determined from :

$$\sigma_o(\theta) = \frac{\sigma_R(\theta) + \sigma_L(\theta)}{2} \qquad (5.2.20)$$

and the corresponding values are listed in the final column of the table. The errors associated with the 'right' and 'left' differential cross sections are due to counting statistics only. However, the total error was estimated to be about 1.6% based on counting statistics (0.8%) and systematic errors associated with the quantities involved in equation (5.2.9), that is, the area of the scatterer presented to the neutron beam (1.0%), distance between scatterer and side detector (0.5%), area of the detector presented to the scatterer (0.5%), transmission (0.4%), number of nuclei in the scatterer (0.1%), and intercalibration factor (0.5%). The errors associated with the differential cross section for unpolarized neutrons corresponded to counting statistics only, but the total error was estimated to be about 1%.

At this point, it is important to emphasise that because of the geometry of the experiment, each of the values reported here represents an average differential cross section in the angular interval from 1.8° to 5.5° measured in the reaction plane containing the neutron beam axis and the centroids of the detectors.

In order to assess the present results, a comparison with published data was made. For this purpose, the differential cross sections reported by Galloway and Maayouf [35], for elastic scattering of unpolarized 3 MeV neutrons scattered through angles from 1.6° to 7.7°, were compared with the value obtained in this experiment at 3.02 MeV neutron energy. The result reported in reference 35 are presented in figure 41, where curve A is the result of optical model calculations [106] for scattering angles from 1° to 10° with parameters appropriate to 3 MeV neutrons. Curve B represents the optical model differential cross sections plus the compound elastic differential cross sections [107]; the Schwinger scattering component was then added to give curve C. Finally, curve D, which fits the corrected experimental points, was obtained by normalising the optical model differential cross sections to which the compound elastic and Schwinger components were added. For comparison purposes, curves A, B, C and D have been extrapolated so as to cover the present finite geometry.

Since the result of the present experiment could not be compared with a single experimental point from the angular distribution represented by curve D, the average value of this distribution, over the angular interval from 0.8° to 6.8° was determined by numerical integration and then compared with the present value. The average value of the angular distribution (curve D) in the mentioned angular interval is 6.1 ± 0.2 b/sr, which is in good agreement with the value 6.6 ± 0.07 b/sr reported here.

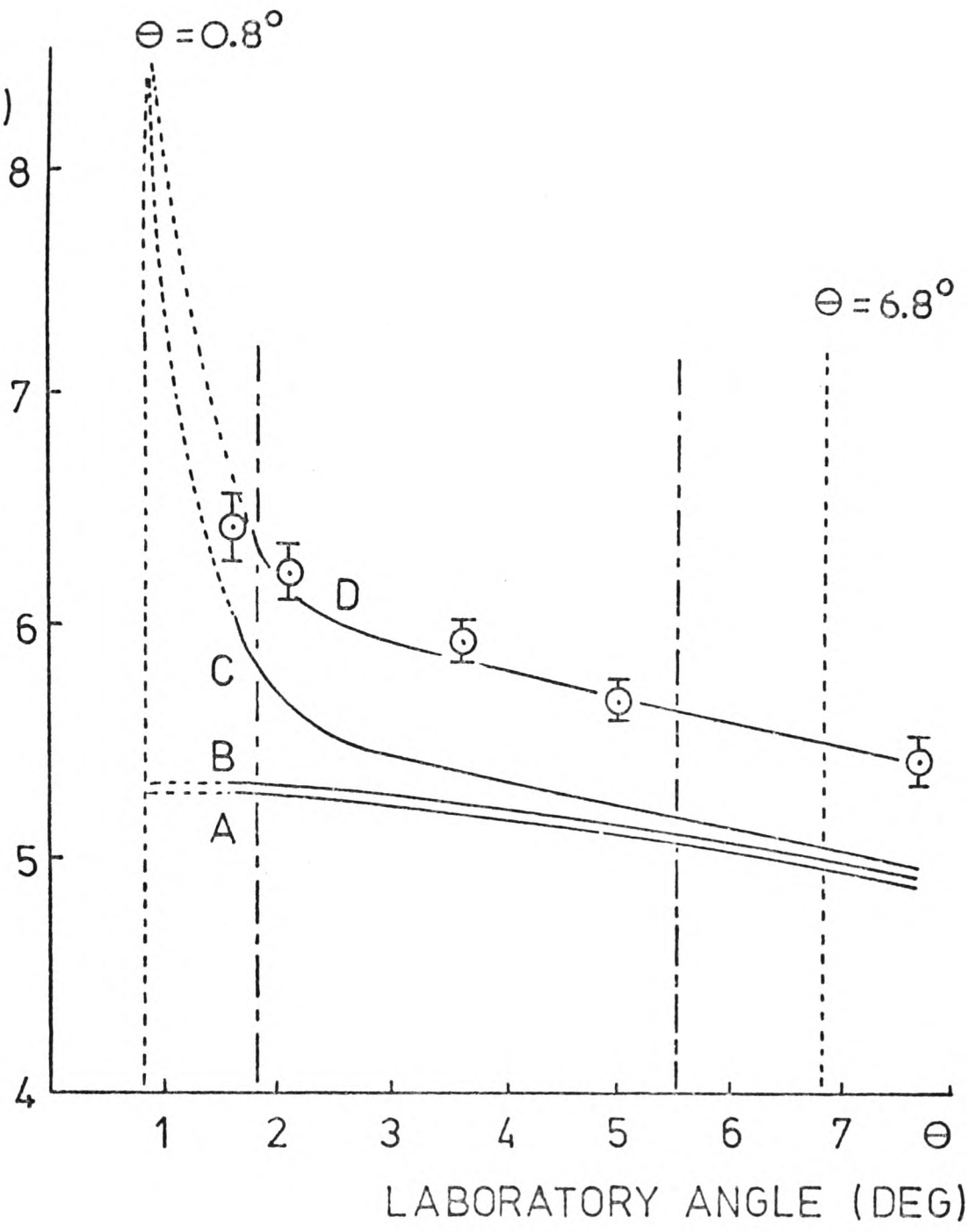

Fig. 41 Differential cross sections for elastic scattering of unpolarized 3 MeV neutrons by lead [35].

For the sake of completeness, the nuclear differential cross sections $\sigma_n(\theta)$ were also compared with published data. The differential cross section due to nuclear interaction was obtained from the equation :

$$\sigma_n(\theta) = \sigma_o(\theta) - \sigma_{sc}(\theta) \qquad (5.2.21)$$

where $\sigma_o(\theta)$ is the differential cross section for unpolarized neutrons defined by equation (5.2.20) and $\sigma_{sc}(\theta)$ is the Schwinger scattering cross section defined by equation (5.2.17).

The values so obtained are presented in figure 42, where the symbols (•) represent the different values of $\sigma_n(\theta)$ obtained for the different neutron energies involved in the present experiment, and the symbol (o) represents the value deduced from reference (35). The symbols (▲) represent the differential cross sections of lead at different neutron energies and scattering angles near to 0^o, calculated from optical potentials [73]. From this figure, it is clear that the magnitude of the present nuclear differential cross sections is in good agreement with the recent value reported in reference (35), and that the trend of the present measurements agrees with that of the calculated values [73]. Fig. 42 also indicates that there is need for suitable normalization in the optical model differential cross sections, so as to have a better agreement between the experimental and calculated values. However, this procedure could not be applied in the present case because angular distributions were not measured.

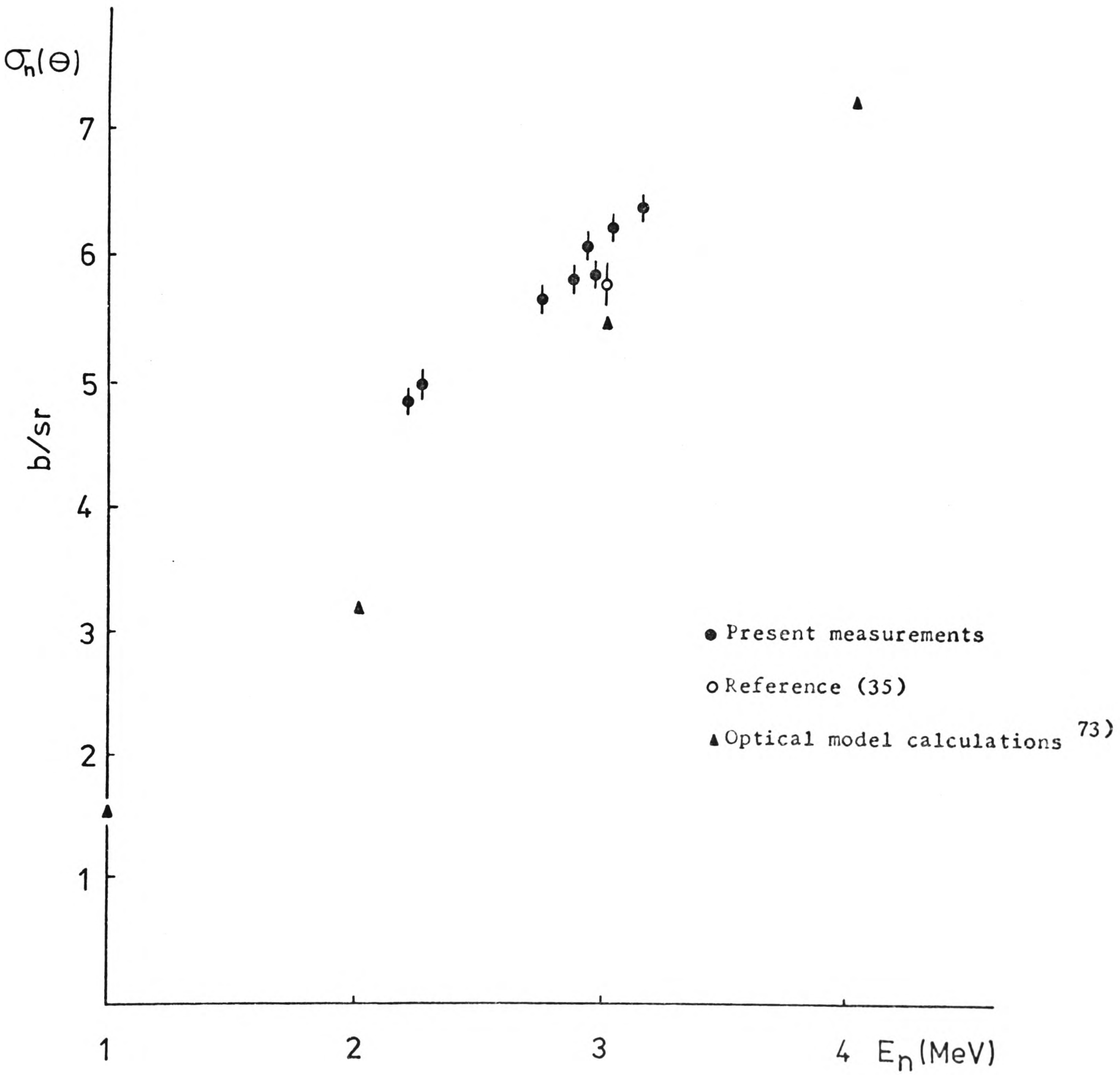

Fig. 42. Nuclear differential elastic scattering cross sections of lead at several neutron energies.

5.3 Calculation of the $H^2(d,n)He^3$ neutron polarization.

In section 1.7, it was pointed out that in a Mott-Schwinger polarimeter the neutron polarization can be calculated directly from the equation :

$$P_n(\theta') = \frac{\sigma(\theta,o) - \sigma(\theta,\pi)}{2\,\sigma_o(\theta)\,P_s(\theta)} \qquad (1.7.1)$$

where $\sigma(\theta,o)$ and $\sigma(\theta,\pi)$ are the differential elastic cross sections measured by the 'right' and 'left' detectors respectively, and the product $\sigma_o(\theta)P_s(\theta)$ is defined by the equation :

$$\sigma_o(\theta)\,P_s(\theta) = k\,\sigma_T \cot(\theta/2)/2\pi \qquad (1.3.6)$$

Thus in order to calculate $P_n(\theta')$ it was required only to measure, as described, the total and differential cross sections, and evaluate the term $\sigma_o(\theta)P_s(\theta)$ over the geometry of both scatterer and side detector by means of the computer program described in chapter two.

The values of $P_n(\theta')$, calculated by this procedure, for the different experimental conditions are listed in column five of the table 5.3. The first four columns of this table are identical to those of table 5.1, and the final column indicates the total charge on target for each particular measurement.

For comparison purposes, the present neutron polarization values are presented in figure 43 in conjunction with the

Polarimeter	Incident deuteron energy (keV)	Target type and thickness (keV)	Mean deuteron energy (keV)	Neutron polarization (%)	Total charge on target (C)
1	150	(st) 88	106	-(12.3 $\pm$ 1.26)	100
2	150	(st) 88	106	+(12.6 $\pm$ 1.60)	99
1	250	(st) 108	196	-(13.9 $\pm$ 1.30)	47
2	250	(st) 108	196	+(14.3 $\pm$ 1.67)	46
1	340	(at) thick	243	-(15.8 $\pm$ 0.93)	46
1	340	(at) 148	266	-(15.0 $\pm$ 1.00)	49
1	400	(at) 140	330	-(14.3 $\pm$ 0.98)	39
1	500	(at) 128	436	-(16.1 $\pm$ 0.95)	32

Table 5.3 $H^2(d,n)He^3$ neutron polarization values.

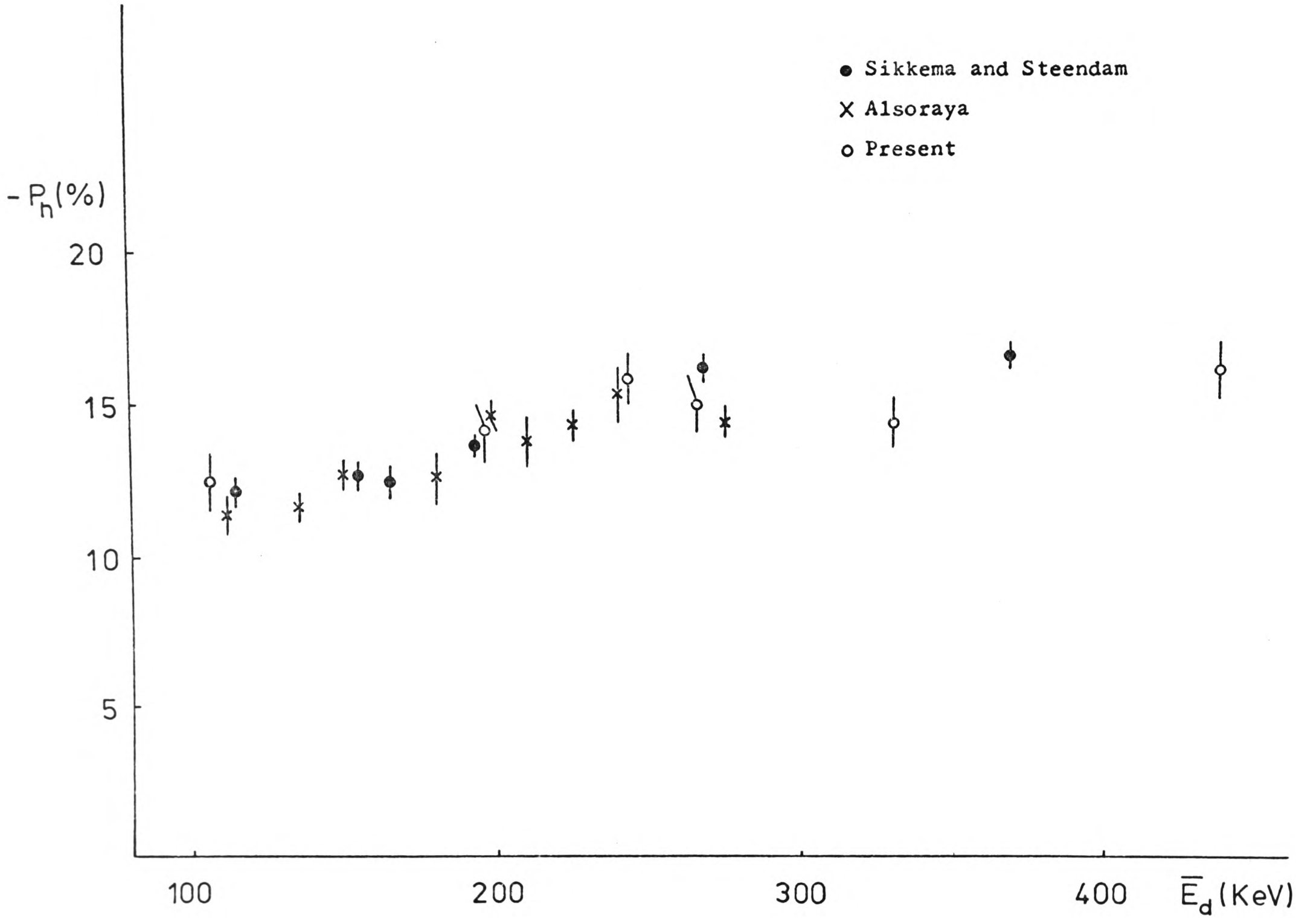

Fig. 43. The present values of P_n compared with other published values.

recent values obtained separately by a typical He^4 scattering polarimeter [108] and the new technique based on a helium filled proportional chamber [72]. The present polarization values corresponding to mean deuteron enegies of 106 and 196 keV were deduced by averaging the magnitude of the values obtained with both polarimeters. It was found, from this comparison, that the polarization values obtained with the present Mott-Schwinger polarimeter are in good agreement with those obtained by the other two techniques, and that the trend of the three sets of values also agree. From here, it was concluded that the present Mott-Schwinger polarimeter can provide a reliable system to measure the source polarization in various neutron producing reactions.

5.4 Efficiency of the present system.

The main objective of this thesis was to design and construct a polarimeter for neutrons of a few MeV energy based on small angle Mott-Schwinger scattering which could have an efficiency of data collection comparable to that of a conventional He^4 scattering polarimeter based on a gas scintillator. The He^4 polarimeter chosen for the comparison is in use in the same laboratory [108]. It consists of a helium gas scintillator operating at a pressure of 1000 psi and scattering neutrons through a mean angle of 117^o into a pair of liquid scintillator neutron detectors.

Therefore, in order to assess the efficiency of data collection of the present system, a comparison was made of the time taken by each system to attain, under similar accelerator conditions, a given statistical accuracy of polarization measurements on neutrons from the $H^2(d,n)He^3$ reaction. Measurements with the first polarimeter of the present system, for neutrons emitted at 45^o lab from this reaction at a mean deuteron energy of 240 keV, gave a polarization value of $P_n = -(15.8 \pm 0.93)\%$ with a total charge on target of 46 coul. The corresponding value obtained with the He^4 polarimeter was $P_n = -(15.5 \pm 0.93)\%$ with a total charge on target of 12 coul.

This comparison indicated that the first polarimeter of the present system takes 3.8 times as long to obtain a polarization value with the same statistical accuracy as a typical He^4 polarimeter. From here, it was concluded that the efficiency of data collection of the first polarimeter of the present system is 30 times larger than that of the Mott-Schwinger polarimeter of reference (46), and that the objective of this thesis has been achieved.

In table 5.3 can be seen that the efficiency of data collection of the second polarimeter of the present system is slightly lower than that of the first polarimeter. This difference was due to a lower neutron yield at backward reaction angles [109], higher neutron background, and a smaller solid angle for acceptance of neutrons. This last condition, as pointed out in

section 2.4, was due to the practical impossibility of placing the collimator at the same distance from the target as in the first polarimeter. Since in the present experiment it was possible to average the magnitude of the polarization values obtained with both polarimeters, it was considered that the present system takes less than 3 times as long to obtain a polarization value with the same statistical accuracy as a typical He^4 polarimeter. However, this averaging procedure cannot be applied when measuring polarization from other neutron producing reactions.

5.5 Possible improvements to the present system.

To conclude the present work, an investigation was made in order to improve further the efficiency of data collection of the present system for future use.

The first obvious improvement can be made by using a scattering sample with higher atomic number, since the Mott - Schwinger contribution depends on the square of the atomic number. This also would improve the scattering ratio because the nuclear differential cross section increases regularly with atomic weight [97]. The second obvious improvement consists in employing a better shielding around the polarimeter, so that the statistical accuracy can be improved by having a lower neutron background.

The possible improvements in the geometry are associated with the solid angle Ω_s subtended by the scatterer at the target, characteristics of the scattering sample, and solid angle Ω_d subtended by a side detector at the sample. However, detailed calculations showed that an increase in solid angles, either by enlarging Ω_s or by moving the side detectors closer to the scattering sample, implies a larger spread in scattering angles, which in turn, reduces the analysing power, and therefore, the figure of merit of the system. Similarly, it was found that if the solid angle Ω_s is kept at its value and the thickness of the scattering sample is enlarged, the increase in the scattering ratio is offset by the decrease in the solid angle Ω_d and the larger attenuation of the scattered flux in the scatterer, requiring therefore, a larger correction due to this attenuation effect. Besides, it is required to take into account triple scattering when correcting for multiple scattering, and also the inscattering contribution is increased. Therefore, it is concluded that the present geometry is adequate for the experiment.

5.6 Conclusions.

Since the polarization measurements obtained with the present system are in good agreement with recent measurements obtained with a typical He^4 polarimeter and the new technique based on a helium filled proportional chamber, and because the efficiency of data collection is comparable to that of a He^4 polarimeter, it is concluded that the advantages of the present Mott-Schwinger

scattering polarimeter outweigh the experimental difficulties and that this system can provide an efficient and reliable alternative technique to determine the source polarization in various neutron producing reactions.

REFERENCES.

1) L. Wolfenstein, Annual Review of Nuclear Science 6(1956)43

2) W. Haeberli, Fast Neutron Physics 2(Interscience, New York, 1963)

3) Sign Convention for Particle Polarization, Nucl. Phys. 118(1960)1054

4) L. Wolfenstein, Phys. Rev. 75(1949)342

5) J. Schwinger, Phys. Rev. 69(1946)681(A)

6) I.I. Levintov, A.V. Miller and V.N. Shamshev, Nucl. Phys. 3(1957)221

7) D.C. Dodder and J.L. Gammel, Phys. Rev. 88(1952)520

8) J.L. Gammel and R.M. Thaler, Phys. Rev. 109(1958)2041

9) S.M. Austin, H.H. Barschall and R.E. Shamu, Phys. Rev. 126(1962)1532

10) S.M. Hoop, H.H. Barschall, Nucl. Phys. 83(1966)65

11) G.L. Morgan and R.L. Walter, Phys. Rev. 168(1968)1114

12) R.A. Arndt and L.D. Roper, Phys. Rev. C1(1970)903

13) Th. Stammbach and R.L. Walter, Nucl. Phys. A180(1972)225

14) H. Davie and R.B. Galloway, Nucl. Instr. and Meth. 92(1971)547

15) E. Baumgartner and P. Huber, Helv. Phys. Acta 26(1953)545

16) J.V. Lepore, Phys. Rev. 79(1950)137

17) J.R. Smith and S.T. Thornton, Can. J. Phys. 50(1972)783

18) L. Drigo, C. Manduchi, G. Noschini, M.T. Russo Manduchi, G. Tornielli and G. Zannoni, Letters Nuovo Cimento 1(1969)237

19) A.S. Hall, Ph.D. Thesis, Edinburgh University, 1976

20) J. Schwinger, Phys. Rev. 73(1948)407

21) N.F. Mott, Proc. Roy. Soc. (London) 124A(1929)425

22) J.T. Sample, Can. J. Phys. 34(1956)36

23) E.M. Purcell and N.F. Ramsey, Phys. Rev. 78(1950)807

24) R. Fox, Nucl. Phys. 43(1963)110

25) M. Walt and D.B. Fossan, Phys. Rev. 137(1965)629

26) Y.A. Aleksandrov, G.S. Samosvat, Zh. Sereter and Tsoi Gen Sor, JETP Letters 4(1966)134

27) IU.A. Aleksandrov, JETP Letters 6(1958)228

28) Y.A.Aleksandrov, G.V. Anikin, A.S. Soldatov, JETP 13(1961)1319

29) A.J. Elwyn, J.E. Monahan, R.O. Lane, A. Langsdorf and F.P. Mooring, Phys. Rev. 142(1966)758

30) G. Breit and M.L. Rustgi, Phys. Rev. 114(1959)830

31) A. Adam, F. Deak, L. Jeki, A. Kiss, Z. Kovessy, G. Palla and P. Hraskv, Sov. J. Nucl. Phys. 8(1969)255

32) G.V. Gorlov, N.S. Lebedeva and V.M. Morozov, Sov. J. Nucl. Phys. 8(1969)630

33) F.T. Kuchnir, A.J. Elwyn, J.E. Monahan, A. Langsdorf and F.P. Mooring, Phys. Rev. 176(1968)1405

34) G.V. Anikin and I.I. Kotoukhov, Sov. J. Nucl. Phys. 12(1971)614

35) R.B. Galloway and R.M.A. Maayouf, Nucl. Phys. A212(1973)182

36) P.W. Martin, R. McFadden and B.L. White, Can. J. Phys. 51(1973)2197

37) E.W. Vogt, Proceedings of the International Conference on Properties of Nuclear States, Montreal, 1969 (Les Presses de l'Universite de Montreal) p. 5

38) Y.V. Dukarevich and A.N. Dyumin, Sov. Phys. JETP 17(1963)89

39) G.V. Anikin, Y.A. Aleksandrov and A.S. Soldatov, Int. Conf. Study of Nucl. Struct. with Neutrons, Antwerpen, July 1965

40) G. Palla, Phys. Lett. 35B(1971)477

41) P.E. Hodgson, The Optical Model of Elastic Scattering, Oxford, 1963

42) H.J. Longley, R.N. Little and J.M. Slye, Phys. Rev. 86(1952)419

43) J.T. Sample, G.C. Neilson and J.B. Warren, Can. J. Phys. 33(1955)350

44) R.G.P. Voss and R. Wilson, Phil. Mag. 1(1956)175

45) P. Hillman, G.H. Stafford and C. Whitehead, Nuovo Cimento 4(1956)67

46) R.B. Galloway and R.M.A. Maayouf, Nucl. Inst. and Meth. 105(1972)561

47) A.J. Elwyn, R.O.Lane, A. Langsdorf and J.E. Monahan, Phys. Rev. 133(1964)B80

48) J.E. Monahan and A.J. Elwyn, Phys. Rev. 136(1964)B1679

49) R.F. Redmond, Phys. Rev. 140(1965)B1267

50) W.S. Hogan and R.G. Seyler, Phys. Rev. 177(1969)1706

51) R. Ricamo, Helv. Phys. Acta 26(1953)423

52) R.B. Galloway, Nucl. Inst. and Meth. 92(1971)537

53) R.W. Meier, P. Scherrer and G. Trumpy, Helv. Phys. Acta 27(1954)577

54) B.M. McCormac, M.F. Steuer, C.D. Bond and F.L. Hereford Phys. Rev. 104(1956)718

55) I.I. Levintov, A.V. Miller, E.Z. Tarumov and V.N. Shamshev, Nucl. Phys. 3(1957)237

56) P.J. Pasma, Nucl. Phys. 6(1958)141

57) P.P. Kane, Nucl. Phys. 10(1959)429

58) P.S. Ot-Stantov, Soviet Phys. JETP 10(1960)1281

59) H.J. Boersma, C.C. Jonker, J.G. Nijenhuis and P.J. Van Hall Nucl. Phys. 46(1963)660

60) J.T. Rogers and C.D. Bond, Nucl. Phys. 53(1964)297

61) H. Hansgen, H. Pose, G. Schrimer and D. Seeliger, Nucl. Phys. 73(1965)417

62) J.P.F. Mulder, Phys. Letters 23(1966)589

63) A.F. Behof, T.H. May and W.I. McGarry, Nucl. Phys. A108(1968)250

64) H. Prade and J. Csikai, Nucl. Phys. A123(1969)365

65) P. Roding and H. Scholermann, Nucl. Phys. A125(1969)585

66) H. Davie and R.B. Galloway, Nucl. Inst. and Meth. 108(1973)581

67) J.R. Smith and S.T. Thornton, Can. J. Phys. 50(1972)783

68) R.L. Walter, Polarization phenomena in nuclear reactions (Eds. H.H. Barschall and W. Haeberli, Univ. Wisconsin, Madison, 1970) p. 317

69) R.M.A. Maayouf and R.B. Galloway, Nucl. Inst. and Meth. 118(1974)343

70) A. Alsoraya, R.B. Galloway and A.S. Hall, Fourth International Symposium on Polarization Phenomena in Nuclear Reactions, August 1975, Zurich, Switzerland.

71) H.J. Boersma, Nucl. Phys. A135(1969)609

72) C.P. Sikkema and S.P. Steendam, Nucl. Phys. A245(1975)1

73) D. Wilmore and P.E. Hodgson, Nucl. Phys. 55(1964)673

74) D.J. Hughes and J.A. Harvey, Neutron Cross Sections, Brookhaven National Laboratory Report BNL - 325(1955)

75) R.B. Owen, I.R.E. Transactions on Nuclear Science, Vol NS - 5(1958)198

76) J. Birks, The Theory and Practice of Scintillation Counting, Pergamon Press, London (1964)

77) L. Varga, Nucl. Inst. and Meth. 14(1961)24

78) F. Du Chaffaut, P. Charmet and R. Trabaud, Nucl. Inst. and Meth. 65(1968)285

79) G. Walter and A Coche, Nucl. Inst. and Meth. 23(1963)147

80) T.G. Miller, Nucl. Inst. and Meth. 63(1968)121

81) R.B. Owen, I.R.E. Trans. on Nuclear Science 9/3(1962)285

82) G.W. McBeth, R.A. Winyard and J.E. Lutkin, Koch - Light Labs. Ltd. Booklet 1971, "Pulse Shape Discrimination with Organic Scintillators".

83) A.S. Hall, M.Sc. Thesis, Edinburgh University, 1972

84) W.B. Reid and R.H. Hummel, Can. Nucl. Tech. 5, 36, Jan/Feb 1966

85) T.K. Alexander and F.S. Goulding, Nucl. Inst. and Meth. 13(1961)244

86) M.L. Roush, M.A. Wilson and W.F. Hornyak, Nucl. Inst. and Meth. 31(1964)112

87) H. Davie, Ph.D. Thesis, Edinburgh University, 1972

88) EMI Photomultiplier Tubes, Catalog Supplement

89) R.B. Owen, Nucleonics 17(1959)92

90) R. Batchelor, W.B. Gilboy, A.D. Purnell and J.H. Towle, Nucl. Inst. and Meth. 8(1960)146

91) A.Simon and C.E. Clifford, Nucl. Sci. and Eng. 1(1956)156

92) D.W. Glasgow et al., Nucl. Inst. and Meth. 114(1974)521

93) A. Langsdorf, Fast Neutron Physics 1(Interscience, New York, 1963) Ch. IV E.

94) A. Alsoraya, private communication, Physics Dept. Edinburgh University

95) J.P. Conner, Phys. Rev. 109(1958)1268

96) Feld, Feshbach, Goldberg, Goldstein and Weisskopf, U.S. Atomic Energy Commission Report NYO - 636, 1951

97) M. Walt, Fast Neutron Physics 2(Interscience, New York, 1963) Ch. V.B

98) S. Schwarz and H.O. Zetterstrom, Nucl. Inst. and Meth. 41(1966)93

99) M.M. Wasson, "The use of stilbene with decay time discrimination as a fast neutron spectrometer", AERE Report 4269(1963)

100) C.D. Swartz and G.E. Owen, Fast Neutron Physics 1(Interscience, New York, 1963) Ch. II.B

101) S.C. Curran, "Luminescence and the Scintillation Counter", (Butterworths Scientific Publications, 1953) p. 153

102) G.C. Wick, Atti accad. d'Ital. 13(1943)1203

103) Yu.V. Dukarevich and A.N. Dyumin, Sov. Phys. JETP 17(1963)89

104) S.A. Cox, Nucl. Inst. and Meth. 56(1967)245

105) L. Cranberg, T.A. Oliphant, J. Levin and C.D. Zafaratos, Phys. Rev. 159(1967)969

106) D. Wilmore, AERE - R4649, Harwell (1964)

107) D. Wilmore, AERE - R5053, Harwell (1966)

108) A. Alsoraya, Ph.D. Thesis, Edinburgh University, 1976

109) J.D. Seagrave, D(d,n)He^3 and T(d,n)He^4 Neutron Source Handbook : LAMS - 2162

ACKNOWLEDGEMENTS.

I thank Professor N. Feather, F.R.S. for the facilities provided for this research at the Edinburgh University, Department of Physics. I am grateful to Dr. R.B. Galloway, under whose supervision I worked on this experiment, for his guidance and valuable advice.

I am grateful to Mr. H.J. Napier for maintaining and operating the accelerator, and also to Mr. G. Turnbull for his willing assistance. I must also express my thanks to Mssrs. A.S. Hall and A. Alsoraya, my colleagues, for their interesting and useful discussions.